**KARADENİZ TECHNICAL UNIVERSITY**
**THE GRADUATE SCHOOL OF NATURAL AND APPLIED SCIENCES**

**DEPARTMENT OF CIVIL ENGINEERING**

# NUMERICAL AND EXPERIMENTAL STUDY OF DAMAGE IDENTIFICATION USING MODAL PARTICIPATION RATIO: DETECTION, LOCALIZATION AND QUANTIFICATION OF SEVERAL DAMAGE SCENARIOS

**MASTER'S THESIS**

**Zafer YILMAZ**

**JULY 2022**
**TRABZON**

**KARADENİZ TECHNICAL UNIVERSITY**

**THE GRADUATE SCHOOL OF NATURAL AND APPLIED SCIENCES**

**DEPARTMENT OF CIVIL ENGINEERING**

# NUMERICAL AND EXPERIMENTAL STUDY OF DAMAGE IDENTIFICATION USING MODAL PARTICIPATION RATIO: DETECTION, LOCALIZATION AND QUANTIFICATION OF SEVERAL DAMAGE SCENARIOS

**Zafer YILMAZ**

**This thesis is accepted to give the degree of**

**"MASTER OF SCIENCE"**

**By**

**The Graduate School of Natural and Applied Sciences at**
**Karadeniz Technical University**

**The Date of Submission** : **10 / 06 /2022**

**The Date of Examination** : **04 / 07 /2022**

**Supervisor** : **Associate Professor Murat GÜNAYDIN**

**Trabzon 2022**

## ACKNOWLEDGEMENT

I would like to express my deepest gratitude to my supervisor Assoc. Prof. Dr. Murat Günaydın for his guidance, recommendations, trust and encouragement throughout this research and preparation of this thesis.

I wish to express my sincere gratitude to Prof. Dr. Ahmet Can Altunışık and Res. Assist. Fatih Yesevi Okur for their constructive feedbacks and support throughtout this research.

I would like to thank Res. Assist. Fezayil Sunca, Res. Assist. Yunus Emrahan Akbulut, Res. Assist. Ali Fuat Genç, Res. Assist. Ali Kaya, Res. Assist. Alihan Baltacı, CE Ali Sarıkoç, CE Mustafa Yılmaz and CE Rıdwan Adebayo Bello for their helpful assistance in the lab.

I would also like to thank The Scientific and Technological Research Council of Turkey (TÜBİTAK), Directorate of Science Fellowships and Grant Programmes (BİDEB 2210-A) for their support throughout my master's studies.

A special thanks to Prof. Dr. Niğmet Uzal for being a perfect academician and influencing me to pursue my dream of being a good researcher.

Finally, my deepest thanks are dedicated to my parents Mümin Yılmaz, Fatma Yılmaz, and my sisters Hümeyra Yılmaz, and Merve Sultan Yılmaz for their endless patience, encouragement and love throughout my research.

Zafer YILMAZ

Trabzon 2022

## DECLARATION

I hereby declare that all information in this master's thesis entitled "Numerical and Experimental Study of Damage Identification Using Modal Participation Ratio: Detection, Localization and Quantification of Several Damage Scenarios" has been obtained and presented in accordance with academic rules and ethical conduct under the supervision of Assoc. Prof. Murat Günaydın. I also declare that, as required by these rules and conduct, I have fully cited and referenced all material and results that are not original to this work.
04/07/2022

Zafer YILMAZ

**TABLE OF CONTENTS**

**Page**

Yüksek Lisans

# ÖZET

## MODAL KATKI ORANINA BAĞLI NUMERİK VE DENEYSEL HASAR TESPİTİ: ÇEŞİTLİ HASAR SENARYOLARININ VARLIĞI, YERİ VE ŞİDDETİNİN BELİRLENMESİ

Zafer YILMAZ

Karadeniz Teknik Üniversitesi
Fen Bilimleri Fakültesi
İnşaat Mühendisliği Dalı
Danışman: Doç. Dr. Murat GÜNAYDIN
2022, 94 Sayfa

Bu tez çalışmasında, hasar tespitinde kullanılmak üzere geliştirilen Modal Katkı Oranı metodunun etkinliğinin numerik ve deneysel olarak değerlendirilmesi amaçlanmıştır. Betonarme bina modeli üzerinde farklı şiddetlerdeki hasar senaryoları sonucu meydana gelen yapısal değişimler numerik olarak ve çelik çerçeve modelin farklı şiddetlerdeki tek kat hasar senaryoları etkisinde geçirdiği yapısal değişimler hem numerik hem deneysel olarak ölçülmüş; hasarın varlığının, yerinin ve şiddetinin tespiti için Modal Katkı Oranının etkinliği değerlendirilmiştir.

Tez çalışması başlıca beş bölümden oluşmaktadır. Birinci bölümde hasar tespitinin önemi vurgulanmış, hasar tespit metotların tarihsel ve teknolojik gelişimi verilmiştir. Ayrıca tez kapsamında kullanılacak formüller ve Modal Katkı Oranı hesap adımları verilmiştir. İkinci bölümde, yapılan çalışmalara, elde edilen bulgulara ve bu bulguların değerlendirmelerine yer verilmiştir. İlk kısımda, numerik betonarme bina modelinin farklı şiddetlerdeki tek kat hasarları ve yığışımlı hasar etkisiyle geçirdiği yapısal değişimler incelenmiş ve hasar tespitinde kullanılmak üzere Modal Katkı Oranı bağıntıları elde edilmeye çalışılmıştır. İkinci kısımda, hem deneysel yetkinliğini test etmek hem de numerik çalışmaları doğrulamak amacıyla, çelik çerçeve modellerine uygulanan farklı şiddetlerdeki tek kat hasar senaryolarının Modal Katkı Oranı üzerinde etkileri incelenmiştir. Üçüncü ve dördüncü bölümlerde çalışmalardan elde edilen sonuçlar sunulmuş ve gelecek çalışmalar için önerilere yer verilmiştir. Son bölümde ise bu çalışmada yararlanılan kaynaklar verilmiştir.

Sonuç olarak bu tezde çalışılmış olan hasar tespit metodunun deneysel ve numerik çalışmalarda etkiliği olduğu ve yapı sağlığı izlemesinde kullanılabileceği çıkarımı yapılmıştır.

**Anahtar Kelimeler:** Deneysel Modal Analiz, Hasar Tespiti, Modal Katkı Oranı, Çevresel Titreşim Testi, Sonlu Elemanlar Yöntemi, Dinamik Karakteristikler

Master's Thesis

# SUMMARY

## NUMERICAL AND EXPERIMENTAL STUDY OF DAMAGE IDENTIFICATION USING MODAL PARTICIPATION RATIO: DETECTION, LOCALIZATION AND QUANTIFICATION OF SEVERAL DAMAGE SCENARIOS

Zafer YILMAZ

Karadeniz Technical University
The Graduate School of Natural and Applied Sciences
Civil Engineering Graduate Program
Supervisor: Assoc. Prof. Dr. Murat GÜNAYDIN
2022, 94 Pages

This thesis aims to numerically and experimentally evaluate the effectiveness of the Modal Participation Ratio method in damage identification. The numerical study of damage identification was carried out on a reinforced concrete building model. Also, numerical and experimental studies of damage identification were performed on a steel frame model under the effect of several damage scenarios. Damage detection, localization and quantification performance of the presented method was examined.

The thesis consists of five chapters. In the first chapter, the importance of damage assessment is emphasized, and the historical and technological development of damage assessment methods is given. In addition, formulas to be used in the thesis and Modal Participation Ratio calculation steps are presented. In the second chapter, case studies, results and discussions are given. In the first part, the structural changes of the numerical reinforced concrete building model due to single story damage scenarios and cumulative damage scenarios with varying damage severity levels were examined, and correlations to be used in damage identification were derived. In the second part, the effect of single story damage scenarios with different severity levels on the Modal Participation Ratio of the steel frame model is investigated to test the experimental and numerical performance of the method. In the third and fourth chapters, conclusions of the study and suggestions for future studies are presented. In the last section, the references and the resume are given.

As a result, it has been deduced that the damage identification method presented in this thesis is effective in experimental and numerical studies and can be utilized in structural health monitoring.

**Key words:** Operational Modal Analysis, Damage Detection, Modal Participation Ratio, Ambient Vibration Test, Finite Element Model, Dynamic Characteristics

## LIST OF FIGURES

**Page**

## LIST OF TABLES

**Page**

## LIST OF SYMBOLS AND ABBREVIATIONS

| | |
|---|---|
| $A_c$ | State Matrix |
| $A_k$ | $k^{th}$ Residue Matrix of the Output PSD |
| AVM | Ambient Vibration Method |
| $B_c$ | System Control Influence Coefficient |
| $c$ | Damping |
| $C_a$ | Acceleration Output Matrix |
| $C_v$ | Velocity Output Matrix |
| $C_d$ | Displacement Output Matrix |
| $C_c$ | Output Matrix |
| CNN | Convolutional Neural Networks |
| COMAC | Coordianate Modal Assurance Criterion |
| $D_c$ | Direct Transmission Matrix |
| $d_k$ | Scalar Constant |
| $DMPR$ | Modal Participation Ratio Value of Damaged State |
| DOF | Degree of Freedom |
| $E$ | Value Operator |
| EFDD | Enhanced Frequency Domain Decomposition |
| EMA | Experimental Modal Analysis |
| $F$ | Force Vector |
| $f_1$ | First Natural Frequency |
| $f_i^r$ | Frequeny Values of i-th Mode within the Filtering Range |
| FDD | Frequency Domain Decomposition |
| FE | Finite Element |
| FFT | Fast Fourier Transform |
| FRF | Frequency Response Function |
| FVM | Forced Vibration Method |

| | |
|---|---|
| $G_{xx}(j\omega)$ | PSD matrix of inputs |
| $G_{yy}(j\omega)$ | PSD matrix of responses |
| $\bar{H}(j\omega)$ | Complex Conjugate of FRF matrix |
| $H(j\omega)^T$ | Transpose of FRF matrix |
| $IMPR$ | Modal Participation Ratio Value of Initial State |
| $k$ | Stiffness |
| $m$ | Mass |
| MAC | Modal Assurance Criterion |
| MLP | Multi Layer Perception |
| MPMR | Modal Participation Mass Ratio |
| MPR | Modal Participation Ratio |
| $\mathrm{MPR}_{\mathrm{i}}^{\mathrm{j}}$ | Modal Participation Ratio of i-th mode and j-th DOF |
| MRRMS | Root Means Square of Modal Response |
| $n_d$ | Number of Measurement Points |
| $n_m$ | Number of Considered Modes |
| OMA | Operational Modal Analysis |
| PSD | Power Spectral Density |
| $R_b$ | Bandpass Filtering Value |
| $R_i$ | Difference between Adjacent Mode Values |
| $R_k$ | Residue Function |
| RC | Reinforced Concrete |
| RF | Reduction Factor |
| SHM | Structural Health Monitoring |
| SSI | Stochastic Subspace Identification |
| $Sub(\omega)$ | Set of Contrubuting Modes |
| SVD | Singular Value Decomposition |
| $T$ | Period |
| $t_k$ | Finite Series Duration |
| $u$ | Displacement |
| $\dot{u}$ | Velocity |

| | |
|---|---|
| $\ddot{u}$ | Acceleration |
| $u_k$ | Deterministic Input |
| $u^j(t)$ | Dynamic Response of j-th Measurement Point |
| $U^j(f)$ | Frequency Domain Data of j-th Measurement point |
| $U_i^j(f)$ | Frequency Domain Data of i-th mode and j-th DOF |
| $w_k, v_k$ | Noise Terms |
| $x_k$ | Discrete Fourier Transform Series |
| $x_l$ | Filtering Value |
| $x_{i(\max)}$ | Maximum Frequency Value of Interval obtained with MAC Rejection Level |
| $x_{i(\min)}$ | Minimum Frequency Value of Interval obtained with MAC Rejection Level |
| $x(t)$ | State vector |
| $y_i^j(f)$ | Modal Response of each measurement point and mode |
| $\lambda_k$ | Pole Function |
| $\phi_k$ | Mode Shape Vector |
| $\phi_n$ | Deflection Shape |
| $\omega_n$ | Natural Angular Frequency |
| $\gamma_k$ | Modal Participation Vector |
| $\gamma$ | User Defined Filtering Coefficient |
| $\delta_{pq}$ | Kronecker Delta |
| $\Delta t$ | Discrete Time Instant |
| $\Delta MPR$ | MPR Variation |
| $\Delta MPR_1^1$ | MPR Variation of i-th mode and j-th DOF |

# 1. GENERAL INFORMATION

## 1.1. Introduction

The constant progress of humanity has led people to come up with solutions to eliminate unnecessary workload and utilize engineering knowledge more in daily life problems. As these developments affect all aspects of life, civil structures which are one of the main indicators of civilization have been among the most influenced. People tend to put remarkable effort into improving and enhancing civil structures because they directly affect the functionality and comfort of everyday life. Structures have been designed and optimized to be safer, economical, more efficient, and environment friendly throughout this progress. After each step forward, engineers realize the flaws of previous designs and will continue to do so. The most notable inadequacy of structures is believed to be their safety which also has the highest rate of change and development. Many studies are carried out in both design and construction phases for safety improvements. However, there is not much development in post-construction maintenance and structural health assessment to maintain structures operational. Therefore, the post-construction maintenance and monitoring studies are of the utmost importance.

Design and construction phases are handled with care to increase structural safety, hence service life. The service life of a structure is the primary indicator of its economic feasibility and structural durability. However, post-construction maintenance is as significant as design and construction. Maintenance can be minor or major depending on its effect on service life and can be performed in many ways from facade cleaning to structural reinforcement. Structural health assessment is utilized to detect inadequacies and damages. In addition to its positive effects on service life, structural health assessment and damage identification before and after disasters such as earthquakes, tsunamis, fire, etc. play a significant role in protecting lives.

Accurate, cost-effective and quick structural assessment of structures after natural or artificial disasters has become critical. Since urbanization caused a considerable increase in the population of cities and the number of civil structures, it is vital to keep structures such as hospitals, dams, bridges, etc. operational after disasters. Therefore, various methods have been developed for structural damage assessment in hopes of preventing adverse outcomes. Just as for all the developments made by humankind, researchers pointed out the flaws of

previously developed methods of damage assessment and provided solutions by idealizing them or creating another method that can replace or assist. These damage assessment methods can be categorized by their comprehensiveness, field of application, accessibility, accuracy, etc., and can be utilized for detection, localization, and quantification of structural damage. A few of these methods are only used to detect the existence of damage, while some methods can even be used to determine the severity of damage on top of its location. Damage detection with primary methods such as visual inspections was limited to local since these methods require access to the damage location. Even if a full-scale assessment could be carried out, it would be time-consuming considering that these methods apply to small areas. From this, researchers developed fast and more reliable methods capable of performing full-scale damage assessment for complex structures by studying the changes in dynamic characteristics.

Structural Health Monitoring (SHM) is a method that has been widely used in the field of civil engineering in recent years. The method is based on the principle of monitoring, controlling and identifying damage by examining the changes in the structural behavior of engineering structures experimentally. The method is divided into two main groups based on its effect on the structure: destructive and non-destructive methods. Non-destructive methods are more preferred for experimental studies. The most widely used non-destructive experimental methods to examine changes in dynamic characteristics are Experimental Modal Analysis (EMA) and Operational Modal Analysis (OMA).

Modal testing techniques are employed to obtain dynamic characteristics such as mode frequency, mode shape and damping ratio of the structure’s current state. Based on the approach these techniques are divided into two methods namely output-only Ambient Vibration Method (AVM) known as OMA and input-output Forced Vibration Method (FVM) known as EMA. In both of these methods, repetitive and non-repetitive vibration signals coming from accelerometers that are placed on the structure are collected in the data acquisition unit and dynamic characteristics are obtained by processing these signals on up-to-date software. Since the dynamic characteristics depend on the mass and stiffness of the structure, changes in these values can be a clear indicator of possible damage.

### 1.2. Literature Review

Inadequate design or faulty analysis might cause a decrease in structural performance over time as well as poor workmanship that results in degradation of a material due to environmental exposures such as humidity and temperature. It is extremely important to determine damage in its early stages before destructive events such as earthquakes in which the dynamic performance of the structure is pushed through its limits. Additionally, quick and effective damage identification after destructive events plays a significant role in maintaining critical services such as transportation and health care operational. For these reasons, various vibration-based damage identification methods which study the dynamic behavior changes by utilizing dynamic characteristics are developed. Periodic or continuous monitoring and control of the engineering structures by using vibration-based methods developed with analytical, numerical and experimental studies presented a promising solution to damage identification. Moreover, these methods can be used to evaluate structural strengthening since dynamic characteristics are affected by any change in the structure's state.

The first developed vibration-based methods were focused on dynamic characteristics such as natural frequency, damping and mode shape. In addition to these, mode-shape curvature changes, dynamic flexibility matrix indices and many other vibration characteristic features of structures have been used for damage identification or utilized in different approaches such as model updating, machine learning and deep learning which attracted more attention with technological advancements. Analytical, numerical and experimental studies on vibration-based damage identification methods are discussed below.

Vandier (1975), carried out a study to evaluate the structural state of fixed offshore platforms by obtaining dynamic characteristics in order to ease the process of damage detection below the waterline. Natural frequencies were calculated from on-site measurements of the Buzzards Bay Tower as well as from the computer simulations of its lumped mass model. Additionally, structural members were removed from the computer model and changes in natural frequencies were examined. It is found that natural frequency variation can be used to detect damage. However, experimental studies were limited because the effect of different liquid levels in tanks located on top of the tower on the natural frequencies was not measured. Also, computer simulations were not effective to detect damage to certain members such as non-load bearing horizontal members.

Adams et. al. (1975), studied the dynamic (vibration) test data to confirm the presence of cracks generated with static and fatigue tests on carbon and glass fiber reinforced plastics. Substantial changes in longitudinal shear modulus and damping have been observed as a result of the static torsion test. In addition, permanent and progressive changes in these parameters have been found as a result of the fatigue torsion test, due to cumulative damage to the specimens. The results proved that vibration data obtained from non-destructive tests can be used for different damage scenarios.

Adams et. al. (1978), stated that determination of natural frequency presents quick detection of damage location and severity compared to other non-destructive tests such as piece-wise investigation or ultrasonic scan. The theory of the method was explained and experimental tests on one-dimensional bar elements were carried out to examine damage through natural frequency changes. According to the authors, the different contribution of localized damage in each mode due to the structure's non-uniform stress distribution presents the possibility for effective and quick detection, localization and quantification of damage.

Cawley and Adams (1979), stated that in addition to natural frequency variation, accurate dynamic analysis of the structure was required for effective detection of location and severity of the damage. The Finite Element (FE) analysis method was included in the study in order to extend the applicability of damage detection to all structures under various effects such as torsional, flexural and axial. Computer analyses were carried out and damages were simulated as stiffness reduction on different parts of an aluminum plate and a cross-ply carbon-fiber-reinforced plastic plate. Results showed that the method can be used to detect, locate and approximately quantify damage in structures.

Yuen (1985), carried out a damage detection on a cantilever beam by studying the changes in eigenparameters (eigenvalues and eigenvectors). FE model of the cantilever beam with a uniform section was studied. Eigenvalues and eigenvectors of 5 modes were calculated for 15 damage scenarios in the form of a decrease in modulus of elasticity at every 15 elements of the beam. Variations in rotation and displacement eigenparameters showed a good correlation with damage location.

Ju and Mimovich (1988), carried out an experimental study to determine fracture on beam structures by studying the changes in modal frequency. They tried an equivalent spring-loaded hinge to model the effect of a cracked section in order to demonstrate the principle of fracture diagnosis. The location of the crack, damage or slit was determined with

a small error when theoretical rigid end condition was used but theoretical predictions and experimental results showed significant errors because of differences in support conditions and crack modeling.

Wolff and Richardson (1989), studied the effect of bolt removal on structure's modal parameters on a flat plate structure with a rib stiffener. Using curve fitting of experimental Frequency Response Function (FRF) data, parameters were determined and the comparisons of mode shapes, mode frequencies and node lines were carried out. Modal Assurance Criterion (MAC) was also used to compare these values. A decrease in natural frequency values pointed out the presence of faults. However, damage location predictions via MAC were not too accurate.

Rizos et. al. (1990), studied the mode shape changes of the beam with the effect of uniformly extending transverse surface crack. Mode shapes were determined by using measured amplitudes from two points on a beam and analytical solution results. Mode shapes of 5 different damage locations with 4 different depths of cracks were examined. The method is found to be effective to determine the location and depth of the moderate cracks (more than 10% of the width). However, cracks smaller than 10% width of the beam were not detected because of low sensitivity. Also, an accuracy decrease in damage detection is expected by authors for more complex structures.

Pandey et. al. (1991), examined curvature mode shape parameters for damage localization and identification. Cantilever and simply supported beam models were analytically studied with damage modeled as the modulus of elasticity decrease. Unlike changes in displacement mode shapes, curvature mode shapes which are related to flexural stiffness of beam cross-sections showed clear changes in damage regions. However, in order to obtain curvature mode shape experimentally, multiple observations from different points are required. Therefore, the authors suggested the use of natural frequency studies to determine the presence of damage prior to localization because the presence of damage through natural frequency change can be done from a one-point measurement.

Kam and Lee (1992), presented a fault diagnosis procedure for single cracks. The accuracy of the procedure was shown on a cantilever beam model. The procedure includes the utilization of measured vibration frequencies and mode shapes for cracked element identification. Also, the strain energy equilibrium equation was created based on the conservation of energy for crack size estimation.

Srinivasan and Kot (1992), studied the dynamic characteristic changes of the thin circular cylindrical shell with the effect of a notch. FE and experimental modal analysis of the shell were carried out for initial state and after damage scenarios. Mode shapes were found to be more sensitive to the presence of cracks than modal frequencies and damping ratios. The largest change in natural frequency was found at 1 percent which meant in most cases it was less than frequency resolution. Also, damping ratios had the highest uncertainty of damage. However, it was suggested to confirm these results by analytical and FE studies on mode shape variations as well as experimental studies on the same structure with different dimensions.

Salawu and Williams (1995), performed full-scale tests on multi-span reinforced-concrete highway bridge before and after structural repairs. Accelerometers were placed on the deck and a hydraulic vibrator was utilized to apply excitation. Changes in frequency response function (FRF), modal frequencies, damping ratios, and mode shapes were studied. The MAC and coordinate modal assurance criterion (COMAC) was used to compare mode shape data. Even though changes were visible in frequency response function, a study on modal parameters was found to be necessary for better determination of damage location. There was no significant change in damping ratio and mode frequencies were decreased after repairs. On the other hand, mode shape comparison and COMAC values showed good relation for the detection of damage location. Locations of two affected points were detected but two false points were also identified and one affected point was not detected. Further investigation of the damage detection on bridge structures was suggested.

Pandey and Biswas (1994), presented a damage detection method examining the changes in the flexibility matrix which is one of the structural parameters. The effectiveness of the method on damage presence and location determination is tested with an analytical beam model and experimental data that is collected from a wide-flange steel beam. The method was highly effective for finding damage at sections with high bending moment. The effect of different support conditions was also presented in order to obtain clear patterns to be later used for damage detection of the same type of structures.

Stubbs et. al. (1995), performed a damage detection study on an I-40 bridge. First, the method was validated with the FE model of the beam. Then, in order to demonstrate the practicality of the method to localize damage in a full-scale structure, modal frequencies and mode shapes of pre-damage and post-damage states of the bridge were determined by modal

analysis. The accurate location of damage was determined by only using data from three modes.

Prime and Shevitz (1995), carried out a study to evaluate the effectiveness of damage detection with conventional mode shapes for crack formation that opens and closes during vibration. Polycarbonate beams were experimentally studied and several techniques were used for crack detection and localization. Compared to conventional mode shapes, harmonic mode shapes were found to be more sensitive to these types of cracks. It was suggested that structural nonlinearities might provide more accurate data for the identification of damage.

Nikolakopoulos et. al. (1997), proposed a new method for damage detection based on creating contours from the first two or three structural eigenfrequencies of the structure. The method provides damage detection and localization by using the value of frequency difference ratio and calculated contour plottings. It was suggested that a good estimation of crack location and depth can be performed by constructing new counter plottings for different boundary conditions.

Liew and Wang (1998), presented a method that utilizes wavelet theory for crack identification. Damage detection through eigenvalue changes and wavelet method was performed on a mathematical model of simply supported cracked beam. It was found that damage identification via the wavelet method was easier than traditional eigenvalue analysis because abrupt changes on eigenvalues were only the case for higher-order modes where results were mostly inaccurate.

Lee and Chung (2000), presented a method of crack detection which utilizes eigenfrequency test data. FE model of the beam-type structure was used to determine the first four mode frequencies which were later used in Armon's Rank-ordering method to approximately detect crack location. Then, a more appropriate FE model was created by using the results of the crack position range in order to detect crack size. Lastly, the actual crack location was determined by using the determined crack size and natural frequencies in Gudmundson's equation. Predictions for damage locations of cracks close to clamped end were not as accurate as predictions of cracks at other parts of the beam.

Razak and Choi (2001), studied the natural frequency and damping ratio changes of concrete beams affected by corrosion. Two concrete beams with moderate cracking and very slight spalling were corroded and modal tests and load tests were performed. Compared with a reference beam and a beam with moderate crack, a beam with very slight spalling had more decrease in natural frequencies and load-carrying capacity. Natural frequency changes of the

first seven modes and damping ratio changes for the first three modes were examined. Decrease in natural frequency of beams with very slight spalling and moderate crack, varied from 4% to 11% and 1% to 4%, respectively. The decreases in load-carrying capacity of beams with very slight spalling and moderate cracking were 57% and 34%, respectively. Damping ratio changes of the first mode were inconsistent. However, damping ratios of second and third modes reflected a consistent trend with severity increase.

Ovanesova and Suarez (2004), presented a wavelet-based method for damage detection by performing several numerical analyses to detect cracks in frame structures. Numerical studies showed that the method was capable of obtaining damage information only by using the damaged response of the structure but response needed to be collected from possible damage locations for robust and reliable results. It was suggested to develop a rigorous method for the selection of optimum wavelet as well as studying different damage scenarios on different structures.

Pawar et. al. (2007), proposed a method of damage detection created with the integration of Spatial Fourier Analysis and Artificial Neural Networks. Fourier coefficients of the mode shapes derived from mode shapes of the FE model by using spatial Fourier series were found to be sensitive to both damage size and location. A damage index was formulated and employed in a neural network which was trained to detect damage. The trained and developed neural network was successful at finding damage location and size. The method was proved to be effective for automated damage detection.

Mehrjoo et. al. (2008), presented a method of damage intensity estimation for truss bridge structures by using a back-propagation-based neural network. Multi-Layer Perceptron (MLP) which is the most commonly used neural network for structural identification problems is utilized. The natural frequencies and mode shapes derived from numerical models of a simple truss and the Louisville Bridge truss were employed in the neural network. It was found that the location and severity of damages in truss bridge joints were predicted with high accuracy. Also, MLP network architecture was found to be effective for damage location and severity determination.

Curadelli et. al. (2008), stated that damping was ignored in damage detection methods because of its high sensitivity to damage it was hard to correlate damping and damage. However, methods utilizing natural frequency and mode shape values were limited because of their low sensitivity to relatively small damages. Therefore, a technique to monitor instantaneous changes in damping coefficient by using wavelet transform was performed. It

was seen from experimental results and numerical simulations that wavelet transform can be used to assess changes in vibration characteristics.

Radizenski et. al. (2011), developed a new damage indicator that utilizes experimentally measured changes in natural frequencies and mode shapes. In addition to this indicator, the method required a baseline model created with numerical simulations. Damage detection on beam-like structures with different fatigue damages was carried out for commonly used modal parameters and newly developed indicators. The proposed method showed consistency with experimental data and was effective for damage localization.

Altunisik et. al. (2017), presented a study on damage detection of multiple cracks on a cantilever beam. The vibration characteristics of the model were determined by using experimental measurements and an updated FE model. Changes in natural frequencies and mode shapes were examined as well as MAC and COMAC factors obtained from mode shapes. Natural frequency changes showed a non-monotonical decrease with increasing crack patterns. It is also found that MAC factors were effective for damage localization. It was suggested to carefully idealize boundary conditions in model updating.

Yu et. al. (2018), proposed a novel method of damage detection based on convolutional neural networks (CNN) for structures equipped with smart control devices. The proposed method offered a more reliable and faster identification of damage with automatic feature extraction and optimal combination selection via a multi-layer fusion. CNN designed and trained for localization and quantification of structural damage was evaluated for five-story laboratory benchmark models subjected to seismic loading.

Khodabandehlou et. al. (2018), presented an approach that utilizes two-dimensional deep CNN for vibration-based SHM. 48 vibration response data sets of a one-fourth-scale model of a reinforced concrete highway bridge were recorded and studied to validate the proposed method. The method was able to predict damage with 100% accuracy. It was found that if accurate network training is carried out, the CNN-based SHM method is scalable to many damage conditions. Moreover, the data required for training could be generated by non-linear FE models. Although obtaining such data takes a considerable amount of time, it offers fast and robust damage identification once the data is ready to use.

Park and Oh (2018), developed a damage detection method where the Modal Participation Ratio (MPR) representing the participation of each mode and each measurement point or degree of freedom (DOF) to the modal behavior of the structure was

examined. Variations of MPR values under the effect of story stiffness reduction were used as indicators of damage. The main focus of the study was on the MPR values of the first mode where damage localization and severity determination was more practical and easier because of the simple correlation between MPR and damage. Lumped mass models with four, eight and twelve DOFs were used to validate obtained correlations. Among the first modes of MPR values, the MPR value of damaged DOF increased the most which was a clear indicator of damage localization. Increasing the severity of damage resulted in bigger changes in all MPR values whether it was an increase or a decrease in the ratio.

Park et al. (2019), studied the applicability of MPR in model updating procedure by creating a baseline model. 4 DOFs lumped mass model was used to obtain a correlation of damage location and severity with MPR value variation. The first mode MPR values of different story damage scenarios were calculated and used to form a fifth-degree polynomial severity function.

Mehboob et al. (2020), proposed a method combining the eigenvalues and modal contributions for each mode to create an index value which was found to be more feasible for damage detection in beams. Numerical models of the simply supported beam were damaged with element stiffness reduction at mid-span and near support. Indexes created for MPR, frequency and mode shape changes were examined. MPR index showed high sensitivity to damage, outperforming traditional natural frequency and mode shape change damage detection methods.

### 1.3. Research Objective

Damage identification has been studied by many researchers over the past 50 years. Because of the limitations of previously developed methods, new approaches and methods were developed. In order to perform full-scale, fast and more reliable damage assessment for complex structures, methods employing dynamic characteristics were studied extensively. Analytical, numerical and experimental models were used to develop and validate many methods. Identifying damage through changes in frequency response function and modal parameters such as natural frequency, mode shape and damping ratio were the first developed vibration-based methods. In addition to these conventional methods, mode-shape curvature, flexibility matrix indices, and many other vibration characteristic features of structures have been used for damage identification or utilized in different approaches

such as model updating, machine learning and deep learning which attracted more attention with technological advancements.

This study aims to contribute to the literature by experimentally and numerically validating the utilization of MPR values in damage identification. To achieve this aim, numerical studies on a four-story reinforced concrete (RC) building model, four-bay in the transverse direction, four-bay in the longitudinal direction was carried out as well as experimental and numerical studies on 4 story steel frame.

### 1.4. Dynamic Characterization

The dynamic characteristics such as mode shapes, mode frequencies and damping ratios can be determined using numerical modal analysis or by modal responses through dynamic response measurements. Modal response of a structure gives an insight into the structure's condition and its possible behavior under different types of vibrations encountered during its service time such as an earthquake. Since modal response requires measurements of the dynamic responses of the structures, the vibrations resulting from ambient or forced excitations need to be collected. The ambient excitations are mostly caused by wind, vehicles, pedestrians and earthquakes, etc. and the forced excitations are artificially generated by shakers, impact hammers, etc. (Trifunac, 1972). Displacement, velocity, and acceleration values measured from the structure as a response to these excitations are referred to as dynamic responses. The experimental modal responses can be obtained by using modal testing techniques. However, additional vibrations are required to simulate the ambient excitations for the numerical modal response. Additionally, dynamic response data can be used to determine the modal response of any type of structure.

#### 1.4.1. Numerical Methods

Dynamic characteristics of a numerical model can be determined by performing modal analysis as well as by using dynamic responses obtained from the transient analysis.

#### 1.4.1.1. Modal Analysis

The modal analysis utilizes the equation of motion for the characterization of structures. Equation of motion is given in Equation 1 where m, c and k denote mass, damping and stiffness matrices, respectively. Also, $\ddot{u}$, $\dot{u}$, u and F denote acceleration, velocity, displacement and force, respectively.

$$m\ddot{u} + c\dot{u} + ku = F \tag{1}$$

An undamped free vibration equation can be employed to calculate dynamic characteristics such as natural frequency and mode shape. Free vibration means that the structure is not affected by external forces and is in an ambient vibration state (Equation 2).

$$m\ddot{u} + ku = 0 \tag{2}$$

Mathematical description of a free vibration undamped system can be shown as in Equation 3 where deflection shape ($\phi_n$) is not time-dependent. (Chopra, 2011)

$$u(t) = q_n(t)\,\phi_n \tag{3}$$

Free vibration is known as simple harmonic motion. Therefore, the simple harmonic function given in Equation 4 is used for time-dependent displacement values of this harmonic motion.

$$q_n(t) = A_n \cos \omega_n t + B_n \sin \omega_n t \tag{4}$$

The constant values A and B are determined by initial conditions (t=0). Combining Equations 3 and 4:

$$u(t) = \phi_n \left( A_n \cos \omega_n t + B_n \sin \omega_n t \right) \tag{5}$$

is obtained. Substituting Equation 5 in Equation 1, Equation 6 is derived.

$$q_n(t)\left[k\phi_n - \omega_n^2 m \phi_n\right] = 0 \tag{6}$$

In order to obtain non-zero solutions for $\phi_n$ and $\omega_n$, the case with $q_n(t) = 0$ is ignored which also meant that the displacement value was zero at all times. In order to calculate the values of $\phi_n$ and $\omega_n$, the square bracket is assumed to be zero. The content of the square bracket in Equation 6 can be simplified as presented in Equation 7.

$$\{\phi_n\}\left(k - \omega_n{}^2 m\right) = 0 \tag{7}$$

Equation 7 gives a trivial solution when $\phi_n = 0$. Therefore, the determinant of the value inside the parenthesis needs to be taken as shown in Equation 8 which is also known as the characteristic equation.

$$\det\left|k - \omega^2 m\right| = 0 \tag{8}$$

By putting known parameters in Equation 8, angular frequencies ($(\omega_1, \omega_2, .....\omega_n)$ as many as the number of DOFs (n) are obtained. Then using Equation 9,

$$T = \frac{2\pi}{\omega} \tag{9}$$

natural periods are obtained. Finally, by taking the inverse of natural periods, the natural frequencies are calculated (Equation 10).

$$f = \frac{1}{T} \tag{10}$$

The smallest natural frequency ( $f$ ) is considered the first mode frequency and the mode shape of that same frequency is named the first mode shape.

### 1.4.1.2. Transient Analysis

One of the ways to obtain dynamic characteristics is through signal processing of transient analysis result data. Artificial vibrations are applied to the numerical model in order to create vibrations. Then, the dynamic responses of the building to these excitations are collected. There are several techniques in both the time domain and frequency domain to determine dynamic characteristics through dynamic responses. Time domain methods are less user-friendly because of their long processing time for parameter estimation. Therefore, in the scope of this thesis, frequency domain methods were employed for determining dynamic characteristics through transient analysis. Fast Fourier Transform (FFT) is employed to transform data into the frequency domain. Figure 1 shows time domain data and logarithmic frequency domain data obtained using the FFT. The data in the frequency domain can be used to determine the natural frequencies and mode shapes of the structure. Ambient excitations can be simulated with white noise acceleration. The time-step and total length of the white noise acceleration are significant for the accurate modal response. The time-step value and duration of white noise acceleration need to be determined by foreseeing the highest possible frequency value to be considered based on the studied structure (Heylen et. al., 1997).

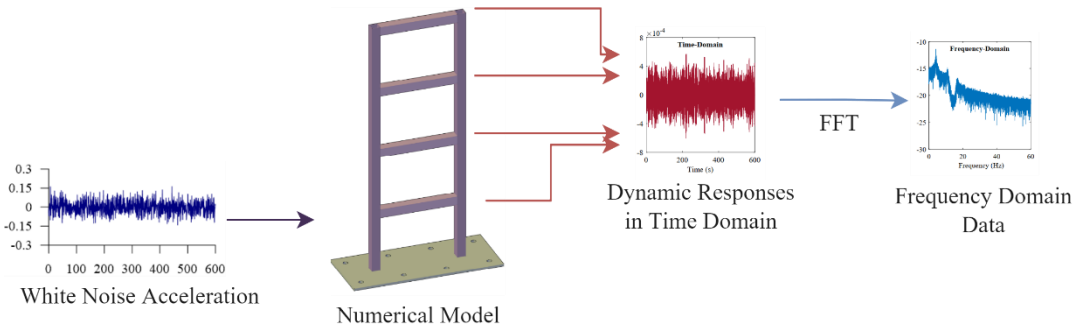


Figure 1. Flow chart of dynamic characterization through transient analysis

### 1.4.2. Experimental Methods

#### 1.4.2.1. Modal Testing

EMA and OMA are vibration-based non-destructive structural health monitoring methods that have been widely used in the field of civil engineering in recent years. These methods are utilized to obtain dynamic characteristics such as frequency, mode shape and damping ratio of the structure's current condition. OMA and EMA are also known as output-only AVM and input-output FVM, respectively. Within the scope of these methods, sensitive accelerometers are placed on the structure considering the geometry and degrees of freedom of the model. Then, vibration signals from accelerometers are stored in the data acquisition unit and dynamic characteristics are obtained by using stored data in up-to-date software.

#### 1.4.2.2. Modal Testing Equipments

##### 1.4.2.2.1. Accelerometers

One of the most fundamental components of modal testing is accelerometers that measure vibrations of the structure they are on. Piezoelectric accelerometers are one of the most commonly used types for measuring structural vibrations. As seen in Figure 2, these accelerometer types consist of a spring-mass-damper system (Ramos, 2007). The piezoelectric element is made of materials such as quartz or ceramic crystals that produce an electric charge at the level of picocoulomb (1E-12 ampere second) under force. When the accelerometer is subjected to vibration, the seismic mass inside the accelerometer attempts to maintain its initial position. The force created by the inertia of this seismic mass causes piezoelectric material to compress and stretch. Therefore, the change of electric charge on the crystal due to acting forces is directly proportional to the change in acceleration. There is a signal conditioning circuit inside the accelerometer body which converts the electrical signal to a portable voltage signal. Then, these signals are simultaneously transferred to the data collection unit with suitable cables (Altunışık, 2010; Sevim, 2010).

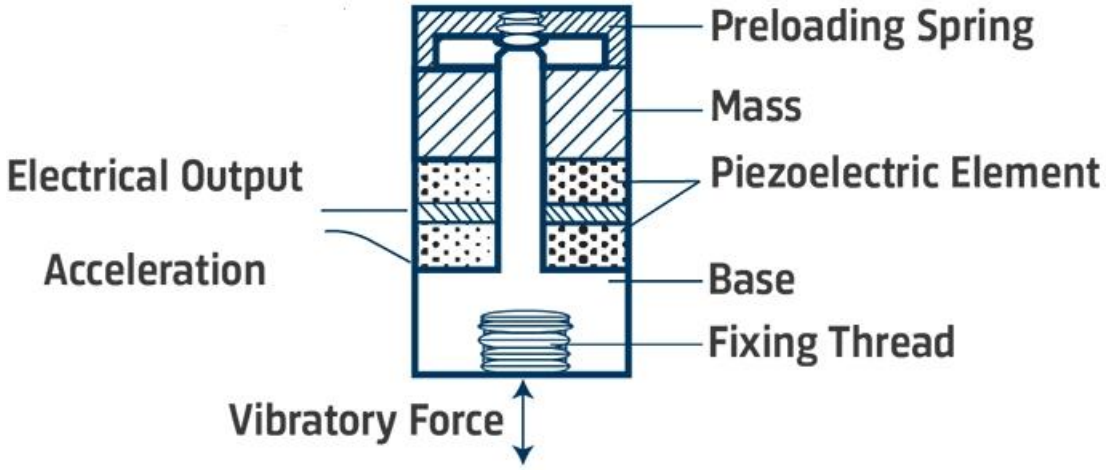


Figure 2. Piezoelectric accelerometer configuration (URL-1).

The selection of an accelerometer has a critical effect on the precision of the results. It is not possible to obtain high-quality signals from the experimental measurements performed with accelerometers that are picked carelessly. Based on the examined structure type and the objective of the study, accelerometer features such as the number of axes, sensitivity and frequency range (bandwidth) should be carefully determined. Based on these parameters, a suitable type of accelerometer needs to be selected. Accelerometer features are briefly described below.

- Frequency Range: Indicates the maximum and minimum frequency range the accelerometer can measure.
- Sensitivity: Specifies the electrical power that the accelerometer can produce proportional to the acceleration.
- Measurement Range: Indicates the maximum acceleration amplitude value that the accelerometer can measure without the electrical signal being distorted or lost.
- Temperature Range: Indicates the maximum and minimum ambient temperature at which the accelerometer can generate a healthy signal.

Within the scope of the thesis, B&K 4507 B 005 type uniaxial accelerometers were used in the experimental measurements (Figure 3). The general features of this accelerometer are listed in Table 1.

Figure 3. Uniaxial B&K 4507 B 005 accelerometer

Table 1. Specifications of uniaxial B&K 4507 B 005 accelerometer (URL-2)

| **Model** | **B&K 4507 B 005** |
|---|---|
| Sensitivity | 1 V/g |
| Frequency Range | 0.4 - 6000 Hz |
| Measurement Range | ±7 g |
| Temperature Range | -54 Cº to +100 Cº |
| Dimensions | 10 x 10 x 10 mm |
| Total Mass | 4.6 grams |

#### 1.4.2.2.2. Data Acquisition Systems

The data collection system consists of a data acquisition unit and systems to transfer data to/from the acquisition unit. Signals from the accelerometers are transmitted from the accelerometers to the data acquisition system via cables. In this data, there are repetitive and non-repetitive vibrations. In order to determine the dynamic characteristics of the structure, these raw data need to be filtered. This step is handled by signal conditioning in the data acquisition system. This step is usually carried out to improve the quality of a low-level signal, reduce the effect of noise signals, filter the unwanted signals, adjust the electrical power and control the behavior of the accelerometers if necessary (Altunışık, 2010; Sevim, 2010). Signal conditioning is critical for filtering unwanted signals, which are high-frequency signals outside the selected frequency measuring range. Then, the processed data is transmitted to the computer via cables for further investigations.

B&K 3053-B-120 type 12-channel input module was used for the experimental measurements carried out within the scope of the study (Figure 4). The data acquisition unit also offers an option to make several sets of measurements with at least one reference measurement.


Figure 4. B&K 3053-B-120 type 12-channel data acquisition module (URL-3).

#### 1.4.2.2.3. Signal Processing Systems

After the completion of signal conditioning in the data acquisition unit, the recorded signals must be processed to be used in the dynamic characterization of the structure. Signal processing is carried out with special software. The signals transferred to the computer are in the time domain. However, for practical reasons, the frequency domain is preferred. Fourier series can be employed to transform the signals from the time domain to the frequency domain. A periodic signal $x(t)$ with a period $T$ can be presented in an infinite series as such (Ramos, 2007):

$$x(t) = \frac{a_0}{2} + \sum_{n=1}^{\infty}\left[ a_n \cos\left(\frac{2\pi n}{T} t\right) + b_n \sin\left(\frac{2\pi n}{T} t\right)\right] \tag{11}$$

where $a_0$, $a_n$ and $b_n$ are:

$$a_0 = \frac{2}{T}\int_0^T x(t)\,dt$$
$$a_n = \frac{2}{T}\int_0^T x(t)\cos\left(\frac{2\pi n}{T}t\right)dt \quad (12)$$
$$b_n = \frac{2}{T}\int_0^T x(t)\,\sin\left(\frac{2\pi n}{T}t\right)dt$$

Discrete Fourier Transform series ($x_k$) can be obtained as Equation 13 by discretization of signal with finite series duration. The finite series duration ($t_k$) is $N$ samples of particular values of the time ($t_k$, $k = 1, 2, 3.....N$).

$$x_k = x(t_k) = \frac{a_0}{2} + \sum_{n=1}^{N/2}\left[a_n \cos\left(\frac{2\pi k}{T}t\right) + b_n \sin\left(\frac{2\pi k}{T}t\right)\right] \;,\; k = 1, 2, 3....N \quad (13)$$

Thus, new $a_0$, $a_n$ and $b_n$ values are:

$$a_0 = \frac{2}{N}$$
$$a_n = \frac{1}{N}\sum_{k=1}^{N} x_k \cos\left(\frac{2\pi nk}{N}\right) \quad (14)$$
$$b_n = \frac{1}{N}\sum_{k=1}^{N} x_k \,\sin\left(\frac{2\pi nk}{N}\right)$$

FFT method presented by Cooley and Tukey (1965) which is significantly faster in terms of the computational process can also be employed. However, since this method requires calculations in the frequency domain, a finite duration of time history needs to be considered which might result in leakage error. The leakage error occurs when the sampling time is not multiple integers of the signal period. In order to solve the leakage problem, the sampling duration can be extended. Additively, windowing in the time domain or filtering in the frequency domain can be used for rescaling.

In this thesis, BK Connect (BK Connect, 2021) software was utilized to introduce the accelerometers to the data acquisition unit, store the signals coming from accelerometers to the data acquisition unit, and transfer the stored signals to the signal processing software.

PULSE Operational Modal Analysis (PULSE, 2021) and Matlab (MATLAB, 2018) software were used to process the recorded signals for the dynamic characterization of structures.

#### 1.4.2.2.4. Excitation Sources

Modal testing techniques make use of vibrations acting on structures. Sources of these vibrations can be environmental or artificial effects. Environmental vibrations are ambient vibrations that do not require any external forces to make the structure vibrate. Noise, wind, earthquakes and traffic are some examples of ambient vibrations. Artificial vibrations, on the other hand, are forced vibrations that require external forces such as a shaker, impact hammer and drop weight system.

Shakers are used in many industries such as automotive, shipbuilding and aerospace to create vibrations with their large force output. Some of the shaker types used in these industries are mechanical, electro-hydraulic and electro-magnetic, which can generate vibrations at the desired level. Since it causes large forces acting on the structure, they need to be fully fixed. Multiple shakers can be employed for large-scale structures, but this would increase the overall cost of measurement. Taking characteristics of the structure into account appropriate shaker(s) need to be selected. Otherwise, it might seriously damage the structure and the device (Okur, 2017).

Impact hammers are often used to vibrate light and medium-sized engineering structures or laboratory models. The main feature of impact hammers is that the tip is replaceable. Replaceable tip offers rubber heads with different hardness (soft, medium, tough and hard) and sensors for impact force measurement. The amplitude of the vibrations given to the structure by the hammer can be measured with the force gauge at the hammer's head. The impact given by the hammer is related to the mass of the head, velocity of the impact and the spectral impact energy depending on the selected tip. So in order to obtain desired force, the tip hardness and the impact velocity can be adjusted. B&K Impact hammer 8210 and the force spectra of different tips are shown in Figure 5.

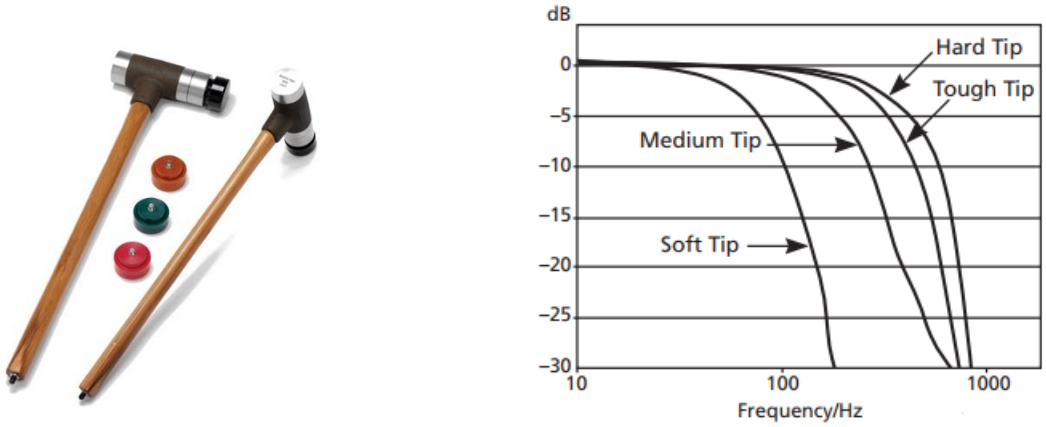


(a) (b)

Figure 5. (a) B&K impact hammer 8210 and (b) the force spectra of different tips (URL-4).

Drop weight systems are utilized to create larger forces than the impact hammer and to have a more controllable impact by adjusting weight and height. (Ramos, 2007)

Within the scope of this thesis, experimental measurements are carried out with ambient vibrations.

#### 1.4.2.3. Modal Testing Techniques

##### 1.4.2.3.1. Ambient Vibration Methods

In this modal testing technique, the structural response to ambient effects is measured and employed in dynamic characterization. Since the excitations cannot be measured and the response function of the input forces cannot be determined, the ambient vibration technique is referred OMA or Output-Only Modal Identification Technique (Brincker et al., 2000). The dynamic characteristics of the structure are determined by using algorithms in the frequency or time domain because the amplitude of the vibrations acting on the structure and their variation with time are unknown.

Depending on the domain type, developed methods can be categorized into two main groups: time domain methods and frequency domain methods. Some of the OMA methods, categorized by their domain of study are given in Table 2. (Ghalishooyan et. al., 2019)

Table 2. OMA algorithms

| **Time Domain** | **Frequency Domain** |
|---|---|
| Natural Excitation Technique (NExT) | Peak Picking (PP) |
| Least Square Complex Estimation (LSCE) | Frequency Domain Decomposition (FDD) |
| Random Decrement (RD) | Enhanced FDD (EFDD) |
| Auto-regressive Moving Average (ARMA) | Least Squares Complex Frequency (LSCF) |
| Stochastic Subspace Identification (SSI) | Polimax |
| Blind Source Seperation (BSS) | Curve Fittting FDD (CFDD) |

In the scope of this thesis, the Enhanced Frequency Domain Decomposition (EFDD) Method and the Stochastic Subfield Identification (SSI) Method are used to obtain the dynamic characteristics. The flow chart of the dynamic characterization through experimental methods is shown in Figure 6.

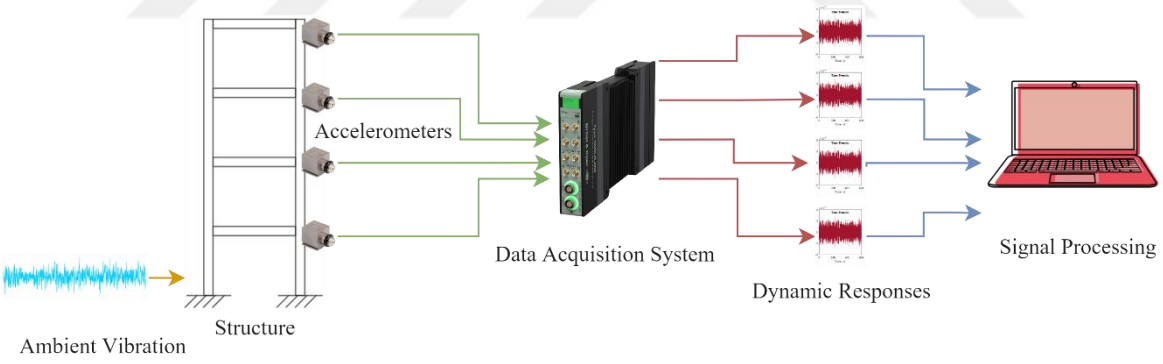


Figure 6. Flow chart of dynamic characterization through AVM

#### 1.4.2.3.1.1. Enhanced Frequency Domain Decomposition

EFDD method is a more developed version of the easy-to-use Frequency Domain Decomposition (FDD) method. FDD method was presented by Brincker et al. (2000) to replace Peak Picking Method which was only effective for well-separated vibrational modes and low damping ratios. In order to determine the natural frequency, the Singular Value Decomposition (SVD) of the response spectral density matrix is initially performed. Then,

a set of auto spectral density functions each representing a single DOF system is obtained. By selecting the peaks in the SVD graphs each representing a different SDOF system, natural frequency and the mode shapes are determined. Since the FDD method is based on the use of a single frequency line from the FFT analysis, the resolution of the FFT is the determinant of an estimated natural frequency precision (Jacobsen et al., 2006).

Brincker et. al. (2001), developed the EFDD algorithm to detect natural frequencies, mode shapes and damping ratios with better precision than FDD. In EFDD, the estimation method for the determination of natural frequencies and damping ratios are different from the FDD. The steps until the estimation of modal parameters for both FDD and EFDD are given below.

As shown in Equation 15, for $r$ number of inputs and $m$ number of responses, $m \times m$ Power Spectral Density (PSD) matrix of the responses $G_{yy}(j\omega)$, $r \times r$ PSD matrix of the inputs $G_{xx}(j\omega)$, complex conjugate and transpose of $m \times r$ FRF matrix ($\bar{H}(j\omega)$ and $H(j\omega)^T$) are used to express the relationship between unknown input $x(t)$ and measured output $y(t)$ in frequency domain (Bendat and Piersol, 2004; Brincker, 2000).

$$G_{yy}(j\omega) = \bar{H}(j\omega) * G_{xx}(j\omega) * H(j\omega)^T \tag{15}$$

The FRF can be written in partial fraction as shown in Equation 16 where $\lambda_k$, $R_k$ and $n$ represent the pole, residue and number of modes, respectively.

$$H(j\omega) = \sum_{k=1}^{n} \frac{R_k}{j\omega - \lambda_k} + \frac{\bar{R}_k}{j\omega - \bar{\lambda}_k} \tag{16}$$

The residue is the multiplication of mode shape vector $\phi_k$ and the transpose of modal participation vector $\gamma_k^T$ (Equation 17).

$$R_k = \phi_k \, \gamma_k^T \tag{17}$$

Supposing that the input has constant matrix PSD such as white noise, Equation 15 can be rewritten as Equation 18 where superscript $H$ represents complex conjugate and transpose.

$$G_{yy}(j\omega) = \sum_{k=1}^{n}\sum_{s=1}^{n}\left[\frac{R_k}{j\omega-\lambda_k}+\frac{\bar{R}_k}{j\omega-\bar{\lambda}_k}\right]G_{xx}(j\omega)\left[\frac{R_s}{j\omega-\lambda_s}+\frac{\bar{R}_s}{j\omega-\bar{\lambda}_s}\right]^H \tag{18}$$

Output PSD can be rewritten in pole/residue form as shown in Equation 19 after some simplifications, multiplying the two partial fractions and using Heaviside partial theorem.

$$G_{yy}(j\omega) = \sum_{k=1}^{n}\frac{A_k}{j\omega-\lambda_k}+\frac{\bar{A}_k}{j\omega-\bar{\lambda}_k}+\frac{B_k}{-j\omega-\lambda_k}+\frac{\bar{B}_k}{-j\omega-\bar{\lambda}_k} \tag{19}$$

$A_k$ is the $k$ th residue matrix of the output PSD and can be calculated using Equation 20 where $C$ denotes $G_{xx}(j\omega)$.

$$A_k = R_k C\sum_{s=1}^{n}\frac{\bar{R}_k^T}{-\lambda_k-\bar{\lambda}_s}+\frac{R_k^T}{-\lambda_k-\lambda_s} \tag{20}$$

The contribution of $k$ th mode to the residue is shown in Equation 21 where $\alpha_k$ is minus the real part of the pole ($\lambda_k = -\alpha_k + j\omega_k$).

$$A_k = \frac{R_k C\bar{R}_k^T}{2\alpha_k} \tag{21}$$

When the damping is light, the term gets dominating, and the residue becomes proportional to the mode shape vector as shown in Equation 22 where $d_k$ is scalar constant.

$$A_k = R_k C\bar{R}_k^{\,T} = \phi_k\,\gamma_k^T\,C\,\gamma_k\,\phi_k^T = d_k\,\phi_k\,\phi_k^T \tag{22}$$

Only a few modes contribute significantly at a certain frequency value $\omega$. For the case of light damping, response spectral density can be expressed as Equation 23 where $Sub(\omega)$ represents the set of modes that contribute.

$$G_{yy}(j\omega) = \sum_{k \in Sub(\omega)} \frac{d_k \phi_k \phi_k^T}{j\omega - \lambda_k} + \frac{\bar{d}_k \bar{\phi}_k \bar{\phi}_k^T}{j\omega - \bar{\lambda}_k} \tag{23}$$

Estimation of modal parameters with EFDD is different from FDD. After the power spectral density matrix of the system response is calculated and SVD analysis on the response is performed, Inverse Discrete Fourier Transform is utilized to transform the Power Spectral Density function identified around a peak of resonance back to the time domain. The outcome of this transformation is a typical response of SDOF namely the auto-correlation response function. Here, the natural frequency is estimated by the number of zero-crossings. And the damping is estimated by logarithmic decrement of the function. (Jacobsen et. al. 2006; Gade et. al. 2006)

#### 1.4.2.3.1.2. Stochastic Subspace Identification

Methods that work directly with time data (i.e. methods that do not need to convert time data to correlations or spectra) are called time-domain methods. They offer modal parameter estimation with high-quality resolution. However, compare to frequency domain methods such as FDD, they are less user-friendly because of the long processing time required for parameter estimation (Ramos, 2007). SSI is an output-only time-domain method that is very applicable for operational modal parameter identification.

General details of the SSI method are presented below. The linear second-order differential equation shown below can be used to express the dynamic behavior of a vibrating structure (Equation 24).

$$M\ddot{U}(t) + C_2\dot{U}(t) + KU(t) = F(t) = B_2u(t) \tag{24}$$

Mass, damping and stiffness matrices of the structure are denoted with $M$, $C_2$ and $K$, respectively. Excitation force $F(t)$ and displacement vector $U(t)$ are at a continuous-time.

After factorization of the force vector $F(t)$ , $B_2$ matrix is obtained which describes inputs in space and a vector $u(t)$ (Yu and Ren, 2005; Peeters and De Roeck, 1999; Okur, 2017).

By using the state vector $x(t)$, the state matrix $A_c$ and the system control influence coefficent matrix $B_c$ as expressed in Equation 25:

$$\begin{aligned} x(t) &= \begin{pmatrix} U(t) \\ \dot{U}(t) \end{pmatrix} \\ A_c &= \begin{pmatrix} 0 & I \\ -M^{-1}K & -M^{-1}C_2 \end{pmatrix} \\ B_c &= \begin{pmatrix} 0 \\ M^{-1}B_2 \end{pmatrix} \end{aligned} \tag{25}$$

Equation 24 can be rewritten as a state equation shown in Equation 26. The amount of independent variables required to describe the state of the system is equal to the number of elements of the state-space vector.

$$\dot{x}(t) = A_c x(t) + B_c u(t) \tag{26}$$

Monitoring all DOFs are unpractical. Therefore in the case of measurements at $l$ numbers of DOFs, whether it is carried out by accelerometers, velocity or displacement transducers, the observation equation is:

$$y(t) = C_a \ddot{U}(t) + C_v \dot{U}(t) + C_d U(t) \tag{27}$$

where output $y(t)$ is $l \times 1$ vector. And $C_a$, $C_v$ and $C_d$ are output matrices for acceleration, velocity and displacement, respectively. Using definitions of output matrix $C_c$ and direct transmission matrix $D_c$ as shown in Equation 28:

$$\begin{aligned} C_c &= [C_d - C_a M^{-1}K \quad C_v - C_a M^{-1}C_2] \\ D_c &= C_a M^{-1}B_2 \end{aligned} \tag{28}$$

Equation 27 can be transformed into Equation 29 (Yu and Ren, 2005).

$$y(t) = C_c x(t) + D_c u(t) \tag{29}$$

The continuous-time state-space model of a vibrating system can be constituted with Equations 26 and 29. Here, continuous-time means that these expressions can be evaluated at each time instant. However, in practice, measurements are available only at discrete time instants $\Delta t$. After sampling, conversion of the continuous-time state-space model to the discrete-time state-space model takes place. Discrete time state-space model is shown in Equation 30 where $x_k = x(k\Delta t)$ is the discrete-time state vector containing the sampled displacements and velocities. Also, $u_k$ and $y_k$ are sampled input and output. Moreover, $A = \exp(A_c \Delta t)$, $B = [A - I]A_c^{-1}B_c$, $C$ and $D$ are discrete state, discrete input, discrete output and direct transmission matrices, respectively (Yu and Ren, 2005).

$$\begin{aligned} x_{k+1} &= Ax_k + Bu_k \\ y_k &= Cx_k + Du_k \end{aligned} \tag{30}$$

In practice, there are system uncertainties such as process noise caused by modeling inaccuracies and measurement noise resulting from sensor inaccuracies. Therefore, process noise $w_k$ and measurement noise $v_k$ are added to Equation 30 to create a discrete-time combined deterministic-stochastic state-space model given in Equation 31.

$$\begin{aligned} x_{k+1} &= Ax_k + Bu_k + w_k \\ y_k &= Cx_k + Du_k + v_k \end{aligned} \tag{31}$$

Both components are unmeasurable vector signals. Therefore, they are assumed to be zero-mean, white and with covariance matrices:

$$E\left[\begin{pmatrix} w_p \\ v_p \end{pmatrix} \begin{pmatrix} w_q^T & v_q^T \end{pmatrix}\right] = \begin{pmatrix} Q & S \\ S^T & R \end{pmatrix}\delta_{pq} \tag{32}$$

where $E$ and $\delta_{pq}$ are the expected value operator and the Kronecker delta. The Kronecker delta is a function of two variables shown in Equation 33.

$$\delta_{pq} = \begin{cases} 1, \text{ if } p = q \\ 0, \text{ if } p \neq q \end{cases} \tag{33}$$

Since the vibration data obtained from structural health monitoring are responses of the structure and there is no information about the operational input vibrations, it is impossible to distinguish deterministic input $u_k$ shown in Equation 30. Consequently, noise terms ($w_k$ and $v_k$) are used to model deterministic input. Thus, the discrete-time purely stochastic state-space model of a vibrating structure is obtained as shown in Equation 34.

$$\begin{aligned} x_{k+1} &= Ax_k + w_k \\ y_k &= Cx_k + v_k \end{aligned} \tag{34}$$

Equation 34, forms the basis of the time domain dynamic characteristics determination from ambient vibrations (Okur, 2017; Gunaydin, 2016).

#### 1.4.2.3.2. Forced Vibration Methods

FVM is one of the most widely used methods to determine the dynamic characteristics of structures, namely the natural frequency, mode shape and damping ratios. Unlike AVM, the structure is excited with known and measurable force, and the structural response to this effect is measured. These forced vibrations are generally produced using electrodynamic shakers, shaking tables and impact hammers. Figure 7 illustrates the process of dynamic characterization with FVM. In FVM, both the artificial force signal and the response of the structure to this effect are measured. Vibration data are collected employing accelerometers and stored in a data acquisition system. Then, signals are processed in signal analyzers. The obtained signals can be used in various numerical techniques to determine the natural frequencies, mode shapes and damping ratios of the measured structure.

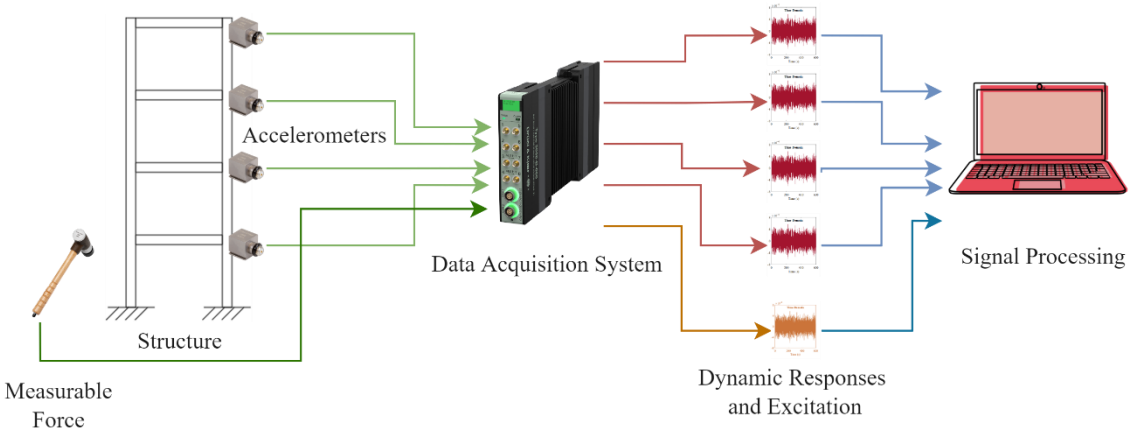


Figure 7. Flow chart of dynamic characterization through FVM

### 1.5. Modal Participation Ratio Methodology

The methodology used for MPR variation through transient analysis is presented below. The only difference between transient analysis and modal testing techniques is that the transient analysis requires input force to simulate ambient vibration conditions. Therefore, this methodology applies to both dynamic characteristic determination techniques.

#### 1.5.1. Fast Fourier Transform

Vibration characteristic in this presented damage identification method represents not only the contribution of mode but also the contribution of measurement points or degrees of freedoms included with modes as distinct from modal participation mass ratio. It creates an opportunity to detect the structural damage between measurement points or DOFs. However, the filtering procedure should be employed in the FFT procedure to separate the effect of each measurement point to each mode and determine the MPR values.

The graphs of applied white noise acceleration and dynamic responses of the structure resulting from white noise excitation are given in Figure 8.

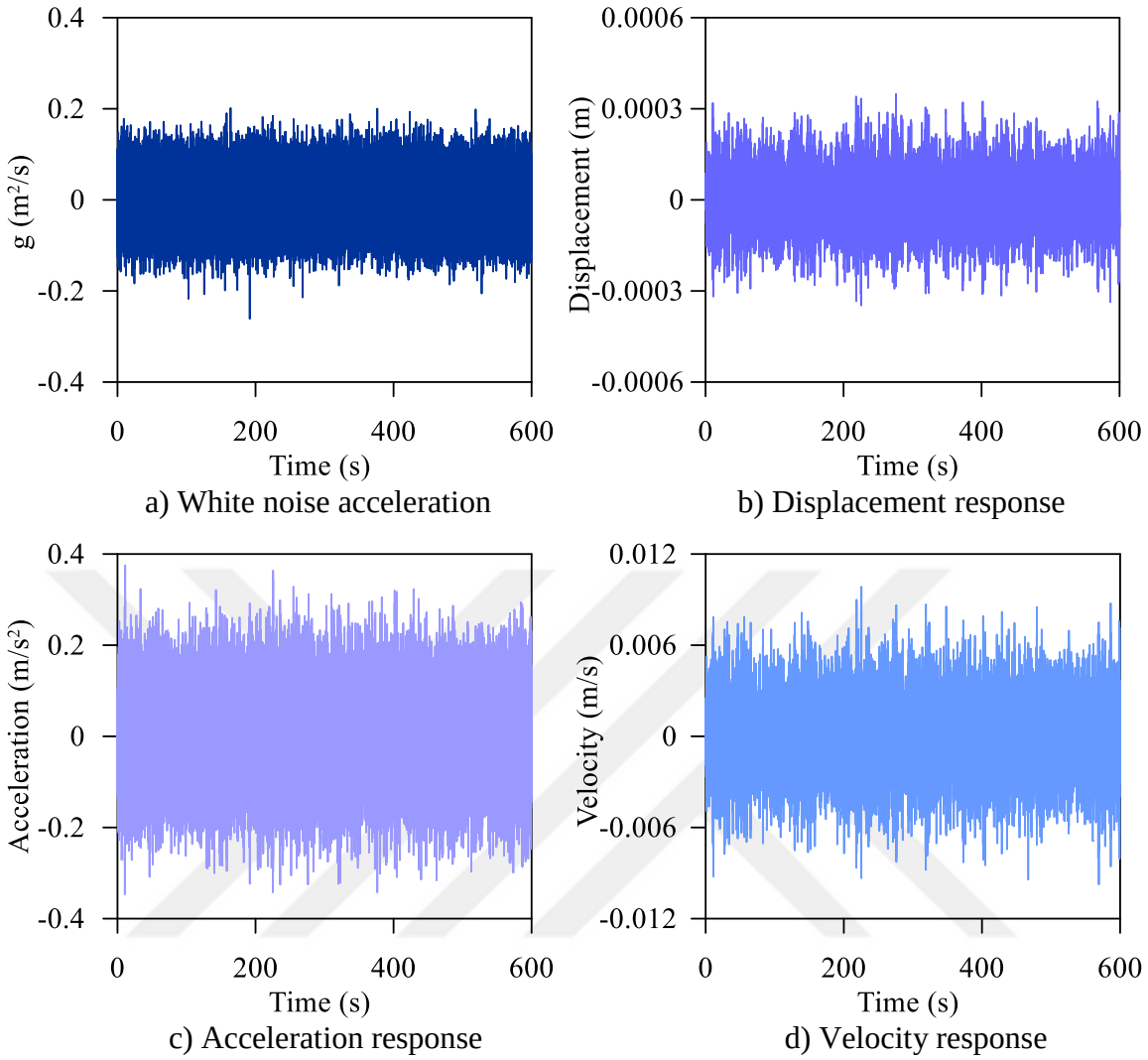


Figure 8. White noise excitation and dynamic responses of the structure

First, the dynamic response of j-th measurement point $u^j(t)$ is converted to frequency domain data of j-th measurement point $U^j(f)$ using FFT as given in Equation 35. FFT is repeated for the number of measurement points ($n_d$) times.

$$U^j(f) = \int_{-\infty}^{\infty} u^j(t) e^{-i\omega t} dt \quad , \; j = 1 \; to \; n_d \tag{35}$$

### 1.5.2. Frequency Filtering

After transforming the time domain data of each measurement point to the frequency domain, bandpass filtering is carried out to divide the frequency domain into the number of considered modes $n_m$ and to form frequency domain data for each mode. The filtering value $R_b$ used for bandpass filtering is calculated using Equation 36 where $f_1$ is the first natural frequency and $R_i$ is the difference between two adjacent mode frequencies (Oppenheim et. al., 2001). The smallest value of differences between adjacent mode frequencies and two times the value of the first natural frequency is selected. Then this value is multiplied by $\gamma$ value that helps adjust the filtering interval with a varying value of 0 to 1. Depending on the length of the data, the filtering coefficient $\gamma$ can be decreased to reduce computational time. However, frequency domain data needs to be graphed and detailed in order to avoid filtering out the peak values within the original range formed by the maximum value of the filtering coefficient.

$$R_b = \gamma \times \min\{2 \times f_1, R_i\} \quad i = 1 \; to \; n_m \tag{36}$$

The frequency domain data of each measurement point is divided into modes using the $R_b$ value as shown in Equation 37 where $f_i$ represents the natural frequency value of $i$-th mode, and $f_i^r$ is the natural frequency value within the filtering range. From this, frequency domain data of each measurement point filtered for each mode $U_i^j(f)$ is obtained. Figure 9 shows the frequency domain graph of one of the measurement points and filtered data graphs of the first, second and third modes.

$$U_i^j(f) = U^j(f_i^r) \quad i = 1 \; to \; n_m \; , \; f_i - \frac{R_b}{2} \le f_i^r \le f_i + \frac{R_b}{2} \tag{37}$$

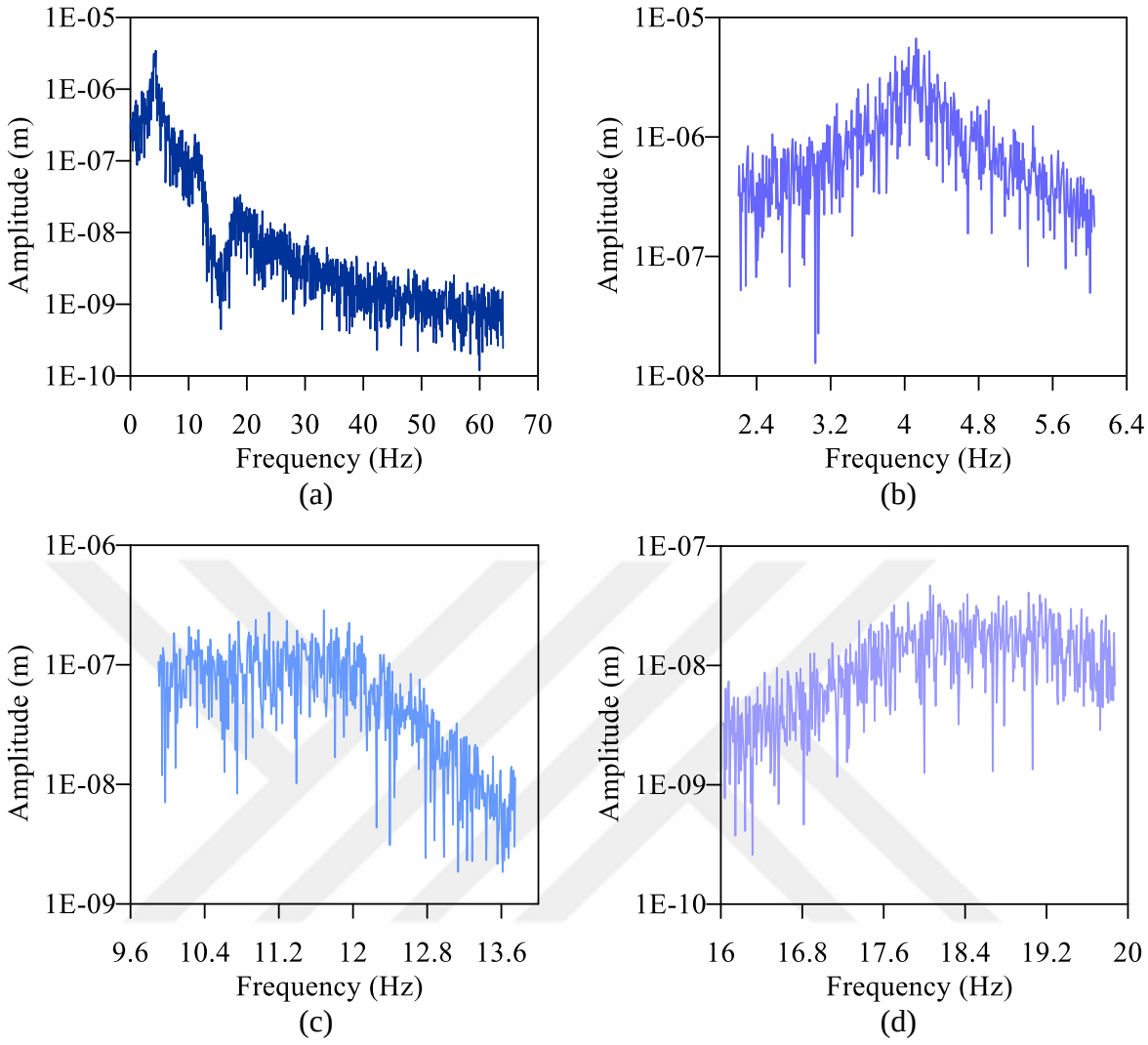


Figure 9. Frequency domain response: (a) of the building, filtered (b) for the 1st mode, (c) for the 2nd mode and (d) for the 3rd mode

### 1.5.3. Inverse Fast Fourier Transform

Finally, inverse FFT is applied, and the modal response of each measurement point and mode $y_i^j(f)$ is extracted using Equation 38. Modal responses of one of the measurement points and the filtered modal responses of the first, second and third modes are obtained (Figure 10).

$$y_i^j(t) = \frac{1}{2\pi}\int_{-\infty}^{\infty} U_i^j(f) e^{ift} df \quad i = 1 \text{ to } n_m,\ j = 1 \text{ to } n_d \tag{38}$$

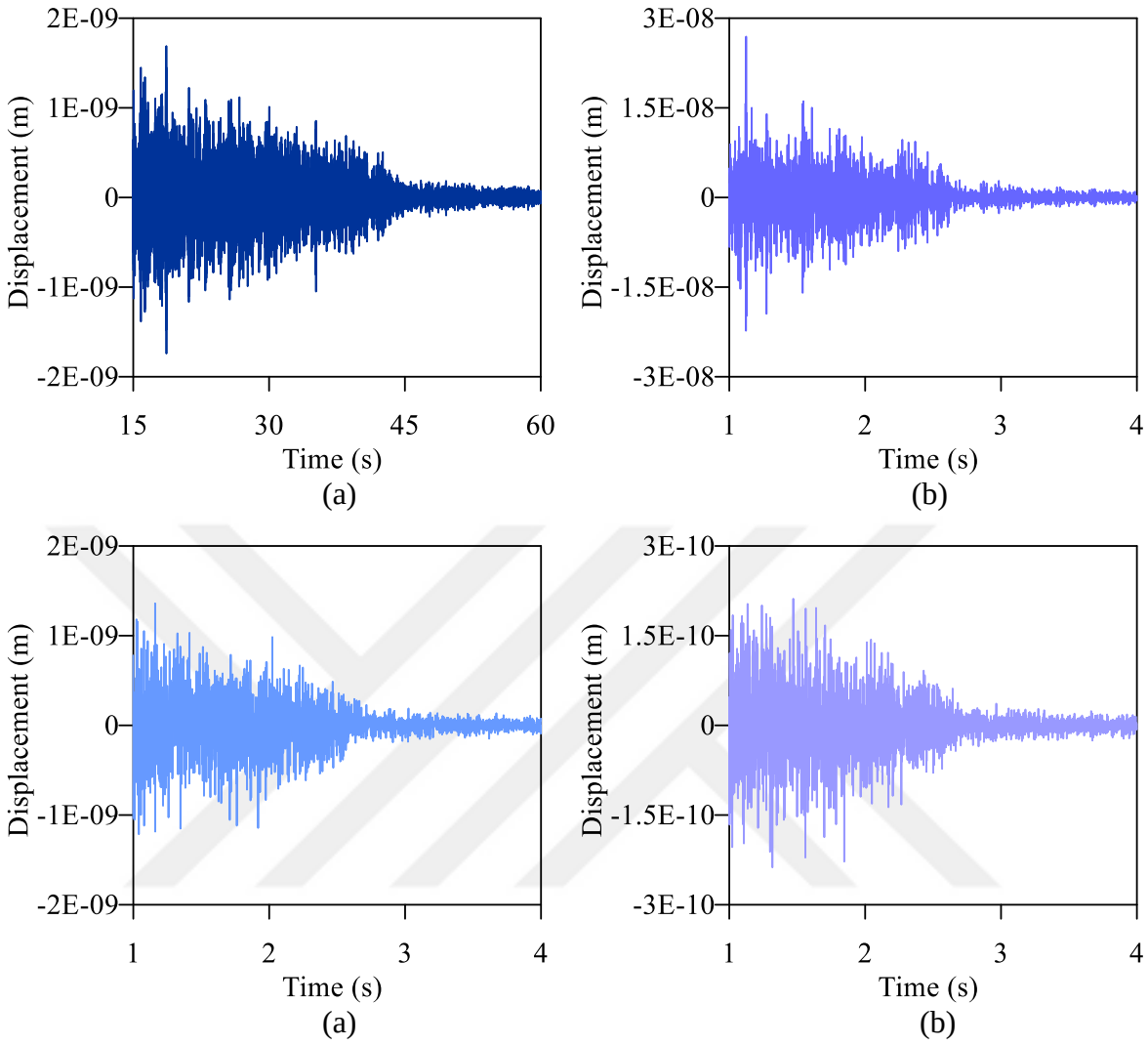


Figure 10. Modal response: (a) for the building, (b) filtered for the 1st mode, (c) for the 2nd mode and (d) for the 3rd mode

### 1.5.4. Modal Response to Modal Participation Ratio

Modal response or modal parameters such as natural frequencies, mode shapes and damping ratios are used for monitoring structural behavior, particularly after any structural damage. Therefore, any change in structural response can be determined by monitoring changes in the modal parameters. The MPR also reflects the modal response of structures and can be used in damage assessment. The relevant steps for the modal response derivation are presented in previous sections. The calculation of the MPR value is detailed in this section.

In order to obtain the MPR value of each measurement point or DOF for each mode, the root means square of modal response ( $MRRMS_i^j$ ) for each measurement point and each mode were separately calculated using Equation 39.

$$MRRMS_i^j = \sqrt{\frac{\sum_{x=1}^{l} u_i^j(x)^2}{l}} \quad i = 1 \; to \; n_m, \; j = 1 \; to \; n_d \tag{39}$$

where $l$ is the data length of the modal response of $i$-th mode and $j$-th measurement point.

MPR value is the ratio of root mean square of modal response for i-th mode and j-th measurement point to a total of root mean squares of considered modal responses, as shown in Equation 40. Consequently, the number of MPR values obtained is equal to the number of modes multiplied by the number of measurement points, and the sum of all MPR values is equal to one.

$$MPR_i^j = \frac{MRRMS_i^j}{\sum_{i=1}^{n_m}\sum_{j=1}^{n_d} MRRMS_i^j} \quad i = 1 \; to \; n_m, \; j = 1 \; to \; n_d \tag{40}$$

Different MPR values can be obtained in accordance with the dynamic response type. When the acceleration was applied as a dynamic response, MPR values for the higher modes were bigger compared to MPR values obtained from velocity and displacement. The comparative studies were carried out by taking displacement, velocity and acceleration into account as dynamic response sources. It was concluded that the sum of MPR values of the same mode for the displacement response is the closest to the modal participation mass ratio ( $MPMR$ ), as shown in Figure 11. However, the variation of the MPR values compare to each other and different damage severities were similar for all dynamic response sources. Therefore, within the scope of this study, displacement responses were utilized for RC structure, and acceleration responses were used for the steel frame model.

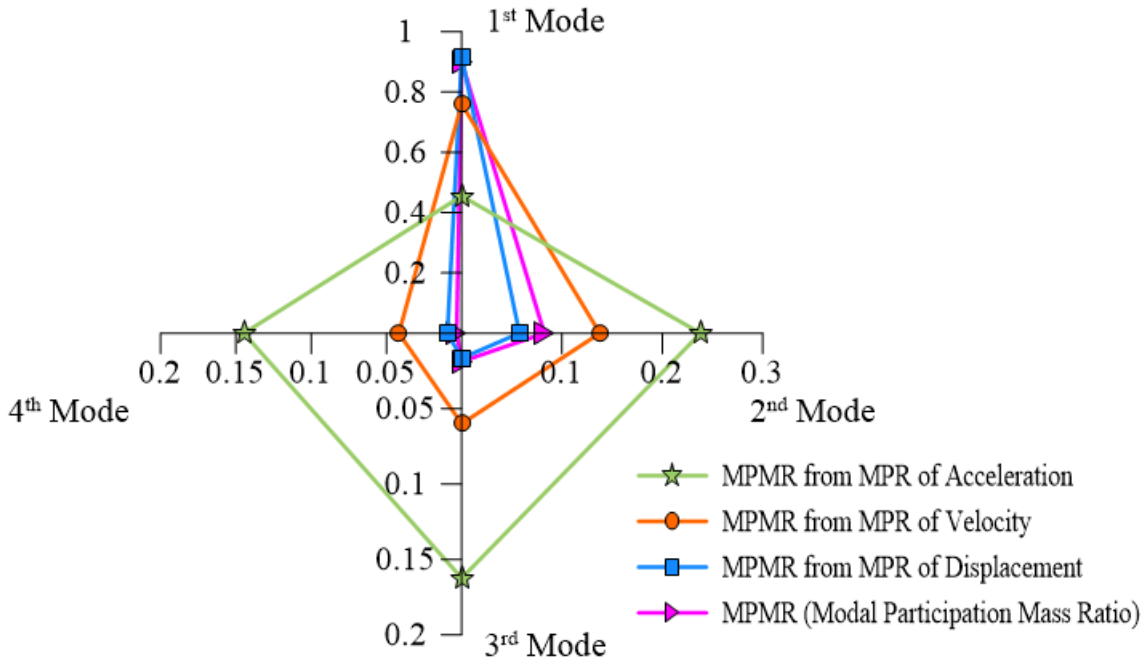


Figure 11. Comparison of MPMR values of the first four modes under different dynamic responses

### 1.5.5. MPR as a Damage Indicator

Damage can be defined as physical harm that decreases functionality, value and strength. It is essential that, prior to damage identification, the initial states of the structures and their components should be detailed. This is also important for structural damage scenarios. Most damage identification methods require information about the initial state of the structure so that localization and quantification would be more effective. Here, the damage identification procedure is carried out using the MPR change percentage set out in Equation 41 where $DMPR$ is the MPR value of the damaged state and $IMPR$ is the MPR value of the initial state.

$$\Delta MPR_i^j = \frac{DMPR_i^j - IMPR_i^j}{IMPR_i^j} \times 100 \quad i = 1 \; to \; n_m, \; j = 1 \; to \; n_d \tag{41}$$

## 2. CASE STUDIES

### 2.1. Introduction

Damage identification through MPR change has been performed on a numerical model of RC building and steel frame as well as a laboratory model of a steel frame.

In the numerical study of the RC building model, structural damage was applied to each story in the form of story stiffness reduction. Both single story and cumulative damage scenarios were practiced to evaluate the utilization of MPR values in damage identification for different damage types. 16 MPR values consisting of a combination of 4 modes and 4 degrees of freedom were evaluated. Single story damage scenarios varied from 1% to 40% for each story with a 1% increment. And the cumulative damage scenarios that represent the earthquake damage were simulated with up to 10% to 40% story stiffness reduction in different stories with 1% increments. Correlations of damage location and severity with MPR value variations were derived. Obtained results of both damage scenarios were evaluated, and the efficiency of MPR values in damage identification was examined.

In the experimental and numerical study of steel frames, structural damage in the form of part cut was applied to each story separately with two different levels of damage severities. Single story damage scenarios were practiced to evaluate the experimental performance of MPR values in the damage identification. An approach to utilize a new filtering technique was presented using the results of the experimental measurements.

### 2.2. Intensive Numerical Study

The effectiveness of MPR values in damage identification was investigated for two types of damage scenarios on the lumped mass model of RC building. These are single story and cumulative damage scenarios.

#### 2.2.1. Model Properties

The numerical model is a four-story RC building with a 3m story height. The model is 20x20m in plan and has a constant span length of 5m. The boundary condition is considered

fixed. All the beams' cross-sections are 25cm wide and 50cm deep. The columns are 50x50cm square cross-sections. The slab thickness is selected as 12cm. The dead load and live load are taken into account as 1.5kN/$m^2$ and 2.0kN/$m^2$, respectively (the live load is taken as 1.0kN/$m^2$ at the top slab). The unit weight of concrete is assumed to be 25kN/$m^3$ and the elasticity modulus is considered 28x$10^6$kN/$m^2$. The three-dimensional (3D) model and plan view of the building is shown in Figure 12.

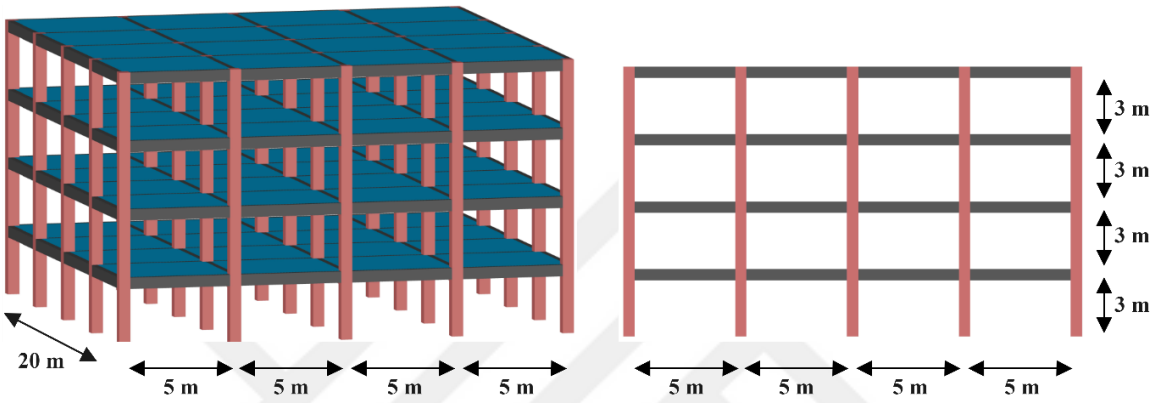


a) The 3D model b) plan view

Figure 12. 3D model and the plan view of the RC building

In this case study, 4 DOF lumped model was employed in order to obtain the relation of MPR changes with the considered damage scenarios. The stiffness for each story was calculated as 1620370kN/m. The masses were calculated as 307tonnes and 266tonnes for the first three stories and the last story, respectively. The dynamic response data of the building resulting from the white noise acceleration were collected from the story levels, as shown in Figure 13.

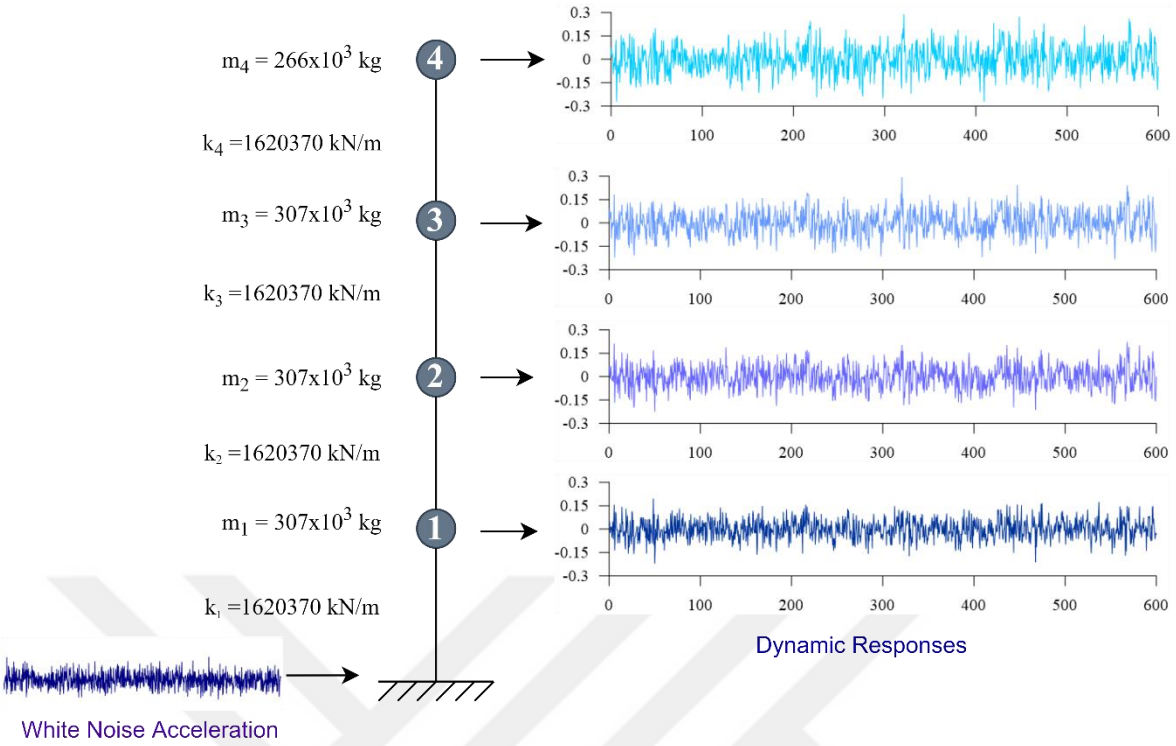


Figure 13. Lumped mass model of the building and its dynamic response data

### 2.2.2. Dynamic Characteristics, MPR Variations and Damage Identification

#### 2.2.2.1. Single Story Damage Scenarios

MPR variation ($\Delta MPR$) for each mode and measurement point gives insight into damage. Therefore, $\Delta MPR$ was detailed to determine the anticipated behavior of MPR under different damage scenarios. For this aim, in order to simulate the increasing damage severity, the stiffness values of each story were decreased within the range of 1-40% with a reduction factor (RF). The change in all 16 MPR values of the first 4 modes and 4 DOFs was then evaluated to establish a relation between the $\Delta MPR$ and the damage. The stiffness reduction of the stories results in a change of modal parameters. The first four natural frequencies were obtained as 4.1312 Hz, 11.8293Hz, 17.9508Hz and 21.8060 Hz for the undamaged (as-built) model. The variation of natural frequencies with the increasing damage severity is given in Figure 14. As shown in Figure 14, a slight decrease in the natural frequencies of the building was observed after the introduction of damage, even at the 40% RF. The first four natural frequencies were obtained as 3.6177Hz, 10.9081Hz, 17.3535Hz and 21.6360Hz after 40% damage occurred at the first story. These were calculated as

3.7274Hz, 11.8262Hz, 16.1410Hz and 20.8244Hz for the second story damage, 3.8981Hz, 10.6464Hz, 17.7726Hz and 20.088Hz for the third story damage, 4.070Hz, 10.6207Hz, 16.1875Hz and 21.1748Hz for the fourth story damage. In Figure 14, there is no specific sign indicating the location of the damage. Therefore, studying only the natural frequency change is not enough for evaluating the presence, severity and location of the damage.

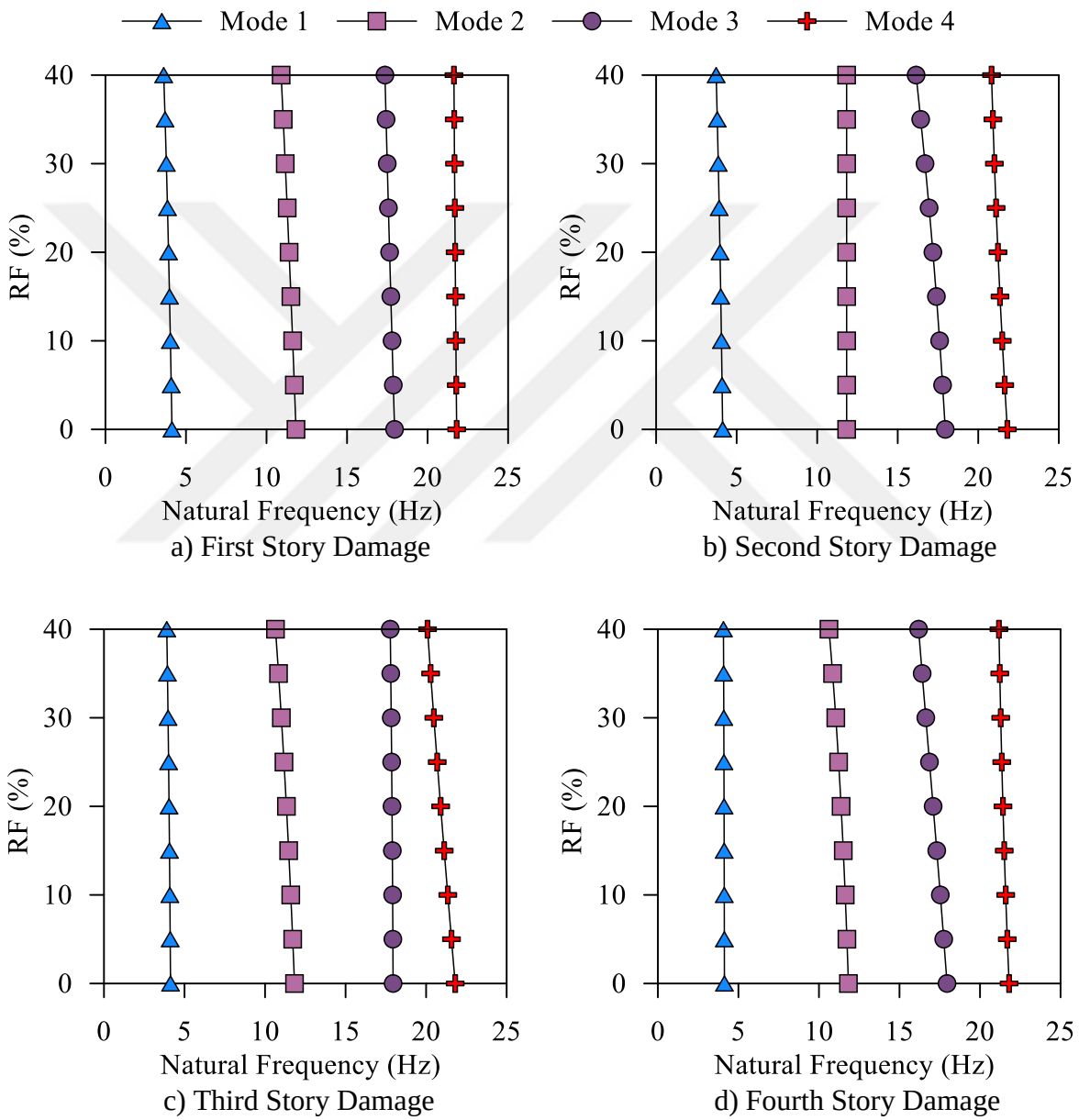


Figure 14. Changes in natural frequencies for different story damages

In addition, the mode shapes do not satisfy for evaluating the presence, severity and location of the damage. Figure 15 shows the variation of the first four mode shapes of the building after 40% of damage occurred on different stories. Figure 16 shows the variation of the fourth mode (most affected mode shape of the first four modes) with the increasing damage severity at different stories. As can be seen in Figure 15 and Figure 16, there is no significant change in the mode shapes of the building after 40% damage occurrence. It should be noted, however, that the presence, severity and location of damage can be effectively evaluated by methods such as mode-shape curvature and mode-shape flexibility.

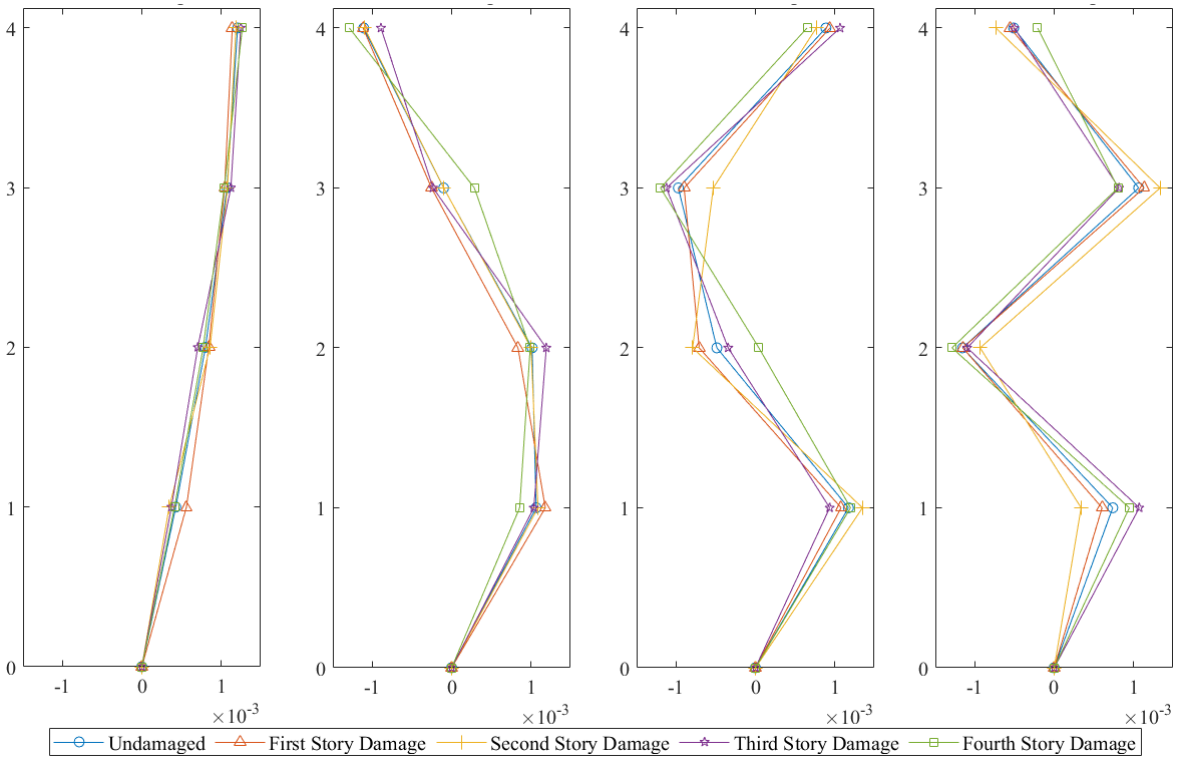


Figure 15. Variations of the first four mode shapes for 40% RF at different stories

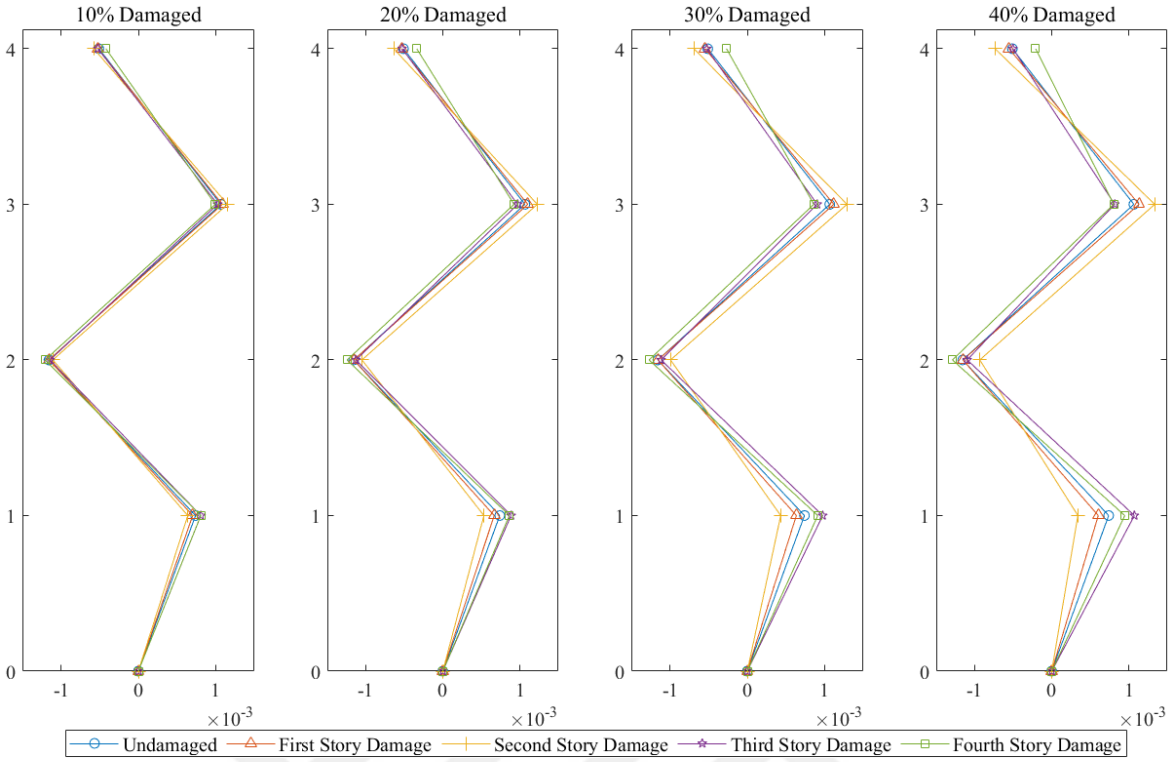


Figure 16. Variations of the fourth mode shape with the increasing damage severity at different stories

To evaluate the effectiveness of MPR values for the damage identification, the variation of MPR values for the first four modes and four DOFs resulting from damage scenarios of 1%-40% at each story with a 1% increment was detailed. For each damage scenario, 16 MPR values were obtained. For instance, the MPR of the first mode at the first DOF is $MPR_1^1$, and the MPR of the fourth mode at the third DOF is $MPR_4^3$. MPR values of each damage scenario were compared to MPR values of the undamaged (as-built) building model. Figure 17 shows the MPR variation of the first mode with the damage severity increase at different stories. In addition, the MPR variation of second, third and fourth modes with the increasing damage severity at different stories are given in Figures 18-20. As shown, each $\Delta MPR$ value moved further away from zero with the increasing damage severity or RF. As can be seen in Figure 17, the $\Delta MPR$ values were obtained highest at the damaged story (DOF). Therefore, it can be concluded that the highest $\Delta MPR$ value indicates the possible damage and its location. $\Delta MPR$ values of DOFs above damaged story also increase but gets smaller at higher stories as shown in Figure 17a-b. And as can be seen in Figure 17c-d the DOFs below-damaged story decreases more at lower stories.

In Figures 18-20, it can be seen that the second, third and fourth modes were not as clear as the first mode MPR variation for the damage assessment. As seen, the damaged story (DOF) was either a turning point or had a dramatic change between adjacent DOFs. From this, it may be concluded that approximate localization of the damage can be performed by the determination of dramatic change in $\Delta MPR$ value.

It should be noted that the MPR values of the first mode provide the information from which a reliable assessment can be made of the damage presence and location. This behavior can be relevant to the high mass participation ratio of the first mode. It is also worth mentioning that with the linear variation of $\Delta MPR$ values under different percentages of damage severity, the linear function for each story damage can be obtained. Then, the damage severity can be determined using these linear functions.

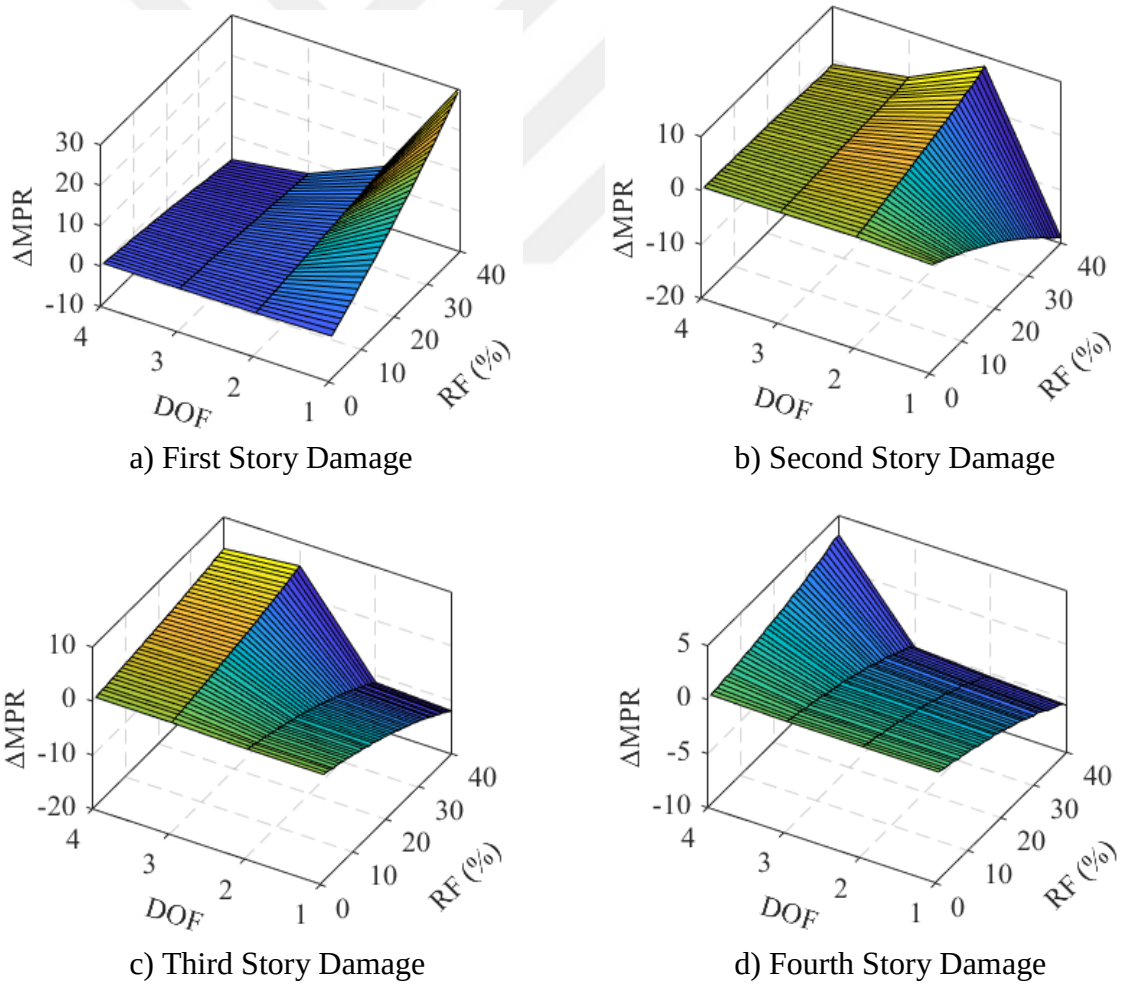


a) First Story Damage

b) Second Story Damage

c) Third Story Damage

d) Fourth Story Damage

Figure 17. Variations of the first mode MPR values by damage severity increase

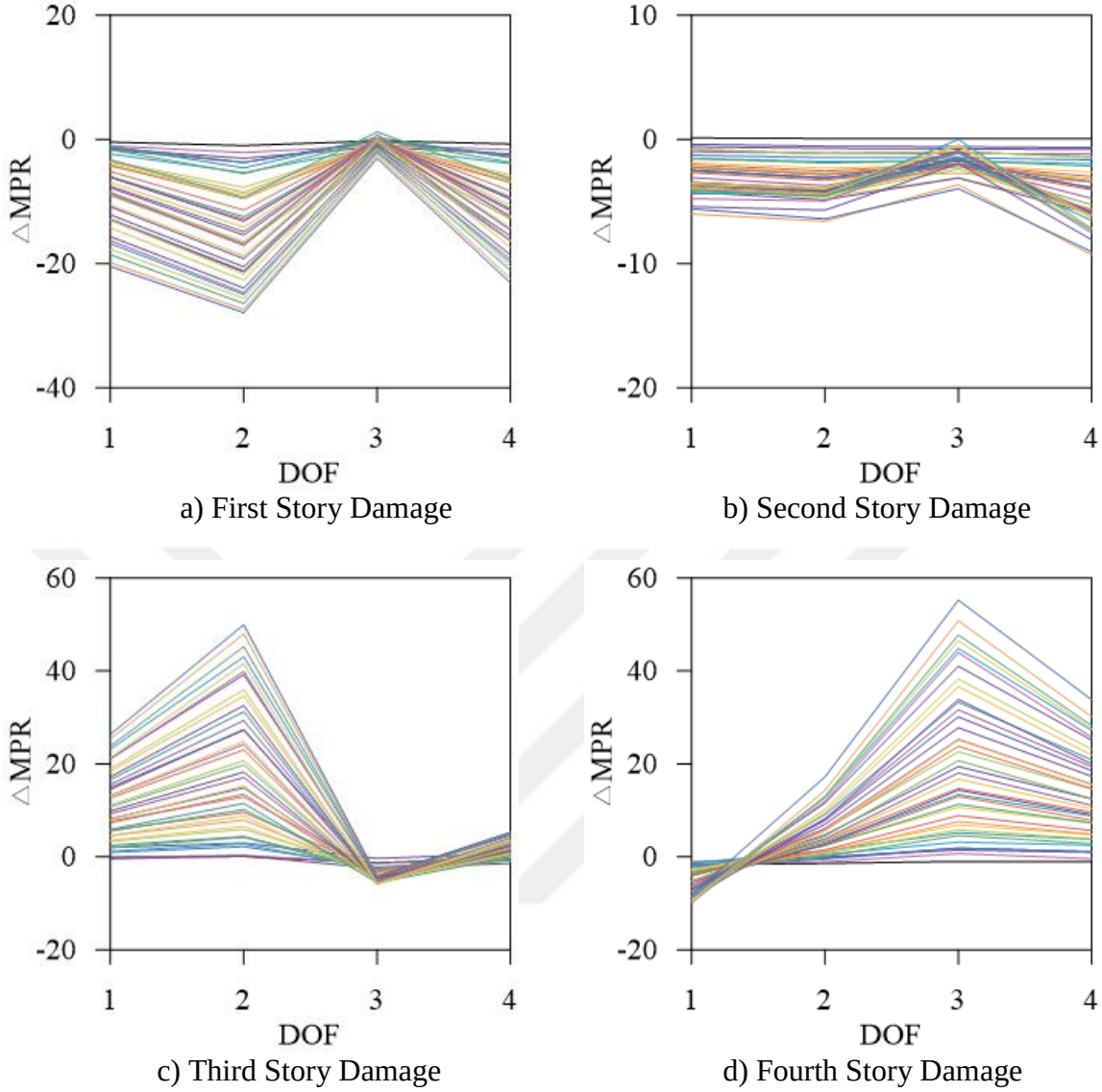


a) First Story Damage

b) Second Story Damage

c) Third Story Damage

d) Fourth Story Damage

Figure 18. Variations of the second mode MPR values by damage severity increase

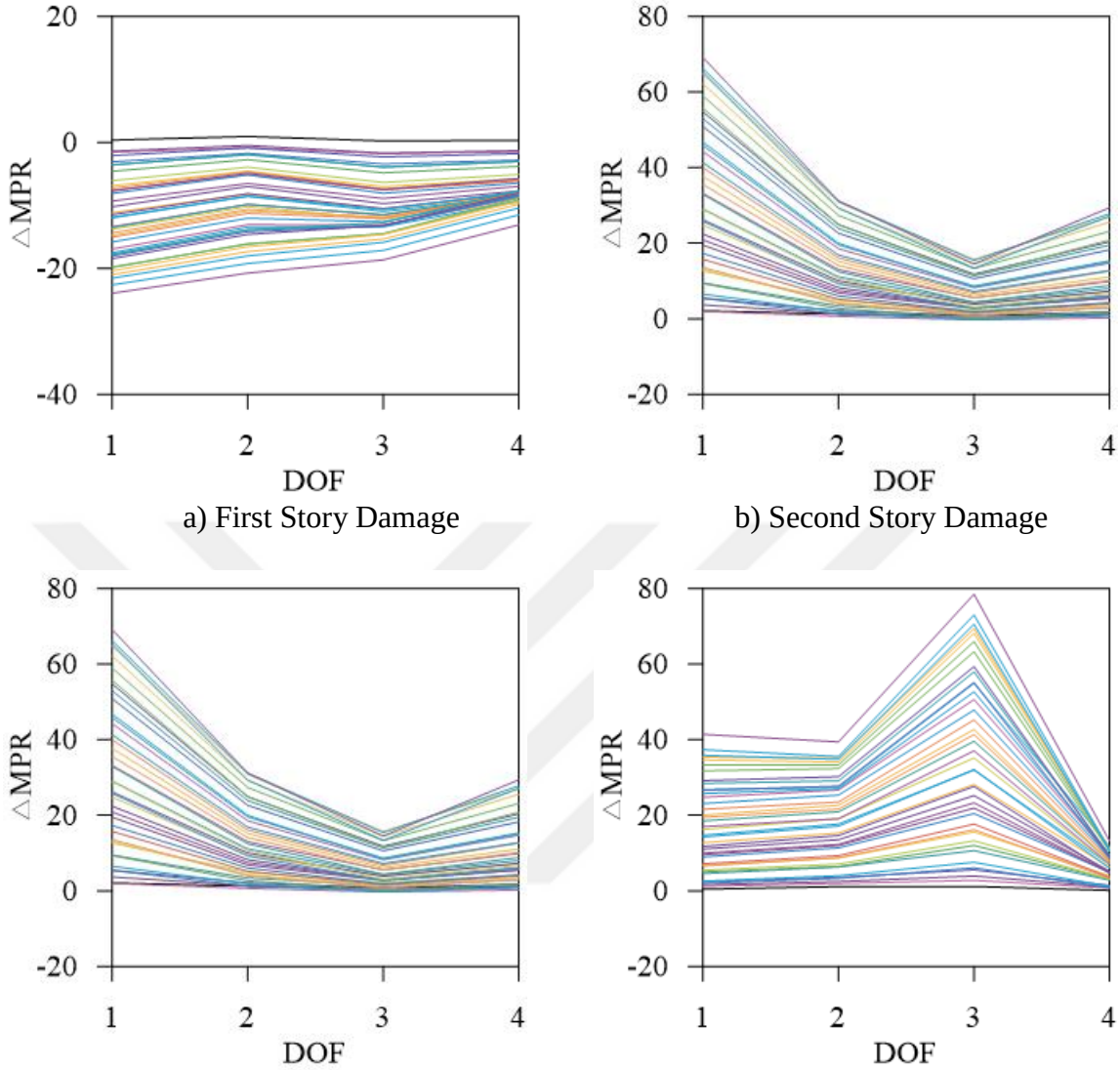


a) First Story Damage b) Second Story Damage

c) Third Story Damage d) Fourth Story Damage

Figure 19. Variations of the third mode MPR values by damage severity increase

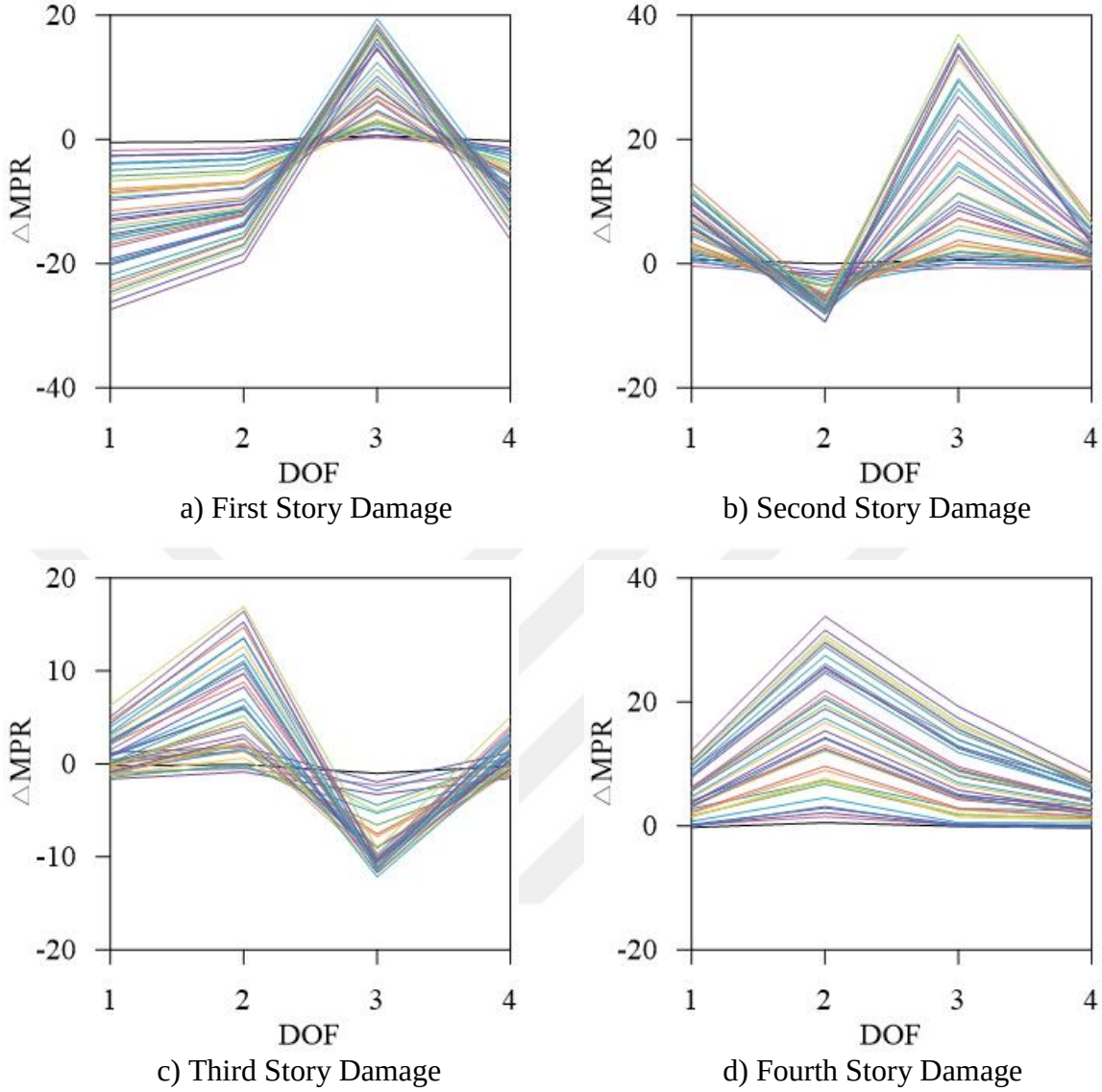


a) First Story Damage b) Second Story Damage

c) Third Story Damage d) Fourth Story Damage

Figure 20. Variations of the fourth mode MPR values by damage severity increase

#### 2.2.2.2. Cumulative Damage Scenario

In most cases of structural damage caused by natural disasters, particularly earthquakes, damage does not only occur on a single story. Depending on the magnitude and duration of the disaster, damage may cumulatively increase and occur in different parts of the structure. The earthquake damage severity is higher in lower stories, as seen in Figure 21 (Gallardo et. al., 2021; Verderame et. al., 2014). The cumulative damage scenarios were performed on the model to simulate the earthquake damage. And the effectiveness of MPR values in damage identification of such damage scenarios was investigated for simulated damage scenarios. Figure 22 shows the cumulative damage scenarios consisting of 40

different rates. The damage in each story was simulated as story stiffness reduction. In the first ten scenarios, the damage was only at the first story increasing one by one to 10%. From the 11$^{th}$ to 20$^{th}$ scenarios, second story damage occurred and increased by 1% at each step until the 20$^{th}$ scenario, while first story damage continued to increase by 1% at each step. From the 21$^{st}$ to 30$^{th}$ scenarios, third story damage occurred and increased by 1% at each step until the 30$^{th}$ scenario, while first and second story damages continued to increase by 1% at each step. Then, from the 31$^{st}$ to 40$^{th}$ scenarios, fourth story damage occurred and increased by 1% at each step until the 40$^{th}$ scenario, while the first, second and third story damage continued to increase by 1% at each step. Finally, in the last scenario, the first, second, third and fourth stories were damaged by 40%, 30%, 20% and 10%, respectively.

Figure 21. Building damage due to earthquake (Demir et. al., 2020).

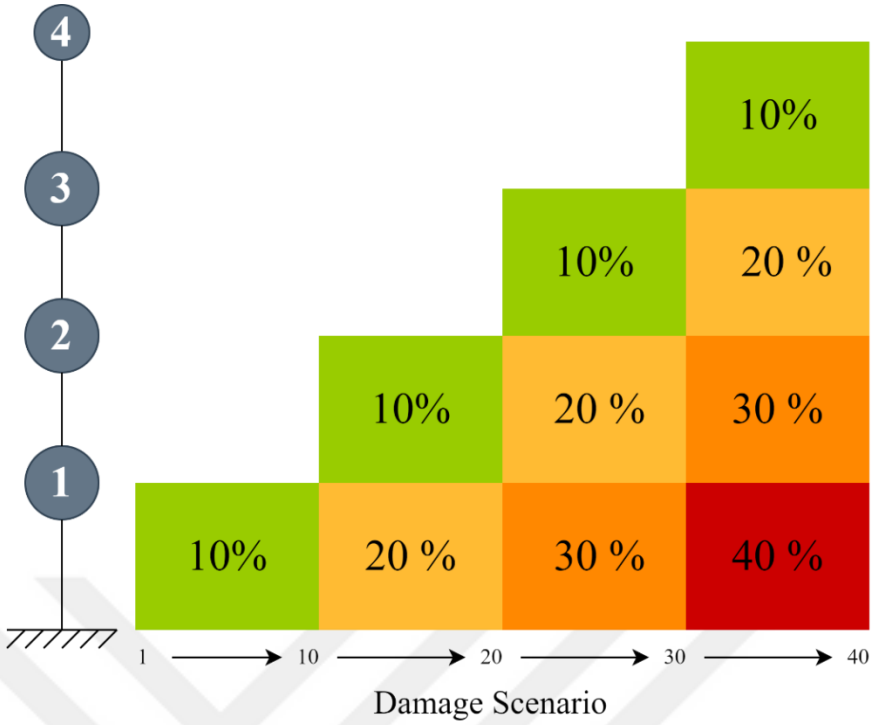


Figure 22. Cumulative damage scenarios

Variation of MPR values compared to the undamaged building model was calculated for each scenario. Figure 23 shows the MPR variation of each scenario for the first four modes. It can be interpreted that the MPR variation graphs for the four modes shown in Figure 23 were similar to four modes of first story damage obtained from the single story damage scenarios. However, the presence of upper story damage can be spotted by small direction changes at 10%, 20%, and 30% RF, as shown in Figure 23a.

As stated earlier, in a single story damage case, MPR values of the first mode gave a better insight into damage. It should also be mentioned that the damage presence in upper stories does not dramatically change the MPR variations of the first mode (Figure 23a). This behavior is due to the dominant behavior of lower story damage compared to upper story damage.

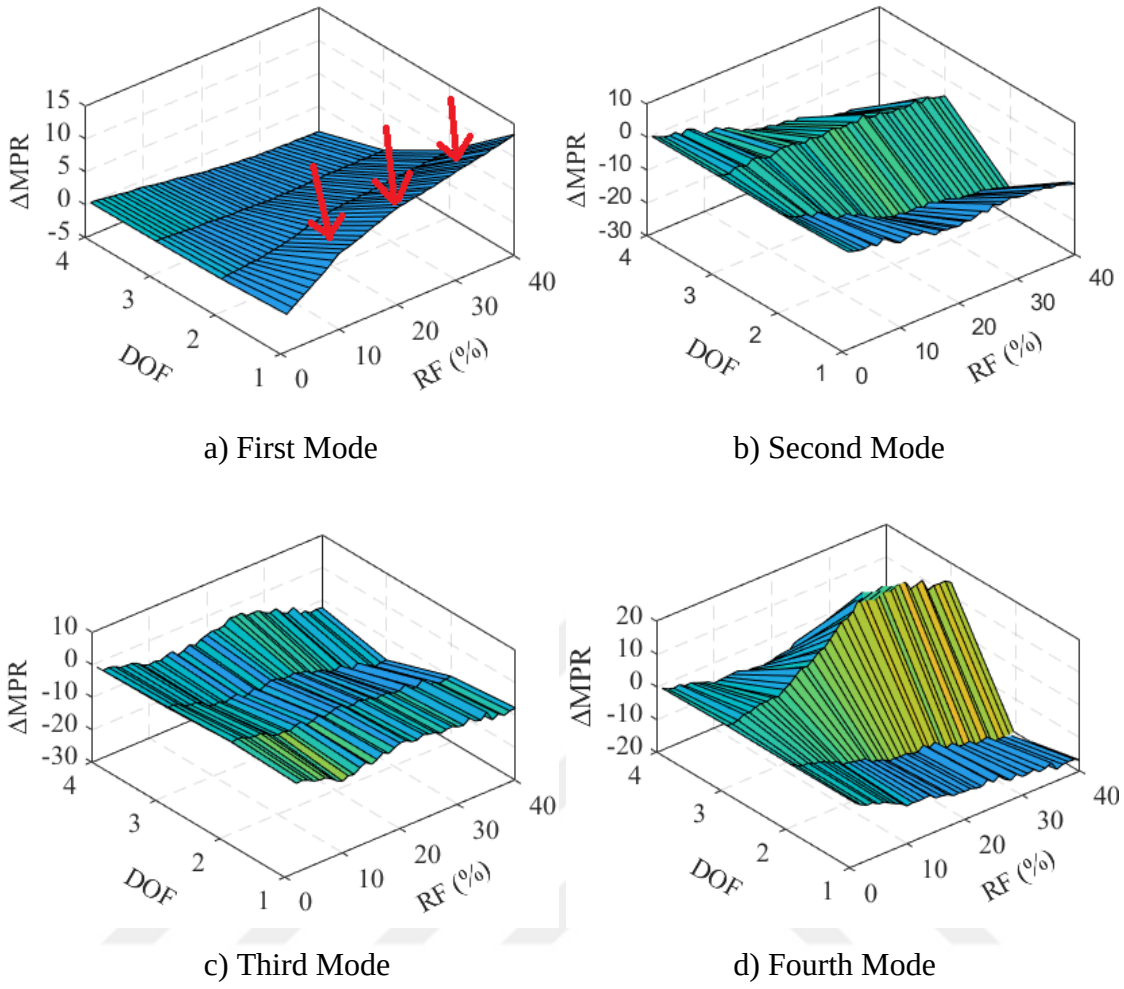


Figure 23. MPR variations of cumulative damage for the first four modes

Figure 24 shows the first mode MPR variation of the first story damage from 1 to 40% obtained from the single story damage scenario and the first mode MPR variation of the cumulative damage scenario. In both graphs, the first story damage increased by 1% to 40%, but in the cumulative damage scenario second, third and fourth story damages were introduced to the model at 10%, 20%, and 30% RF. It can be seen in Figure 24 that the $\Delta MPR_1^1$ value in Figure 24b deviates further away from the $\Delta MPR_1^1$ value of the single story damage scenario shown in Figure 24a. This slight directional change indicates the presence of additional story damage. Therefore, the sensitivity of MPR variation to additional story damage makes it applicable to multiple story damage scenarios.

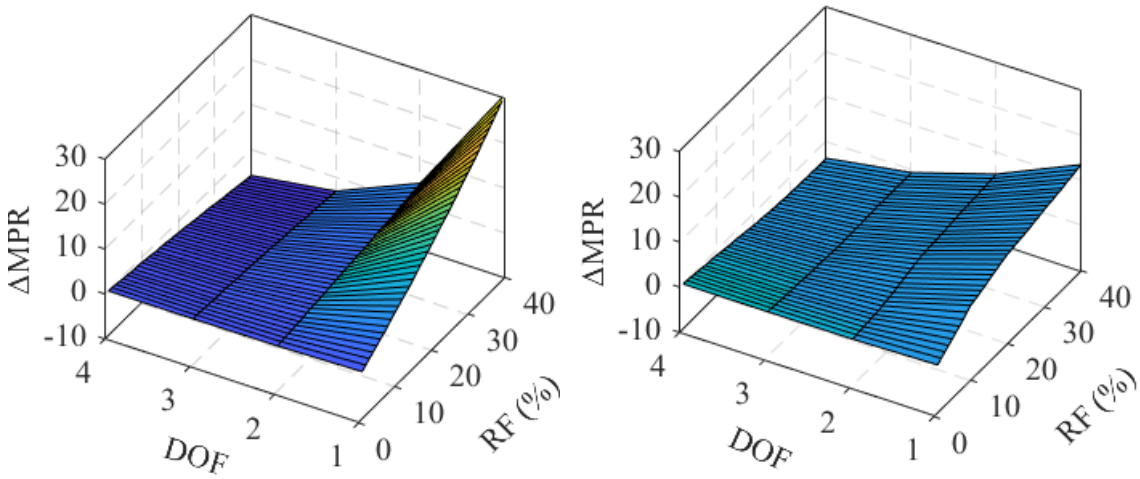


Figure 24. Variations of first mode MPR values: (a) for the single story damage scenario and (b) for the cumulative damage scenario

### 2.2.3. Results and Discussion

The utilization of the MPR values in damage identification was numerically evaluated. In order to extend the evaluation of the presented method, single story and cumulative damage scenarios were practiced on a four-story RC building model. For the structural damage, the story's stiffness was reduced. From the study, the following conclusions can be drawn:

- ✓ As expected, the natural frequencies decreased with the increasing damage severity. However, even after a 40% stiffness reduction of each story the natural frequencies decreased slightly. Also, the mode shapes of the building did not change with the increasing damage severity. The presence, severity and location of damage were not evaluated based on these parameters.

The Single Story Damage Scenario:

- ✓ The MPR variation of a four-story building was calculated under the effect of stiffness reduction. 16 MPR values consisting of combinations of 4 modes and 4 DOF were evaluated for each story damage ranging from 1-40% (RF) stiffness reduction. A higher RF percentage resulted in greater changes in the MPR value of each mode and each DOF. This behavior means that the severity of the damage can efficiently be determined through this method. $\Delta MPR$ value of damaged DOF was the biggest

among other DOFs of the first mode. Also, $\Delta MPR$ was positive for DOFs above the damaged story and negative for DOFs below the damaged story. Moreover, the MPR variation of other modes can also be used to approximately localize the damage by spotting dramatic changes between adjacent DOFs.

The Cumulative Damage Scenario:

- ✓ The cumulative damage scenarios representing earthquake damage to buildings were provided. 16 MPR values consisting of 4 modes and 4 DOF combinations were calculated for each step of the scenario. Increasing the RF by 1% at each step and introducing new damage to the upper story at every 10% RF, 40 different damage scenarios were taken into account. It should also be stated that similar MPR variation graphs were obtained for both the single story and the cumulative damage scenarios. However, the presence of upper story damage can be spotted by little direction changes at 10%, 20%, and 30% RF (for the first mode). This referred to the new damage location in the relevant story. Also, even though the variation of other modes is not as linear as the variation of the first mode, slight slope changes and inverting points can be interpreted as new damage locations.

Based on the results of these cases, it was concluded that the MPR variation was effective in damage detection and assessment. The MPR values provided information on the damage presence, severity and location. Also, MPR variation was capable of detecting changes due to additional damage location. It should be noted, however, that the method requires knowledge about the initial condition of the structures. Because the method is based on a comparative approach.

Finally, it should be emphasized that the presented method can provide valuable data for damage identification practice. Moreover, the method detailed in this study can be adopted for structural health monitoring. For this reason, the numerical study employed can be used, with some modification, for field applications.

### 2.3. Experimental and Numerical Study

The effectiveness of MPR values in damage identification was investigated for single story damage scenarios on the steel frame model. Experimental and numerical measurements were performed and MPR variations were examined for both.

#### 2.3.1. Model Properties

Within the scope of this thesis, a steel frame model that simulates the behavior of the building is constructed for experimental studies. Steel was picked as a building material because it offers unlabouring assembly and uniform behavior. As can be seen in Figure 25, the frame model has four stories and one bay in the longitudinal direction. Dimensions of the steel frame model are shown in Figure 26. 40 mm x 40 mm x 2 mm rectangular hollow sections were welded to form a frame shape, and 700 mm x 300 mm x 6 mm steel plate with eight holes were used to create fixed support boundary conditions.

(a) (b)

Figure 25. 3D model of the steel frame (a) experimental model and (b) numerical model

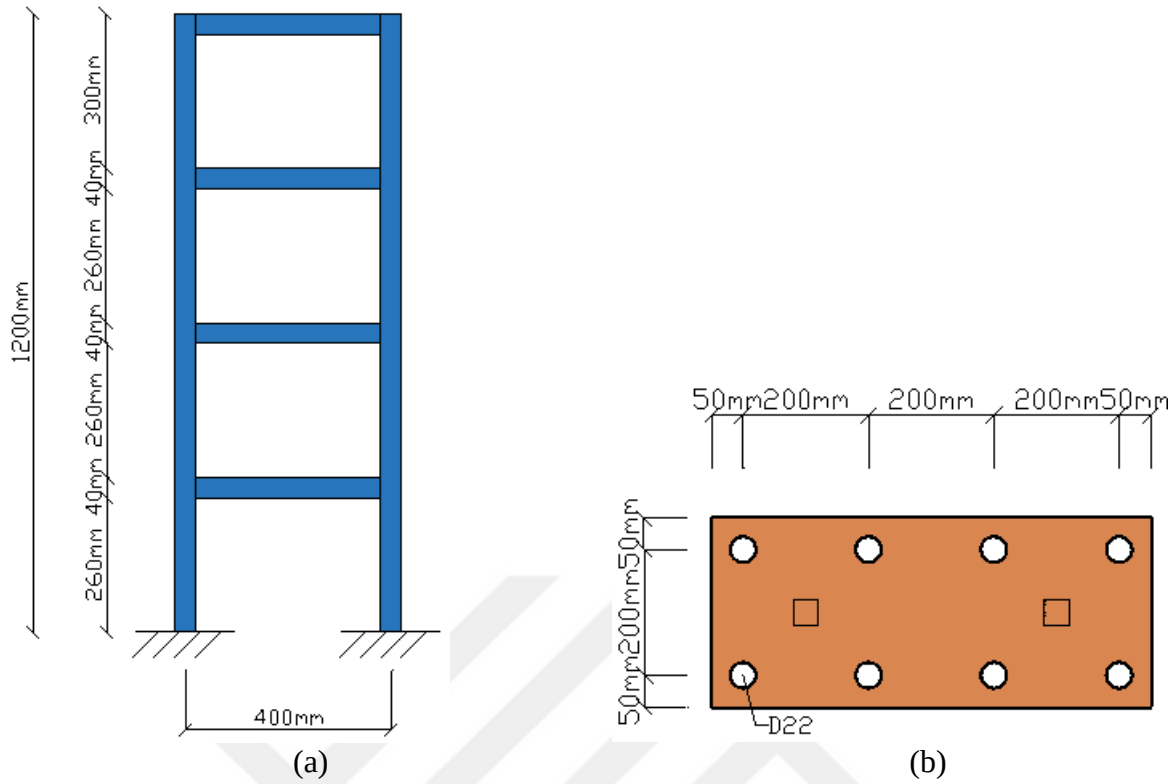


Figure 26. Dimensions of the (a) steel frame and (b) steel plate

### 2.3.2. Damage Scenarios

Considering the level of workmanship required and the risks of incorrect measurements, a simple steel frame model is selected for experimental study. Undamaged and eight damaged models that consist of 4 different single story damages with two severity levels were examined. In Figure 27, it can be seen that the first level damage was simulated as the removal of part with 14 cm height and 1.5 cm width from the middle of the story. The process was followed to simulate second level damage by increasing the part cut width to 2 cm. Consequently, these undamaged and damaged models can be used to examine the performance of MPR as a damage identification method.

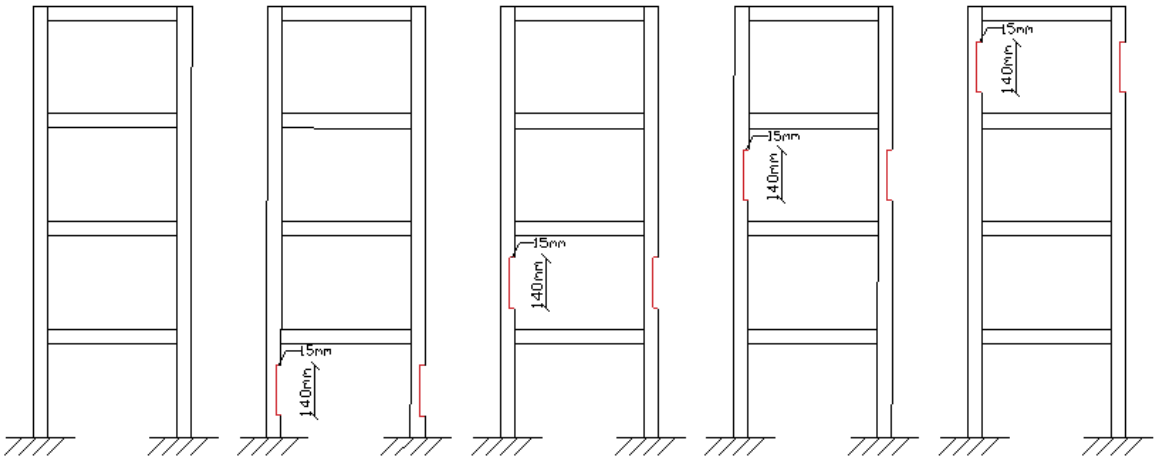


Figure 27. Undamaged model and the first level damage scenarios

### 2.3.3. Dynamic Characteristics of Numerical Study

FE method has been used to examine the dynamic characteristics of the steel frame model. Dynamic characteristics of the undamaged and eight different damage scenarios were obtained using SAP2000 (SAP, 2021). Steel material properties were selected as S235 properties. Both rectangular hollow sections and base plate were divided into small finite elements to increase precision. Undamaged steel frame model and models with damage scenarios are shown in Figure 28. And the first three in-plane modes of undamaged and damaged models are given in Figure 29.

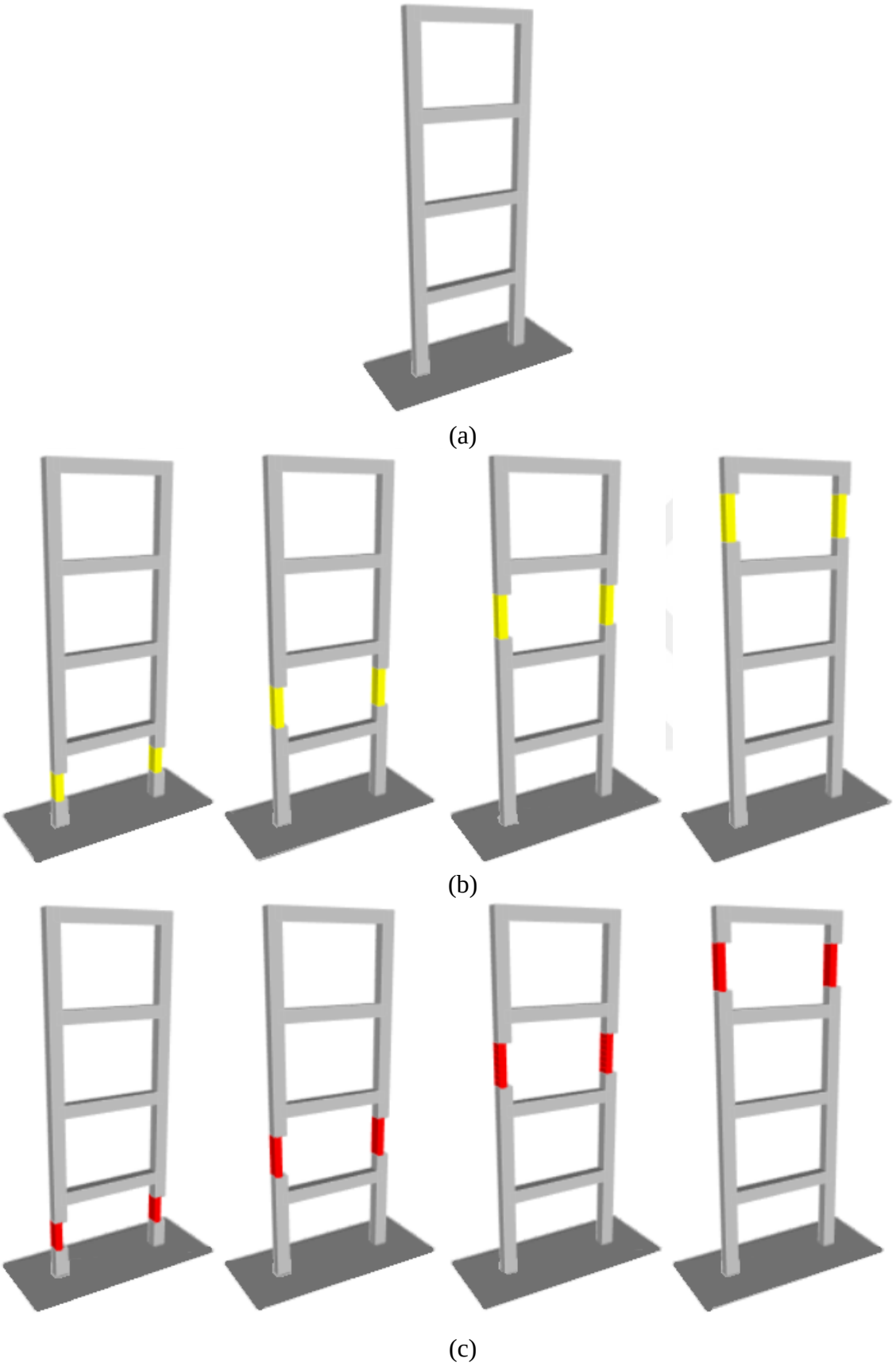

(a)

(b)

(c)

Figure 28. (a) Undamaged, (b) level 1 damaged and (c) level 2 damaged models

Mode 1 (65.248 Hz) Mode 2 (227.732 Hz) Mode 3 (458.989 Hz)

(a)

Mode 1 (58.878 Hz) Mode 2 (209.526 Hz) Mode 3 (433.068 Hz)

(b)

Mode 1 (55.776 Hz) Mode 2 (200.864 Hz) Mode 3 (421.78 Hz)

(c)

Figure 29. Mode shapes of undamaged and damaged states of the steel frame

Figure 29 continued.

Mode 1 (64.057 Hz)

Mode 2 (223.367 Hz)

Mode 3 (424.473 Hz)

(d)

Mode 1 (62.666 Hz)

Mode 2 (221.288 Hz)

Mode 3 (399.393 Hz)

(e)

Mode 1 (65.616 Hz)

Mode 2 (215.512 Hz)

Mode 3 (450.838 Hz)

(f)

Figure 29 continued.

Mode 1 (65.048 Hz)

Mode 2 (206.9 Hz)

Mode 3 (446.798 Hz)

(g)

Mode 1 (66.723 Hz)

Mode 2 (223.968 Hz)

Mode 3 (427.197 Hz)

(h)

Mode 1 (66.839 Hz)

Mode 2 (217.989 Hz)

Mode 3 (404.473 Hz)

(i)

The first three in-plane mode frequencies of undamaged and eight damaged models and the increase/decrease rate of damaged scenarios compared to the undamaged state are given in Table 3. The first mode frequencies of all models were between 55.776 Hz and

66.839 Hz. The maximum difference in first mode values was observed at first story level 2 damage in which the frequency decreased by 14.517%.

Table 3. Mode frequencies of FE models and frequency variations

| Mode Number | Initial State (Hz) | First Story Damage (Hz) | | Second Story Damage (Hz) | | Third Story Damage (Hz) | | Fourth Story Damage (Hz) | |
|---|---|---|---|---|---|---|---|---|---|
| | | Level 1 | Level 2 | Level 1 | Level 2 | Level 1 | Level 2 | Level 1 | Level 2 |
| 1 | 65.248 | 58.878 | 55.776 | 64.057 | 62.666 | 65.616 | 65.048 | 66.723 | 66.839 |
| 2 | 227.732 | 209.526 | 200.864 | 223.367 | 221.288 | 215.512 | 206.9 | 223.968 | 217.989 |
| 3 | 458.989 | 433.068 | 421.78 | 424.473 | 399.393 | 450.838 | 446.798 | 427.197 | 404.473 |
| | | Frequency Variation (%) | | | | | | | |
| 1 | 0 | -9.763 | -14.517 | -1.825 | -3.957 | +0.564 | -0.307 | +2.261 | +2.438 |
| 2 | 0 | -7.994 | -11.798 | -1.917 | -2.830 | -5.366 | -9.148 | -1.653 | -4.278 |
| 3 | 0 | -7.514 | -10.927 | -10.667 | -17.830 | -6.538 | -9.196 | -9.029 | -16.041 |

### 2.3.4. Dynamic Characteristics of Experimental Study

Dynamic responses of the steel frame model to ambient vibrations are measured using one directional B&K 4507 accelerometers. Dynamic responses of each model were monitored for 10 minutes and data was collected in B&K 3053 data acquisition system. Then, stored data was processed using BK Connect software. Lastly, dynamic characteristics such as natural frequency, mode shape and damping ratio of each model were determined using OMA software (BK connect, 2021; PULSE, 2021).

For this thesis, accelerometers are placed in the longitudinal direction to measure in-plane dynamic responses. The placement of accelerometers on the model structure is given in Figure 30.

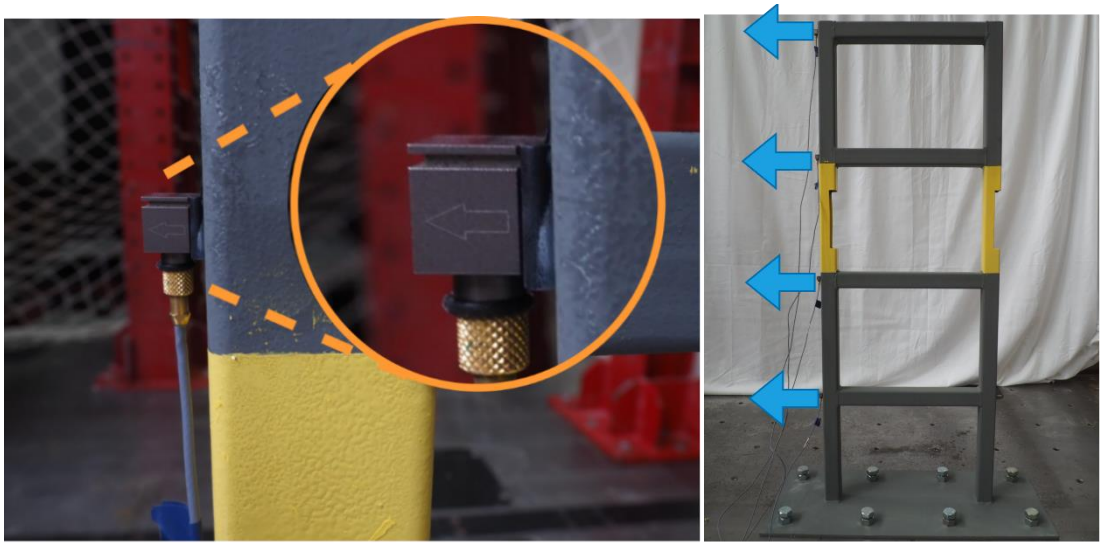

Figure 30. Accelerometer placement on the steel frame

Experimental measurements are carried out for undamaged and the eight different damaged steel frame models given below in Figure 31. And a few pictures of the vibration measurement setup are shown in Figure 32.

(a) (b)

Figure 31. The undamaged model with (a) first level damaged models and (b) second level damaged models

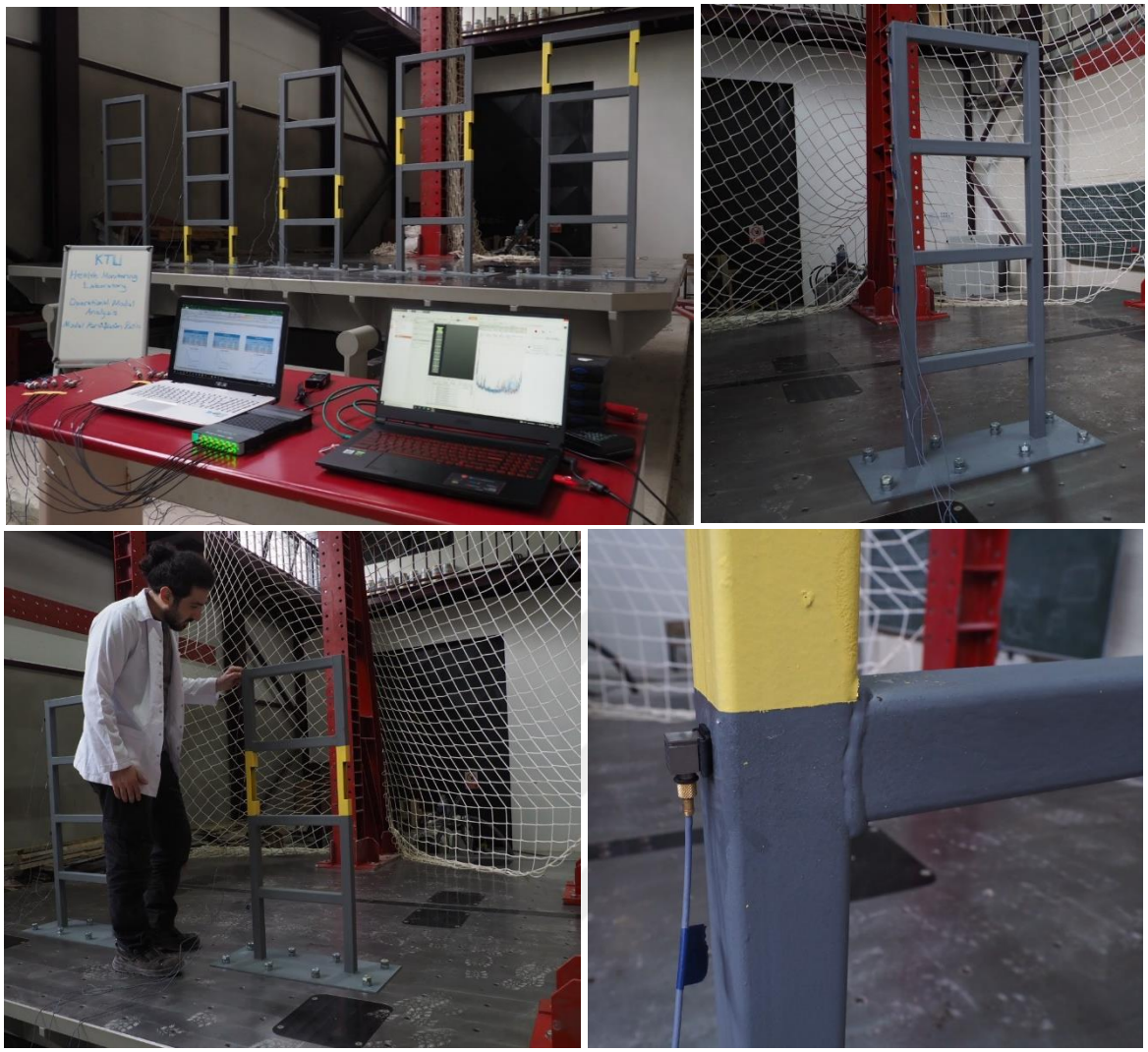


Figure 32. Pictures of the vibration measurement setup

Singular values of spectral densities and the average of these matrices obtained by the EFDD method as well as stabilization diagrams and singular values obtained by the SSI method are given in Figures 33-50.

The first three in-plane mode shapes of the undamaged state and all damaged models are shown in Figure 51. Mode frequencies of each structural state (undamaged and damaged) obtained with EFDD and SSI methods and the variation of each mode frequency from the undamaged state are given in Tables 4-5. Damping ratios of all steel frame models are listed in Table 6 along with the variation of ratios from the undamaged values.

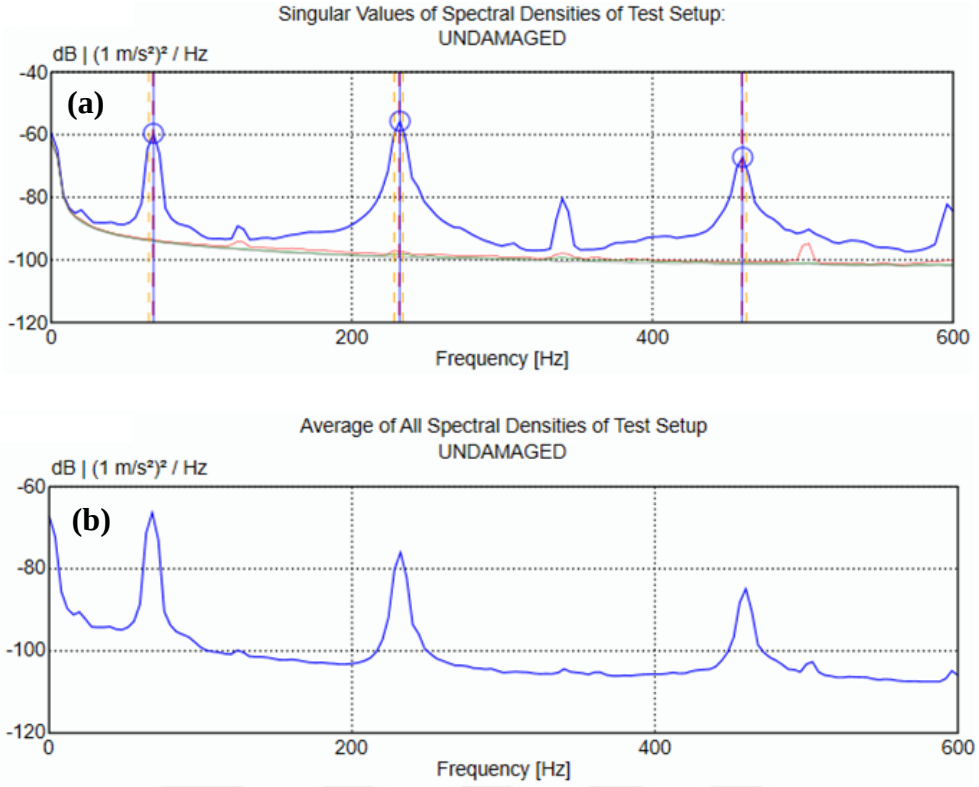


Figure 33. The undamaged state (a) singular values of spectral densities and (b) the average of all spectral densities

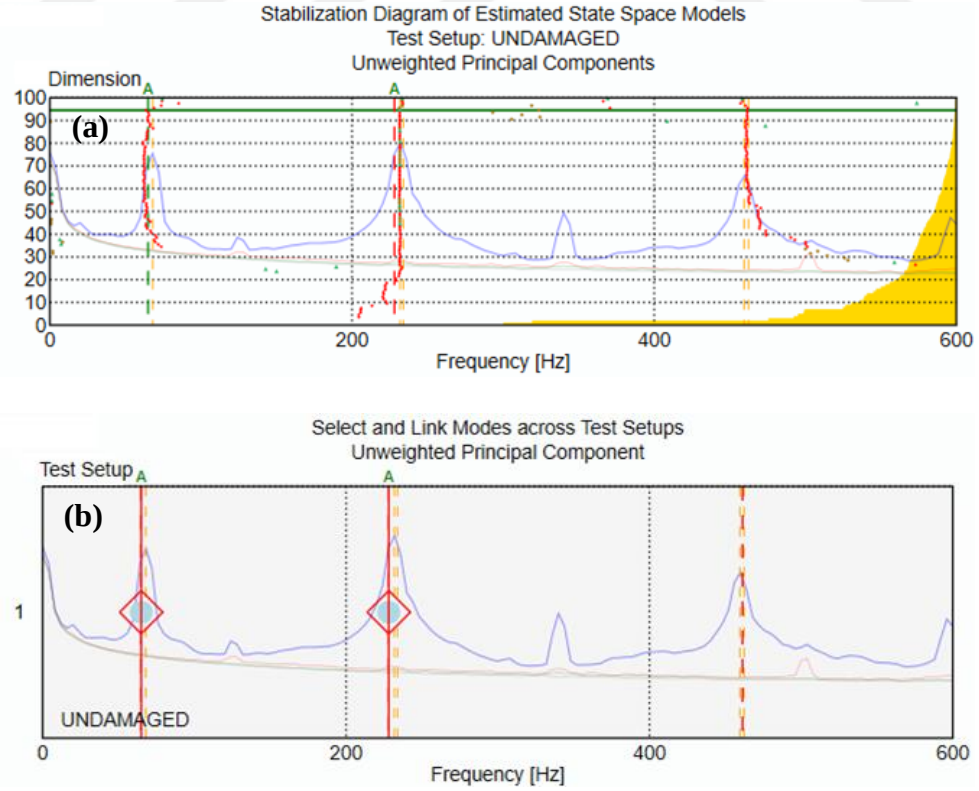


Figure 34. The undamaged state (a) the stabilization diagram and (b) the singular values diagram

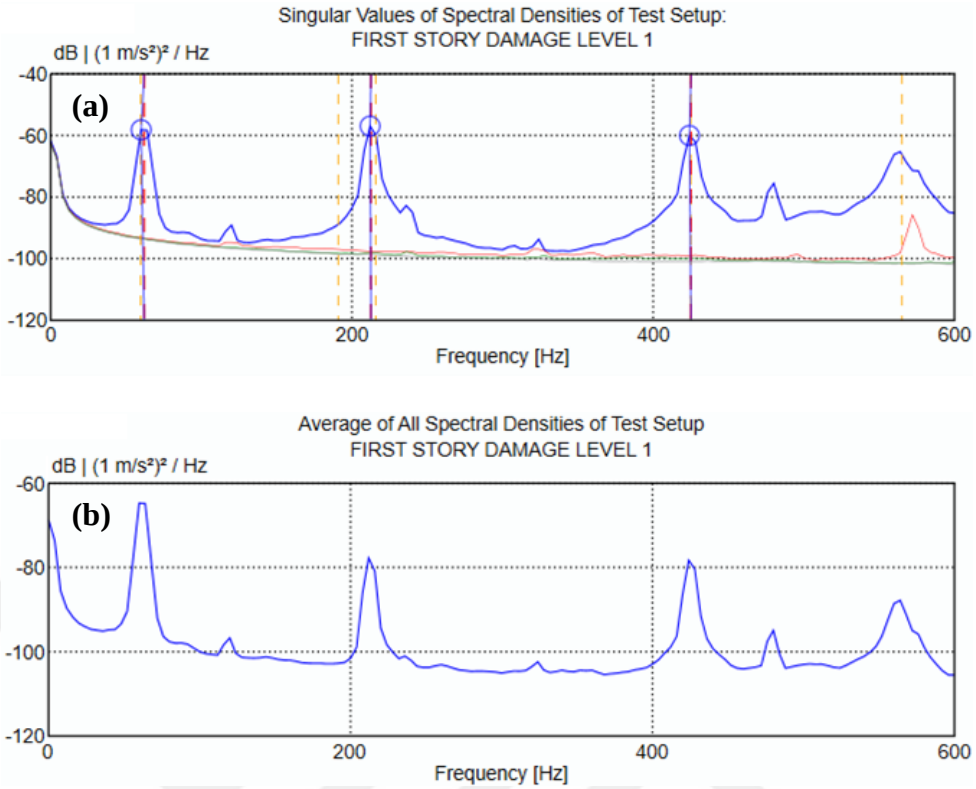


Figure 35. The first story level 1 damage (a) singular values of spectral densities and (b) the average of all spectral densities

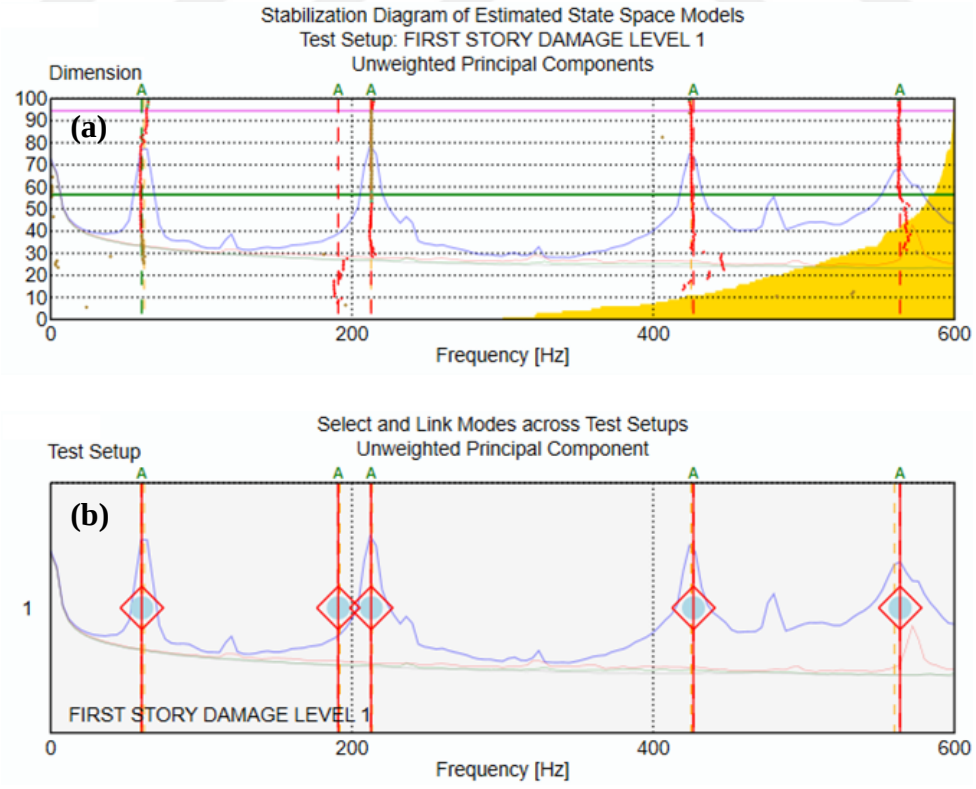


Figure 36. The first story level 1 damage (a) the stabilization diagram and (b) the singular values diagram

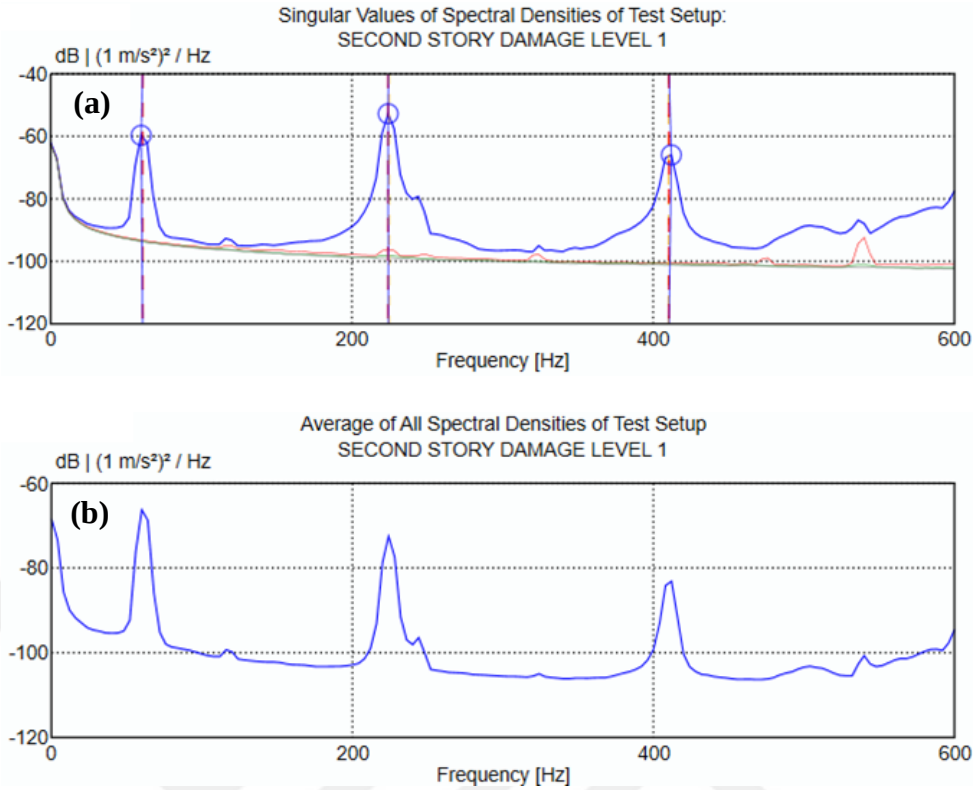


Figure 37. The second story level 1 damage (a) singular values of spectral densities and (b) the average of all spectral densities

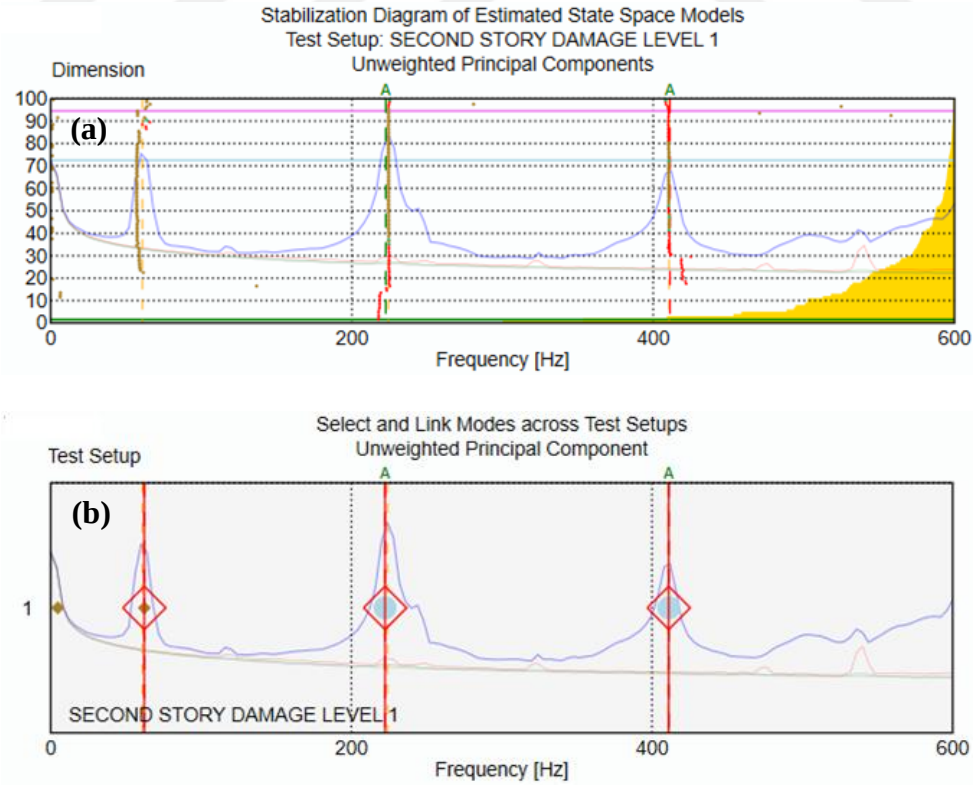


Figure 38. The second story level 1 damage (a) the stabilization diagram and (b) the singular values diagram

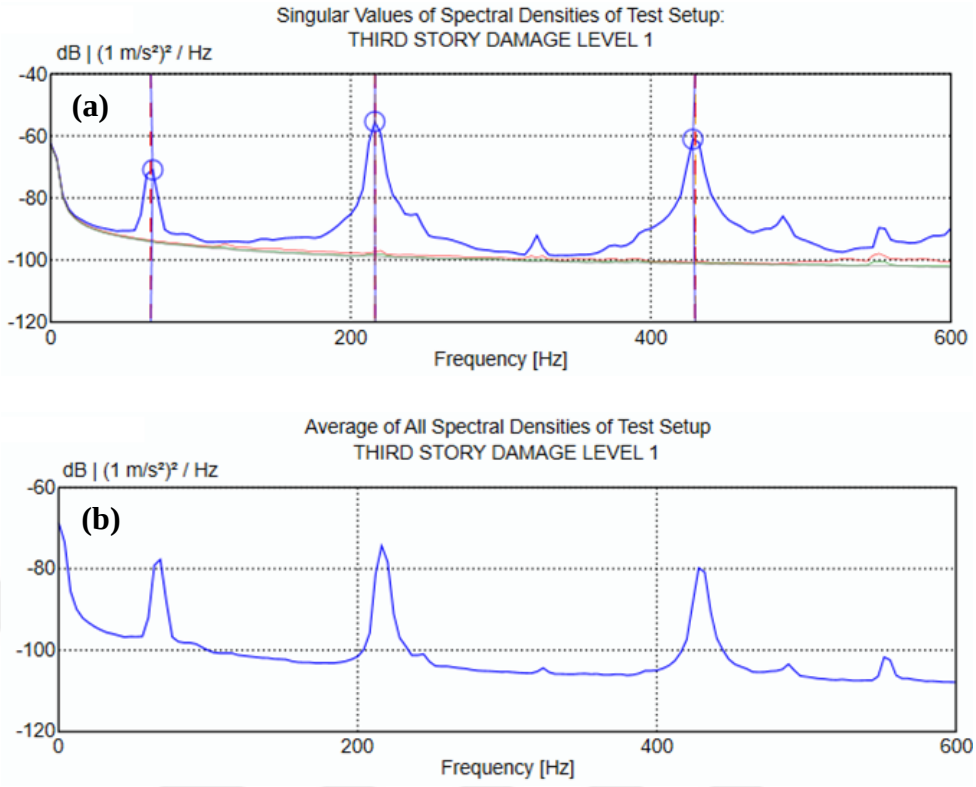


Figure 39. The third story level 1 damage (a) singular values of spectral densities and (b) the average of all spectral densities

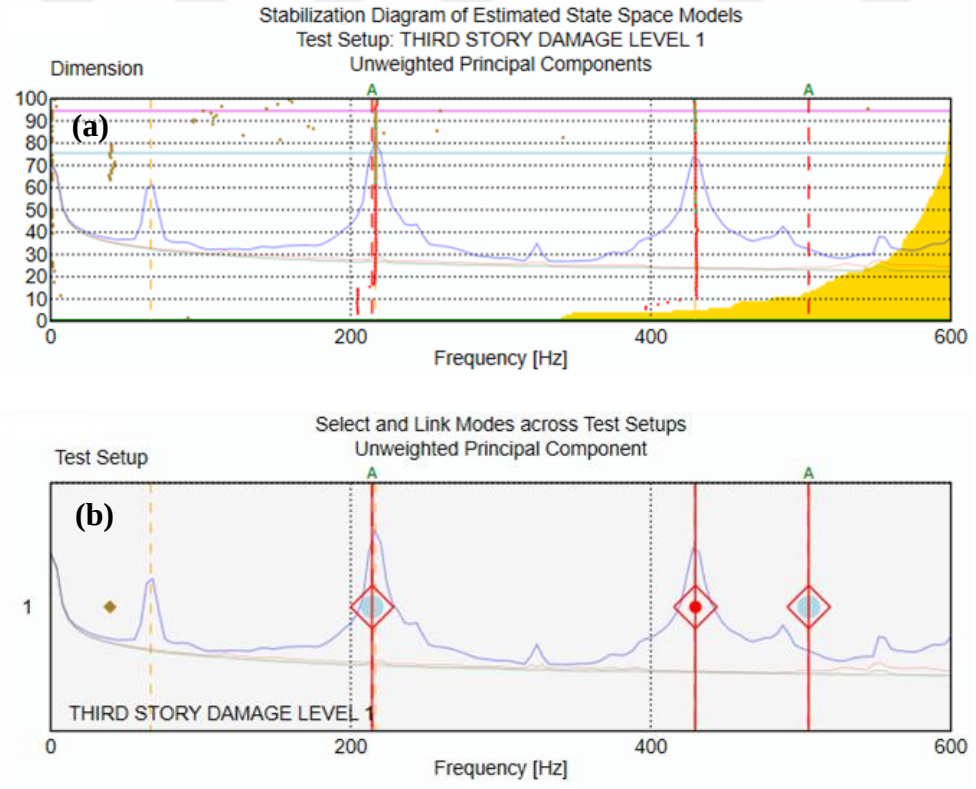


Figure 40. The third story level 1 damage (a) the stabilization diagram and (b) the singular values diagram

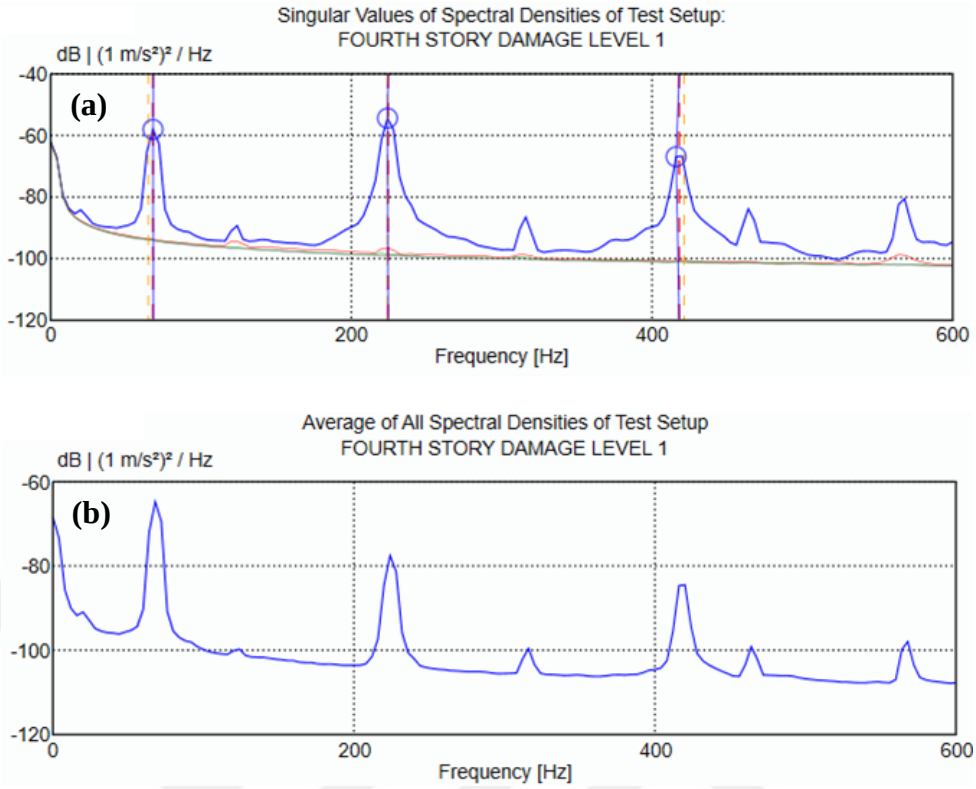


Figure 41. The fourth story level 1 damage (a) singular values of spectral densities and (b) the average of all spectral densities

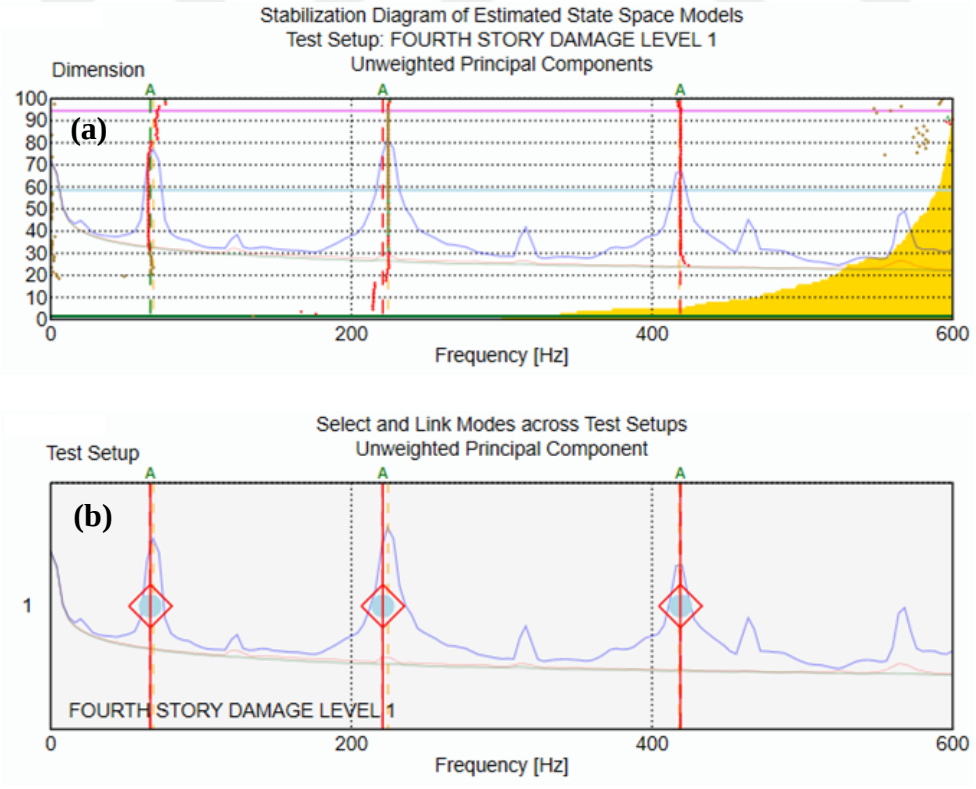


Figure 42. The fourth story level 1 damage (a) the stabilization diagram and (b) the singular values diagram

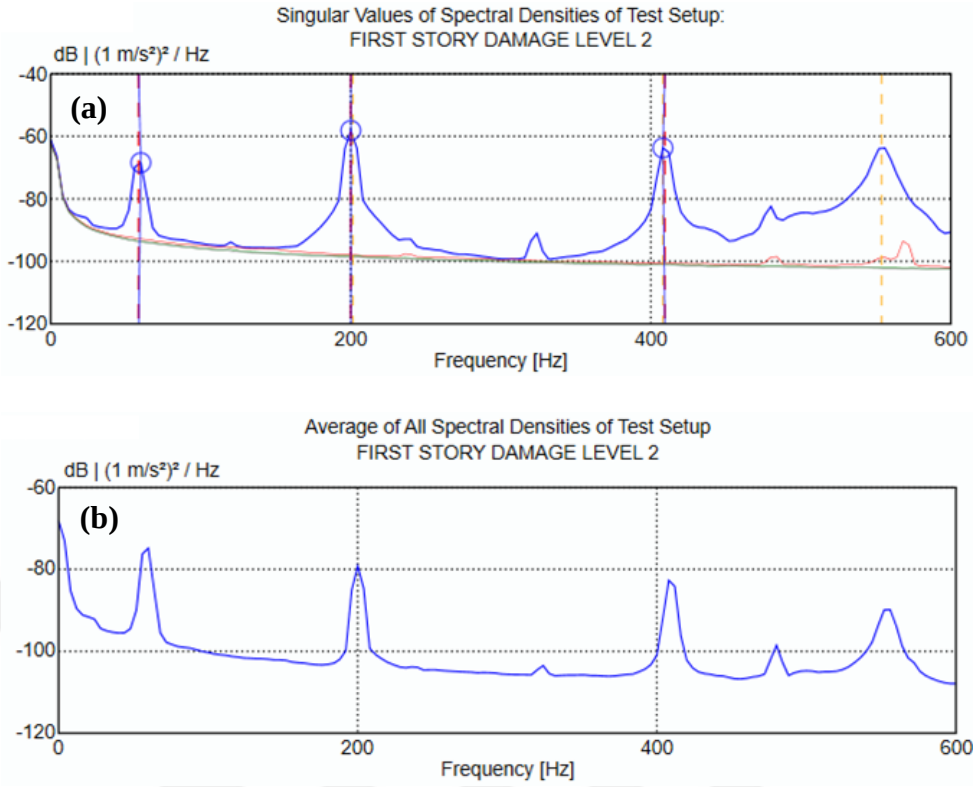


Figure 43. The first story level 2 damage (a) singular values of spectral densities and (b) the average of all spectral densities

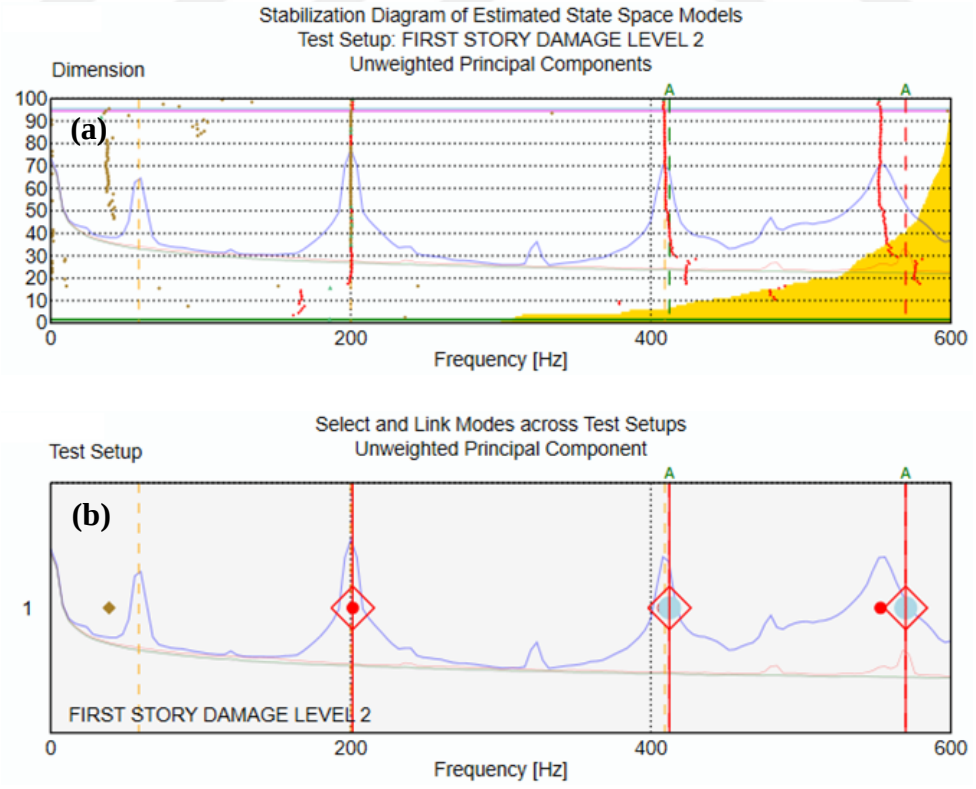


Figure 44. The first story level 2 damage (a) the stabilization diagram and (b) the singular values diagram

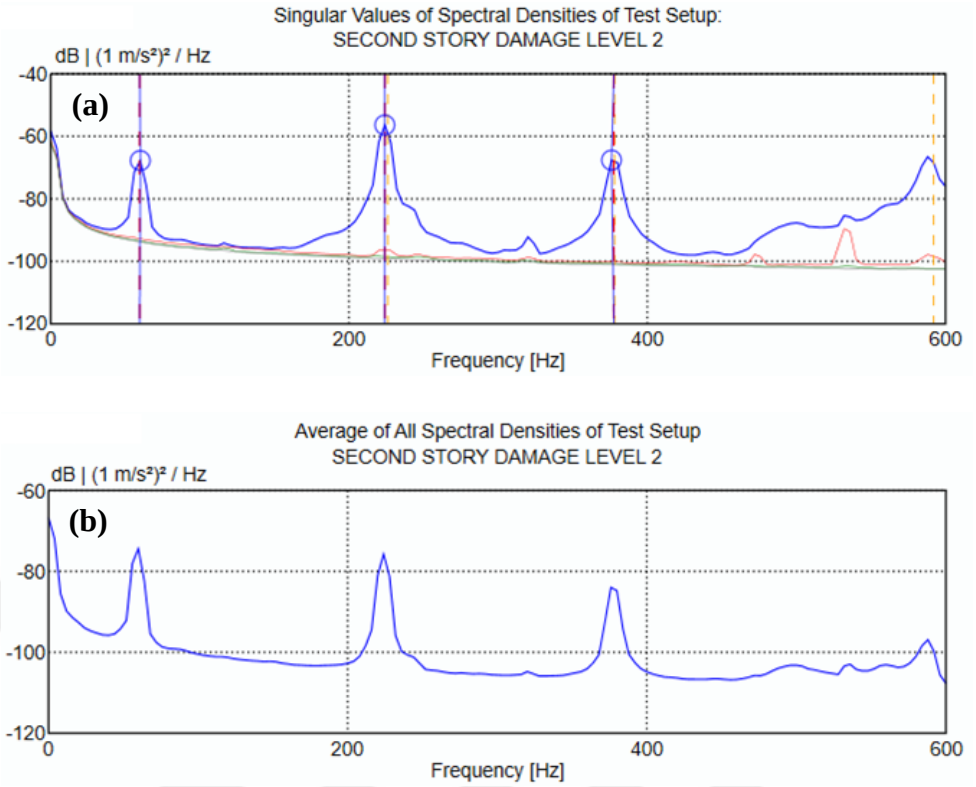


Figure 45. The second story level 2 damage (a) singular values of spectral densities and (b) the average of all spectral densities

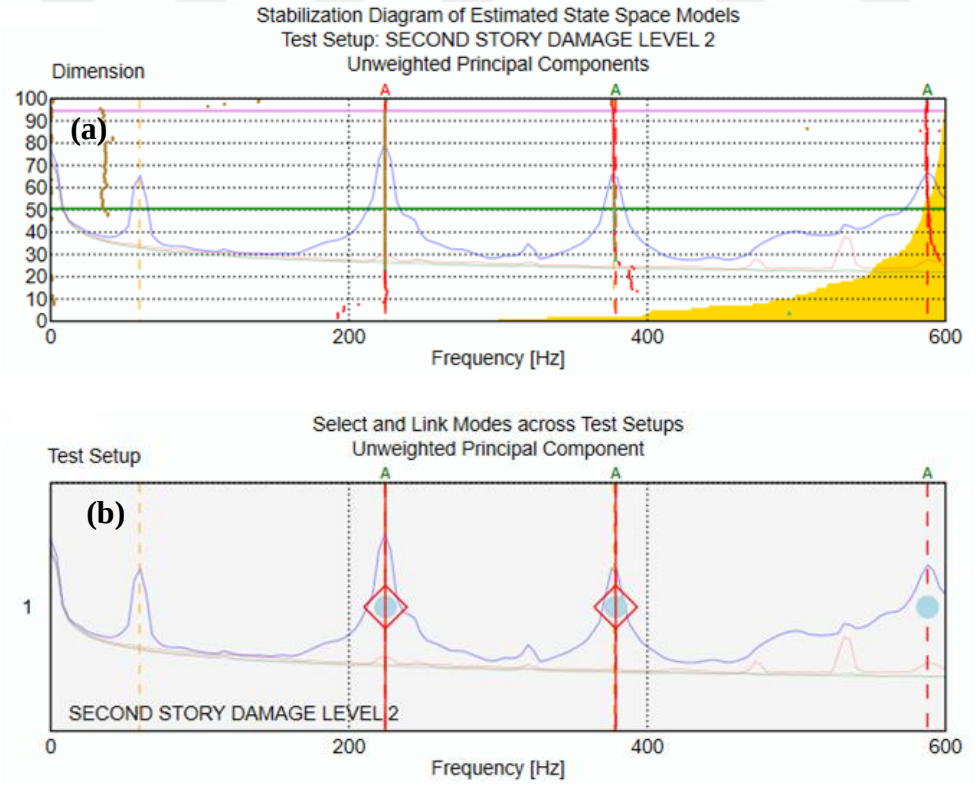


Figure 46. The second story level 2 damage (a) the stabilization diagram and (b) the singular values diagram

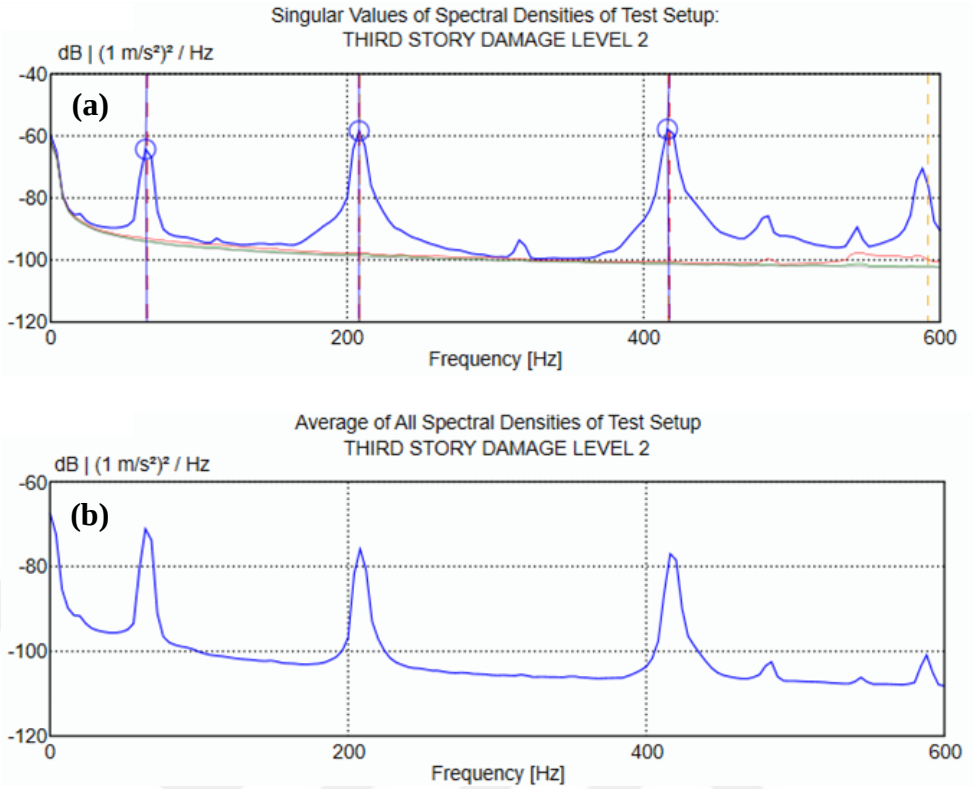


Figure 47. The third story level 2 damage (a) singular values of spectral densities and (b) the average of all spectral densities

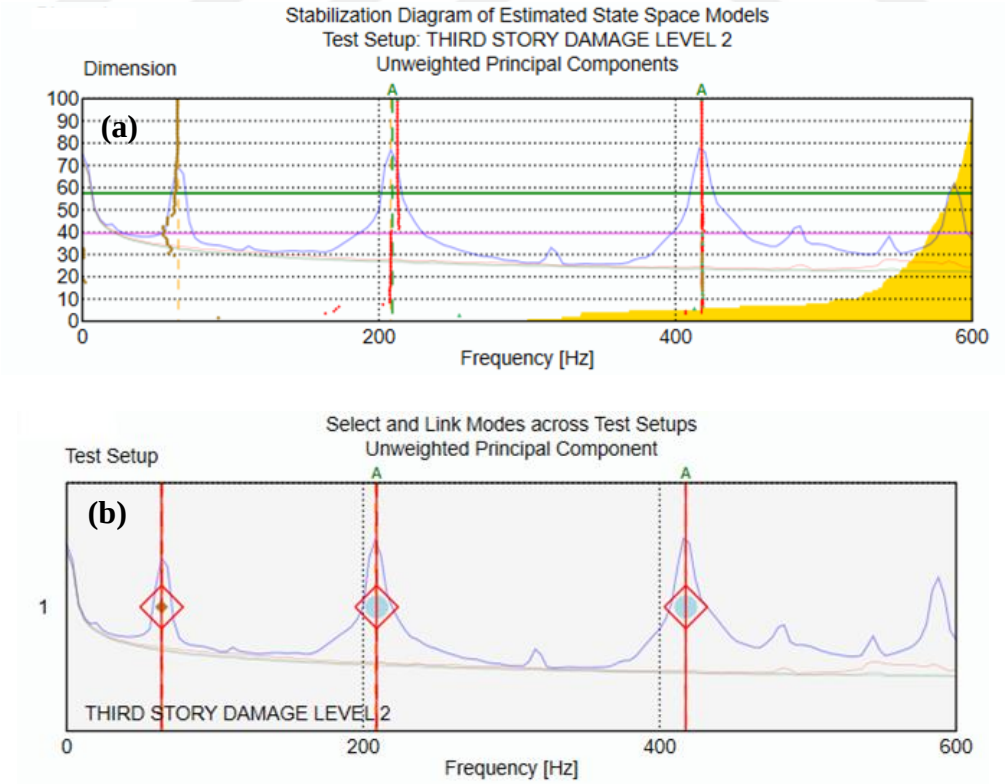


Figure 48. The third story level 2 damage (a) the stabilization diagram and (b) the singular values diagram

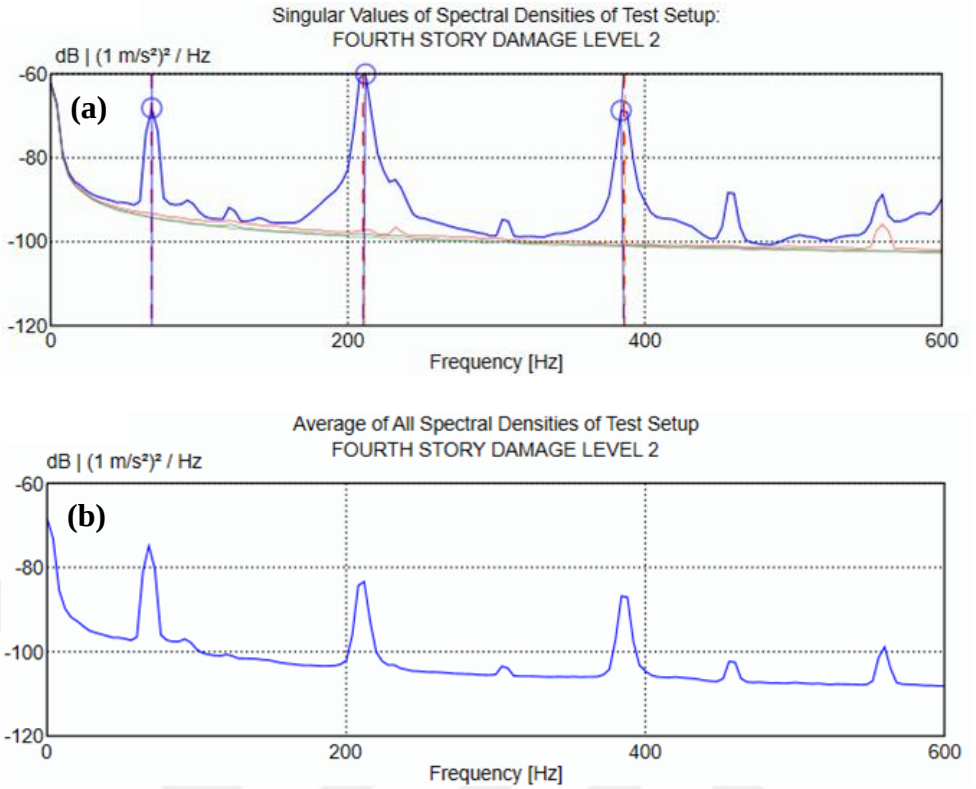


Figure 49. The fourth story level 2 damage (a) singular values of spectral densities and (b) the average of all spectral densities

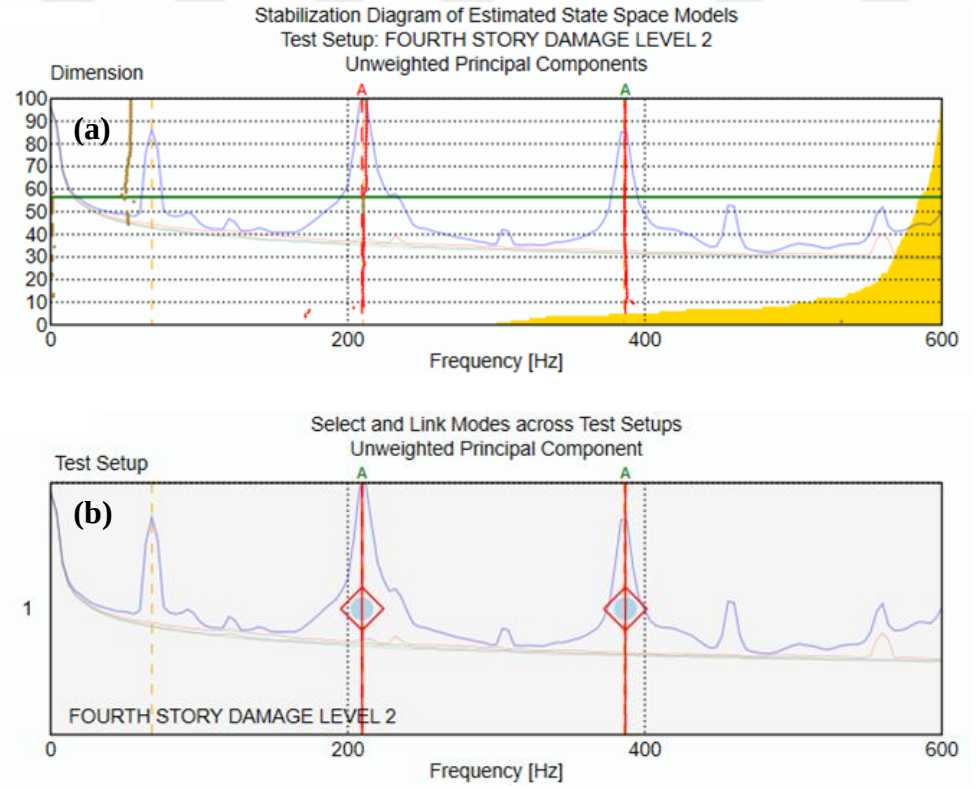


Figure 50. The Fourth story level 2 damage (a) the stabilization diagram and (b) the singular values diagram

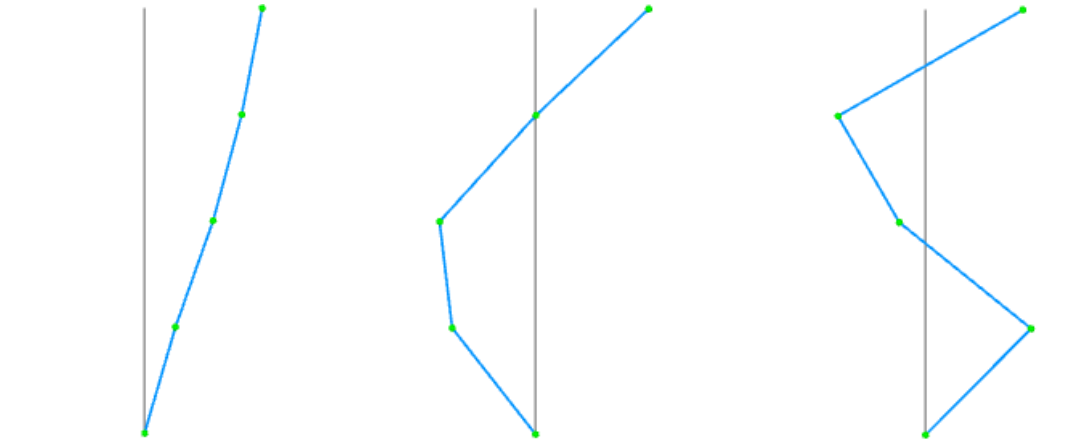

1st mode (67.958 Hz) 2nd mode (231.753 Hz) 3rd mode (459.544 Hz)

a) Undamaged

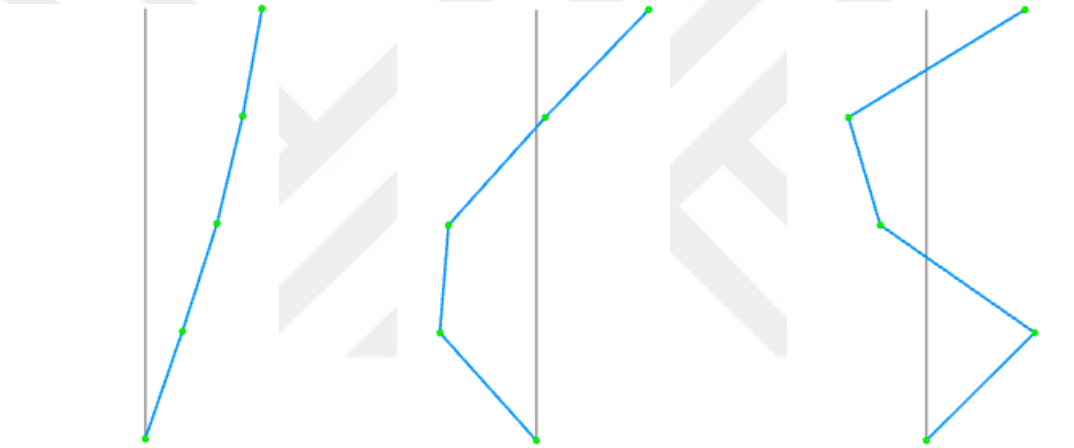

1st mode (61.911 Hz) 2nd mode (212.612 Hz) 3rd mode (425.015 Hz)

b) The first story level 1 damage

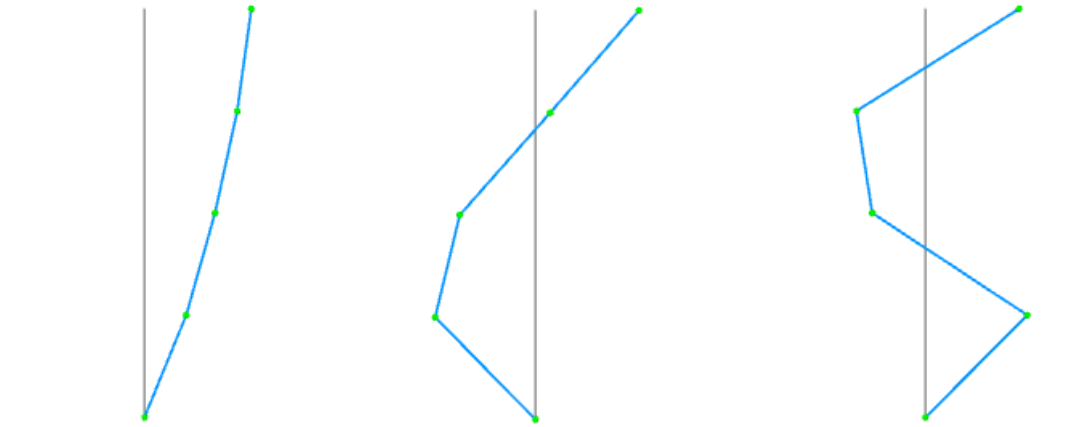

1st mode (58.66 Hz) 2nd mode (200.018 Hz) 3rd mode (409.331 Hz)

c) The first story level 2 damage

Figure 51. First three modes of all models obtained with EFDD

Figure 51. continued.

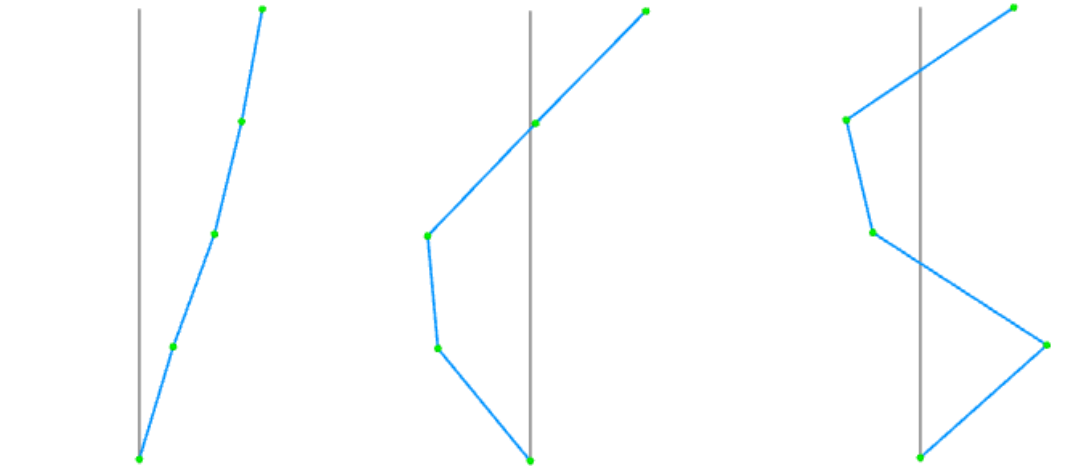

1st mode (60.955 Hz) 2nd mode (224.117 Hz) 3rd mode (410.526 Hz)

d) The second story level 1 damage

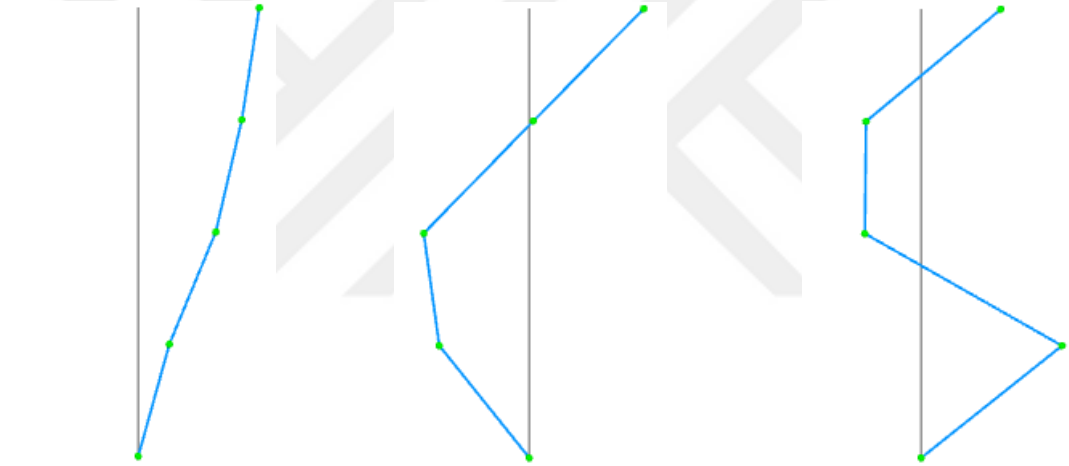

1st mode (59.674 Hz) 2nd mode (224.004 Hz) 3rd mode (377.608 Hz)

e) The second story level 2 damage

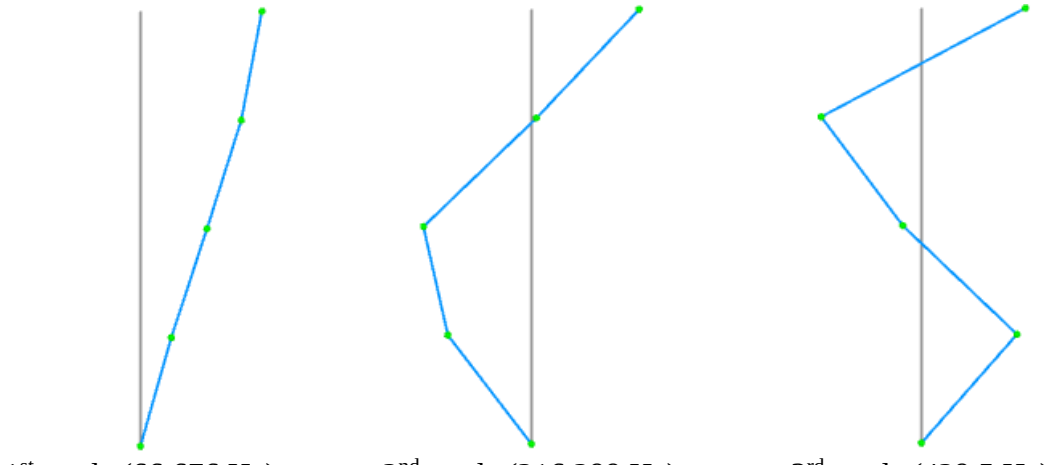

1st mode (66.676 Hz) 2nd mode (216.299 Hz) 3rd mode (429.5 Hz)

f) The third story level 1 damage

Figure 51. continued.

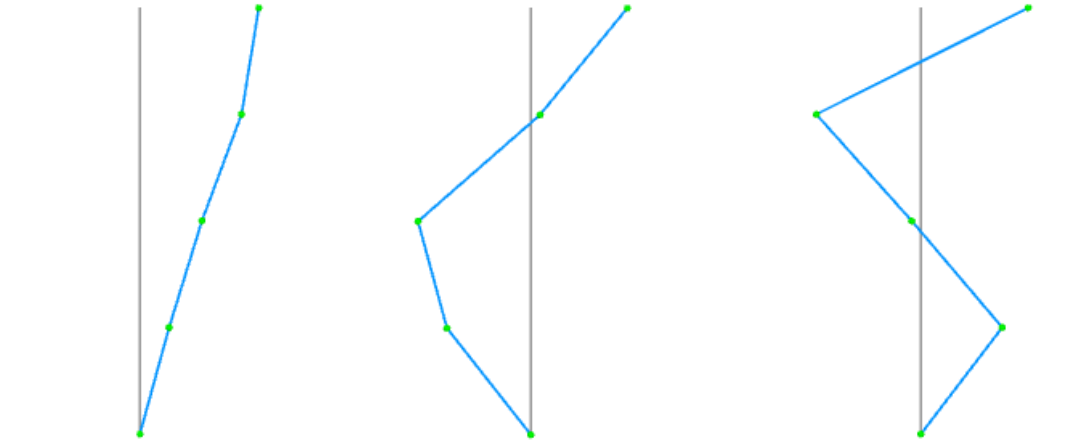

1st mode (64.868 Hz) 2nd mode (208.044 Hz) 3rd mode (417.284 Hz)

g) The third story level 2 damage

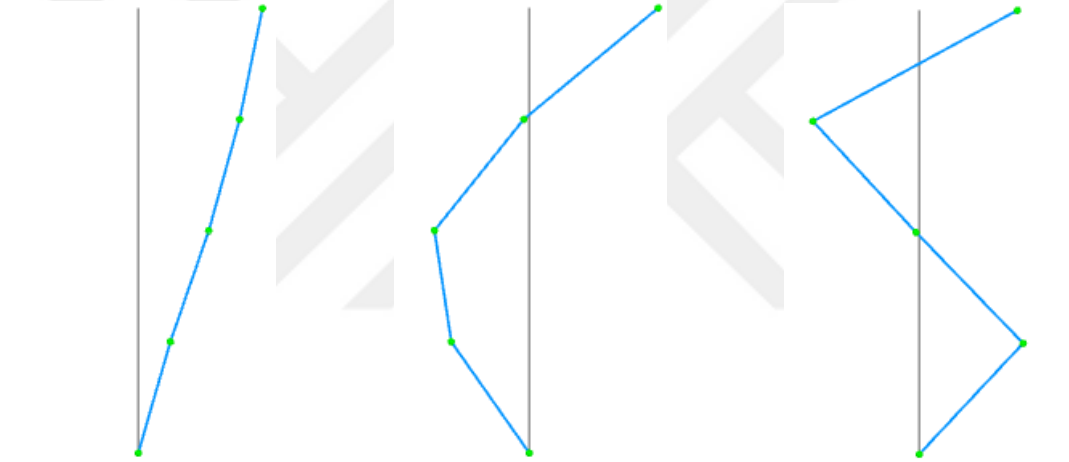

1st mode (68.164 Hz) 2nd mode (224.424 Hz) 3rd mode (418.054 Hz)

h) The fourth story level 1 damage

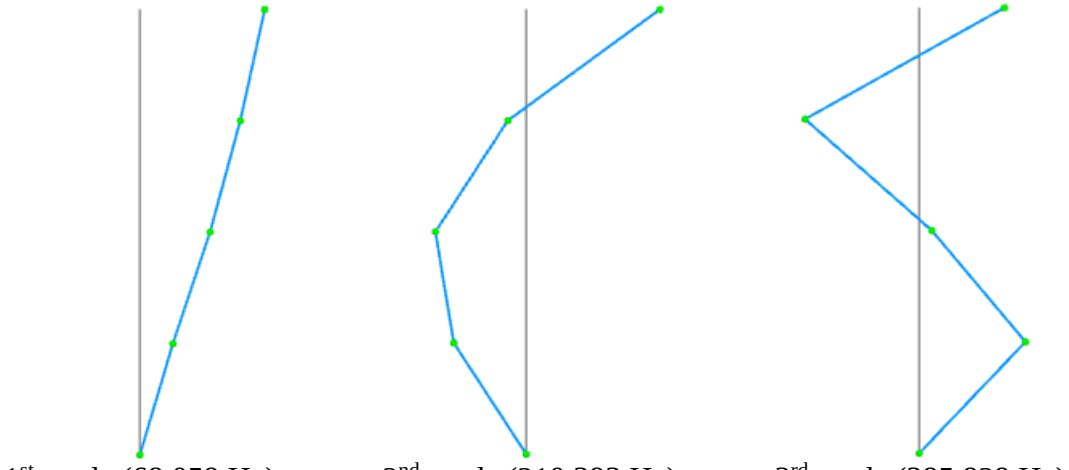

1st mode (68.059 Hz) 2nd mode (210.393 Hz) 3rd mode (385.829 Hz)

i) The fourth story level 2 damage

Table 4. Mode frequencies of steel frame models obtained with EFDD

| Mode Number | Initial State (Hz) | First Story Damage (Hz) | | Second Story Damage (Hz) | | Third Story Damage (Hz) | | Fourth Story Damage (Hz) | |
|---|---|---|---|---|---|---|---|---|---|
| | | Level 1 | Level 2 | Level 1 | Level 2 | Level 1 | Level 2 | Level 1 | Level 2 |
| 1 | 67.958 | 61.911 | 58.66 | 60.955 | 59.674 | 66.676 | 64.868 | 68.164 | 68.059 |
| 2 | 231.753 | 212.612 | 200.018 | 224.117 | 224.004 | 216.299 | 208.044 | 224.424 | 210.393 |
| 3 | 459.544 | 425.015 | 409.331 | 410.526 | 377.608 | 429.5 | 417.284 | 418.054 | 385.829 |
| Frequency Variation (%) | | | | | | | | | |
| 1 | 0 | -8.808 | -13.682 | -10.305 | -12.190 | -1.886 | -4.547 | +0.303 | +0.149 |
| 2 | 0 | -8.259 | -13.693 | -3.295 | -3.344 | -6.668 | -10.230 | -3.162 | -9.217 |
| 3 | 0 | -7.514 | -10.927 | -10.667 | -17.830 | -6.538 | -9.196 | -9.029 | -16.041 |

Table 5. Mode frequencies of steel frame models obtained with SSI

| Mode Number | Initial State (Hz) | First Story Damage (Hz) | | Second Story Damage (Hz) | | Third Story Damage (Hz) | | Fourth Story Damage (Hz) | |
|---|---|---|---|---|---|---|---|---|---|
| | | Level 1 | Level 2 | Level 1 | Level 2 | Level 1 | Level 2 | Level 1 | Level 2 |
| 1 | 65.015 | 63.654 | - | 62.26 | - | - | 63.975 | 66.289 | - |
| 2 | 228.129 | 212.88 | 201.321 | 224.311 | 224.449 | 216.523 | 212.424 | 220.948 | 209.57 |
| 3 | 461.406 | 425.221 | 408.237 | 410.074 | 378.879 | 429.71 | 417.687 | 418.865 | 386.911 |
| Frequency Variation (%) | | | | | | | | | |
| 1 | 0 | -2.138 | - | -4.328 | - | - | -1.634 | +2.001 | - |
| 2 | 0 | -6.684 | -11.751 | -1.674 | -1.613 | -5.087 | -6.884 | -3.148 | -8.135 |
| 3 | 0 | -7.842 | -11.523 | -11.125 | -17.886 | -6.869 | -9.475 | -9.220 | -16.145 |

Table 6. Damping ratios of steel frame models obtained with EFDD

| Mode Number | Initial State (%) | First Story Damage (%) | | Second Story Damage (%) | | Third Story Damage (%) | | Fourth Story Damage (%) | |
|---|---|---|---|---|---|---|---|---|---|
| | | Level 1 | Level 2 | Level 1 | Level 2 | Level 1 | Level 2 | Level 1 | Level 2 |
| 1 | 2.943 | 3.536 | 4.088 | 3.699 | 3.715 | 3.295 | 3.464 | 2.938 | 2.897 |
| 2 | 0.972 | 1.034 | 0.991 | 0.954 | 0.936 | 1.022 | 1.022 | 1.003 | 1.103 |
| 3 | 0.505 | 0.533 | 0.542 | 0.571 | 0.625 | 0.551 | 0.554 | 0.507 | 0.579 |

Table 6. continued.

| | | Ratio Variation (%) | | | | | | | |
|---|---|---|---|---|---|---|---|---|---|
| 1 | 0 | +20.15 | +38.906 | +25.688 | +26.232 | +11.961 | +17.703 | -0.17 | -1.563 |
| 2 | 0 | +6.379 | +1.955 | -1.852 | -3.704 | +5.144 | +5.144 | +3.189 | +13.477 |
| 3 | 0 | +5.545 | +7.327 | +13.069 | +23.762 | +9.109 | +9.703 | +0.396 | +14.653 |

### 2.3.5. MPR Variations and Damage Identification

MPR is a parameter created to effectively present the participation of a measurement point or degree of freedom in a structure's behavior along with the participation of each mode. MPR differs from the modal participation mass ratio because its approach includes the effect of measurement points or DOFs in addition to mode participations. It is an output of dynamic characterization as natural frequency, mode shape and damping ratio. Therefore, through a study of the MPR variation, damage identification can be performed. For this reason, numerical and experimental dynamic characterization of the steel frame model has been carried out and the MPR variations caused by different damage scenarios were examined. In order to determine the effectiveness of MPR as a damage parameter, eight damage scenarios which are combinations of four different locations and two different damage severity levels were taken into consideration. Then, changes were studied to establish a relation between the MPR values and damage. It has been mentioned earlier that the other mode MPR variations were not as easy to interpret as the first mode MPR variations to perform the damage identification. MPR values of the first mode provided the information from which a reliable assessment can be made for the damage presence and location. Since the MPR variations of the first mode showed great potential for damage identification, this part of the study is focused on the first mode MPR variations in detail. 4 MPR values were obtained for each model. $MPR_1^1$, $MPR_1^2$, $MPR_1^3$ and $MPR_1^4$ values are MPR values of the first mode at first, second, third and fourth DOF, respectively.

### 2.3.5.1. MPR Variations of Numerical Study

In this section, MPR values obtained through processing the dynamic responses of the FE model are presented. White noise acceleration is used in transient analysis to excite steel frame in order to create dynamic responses. Then, by using these dynamic responses as stated in the methodology section, MPR values were derived. User-defined filtering value is assumed to be 1. MPR values of undamaged and damaged models are shown in Figure 52.

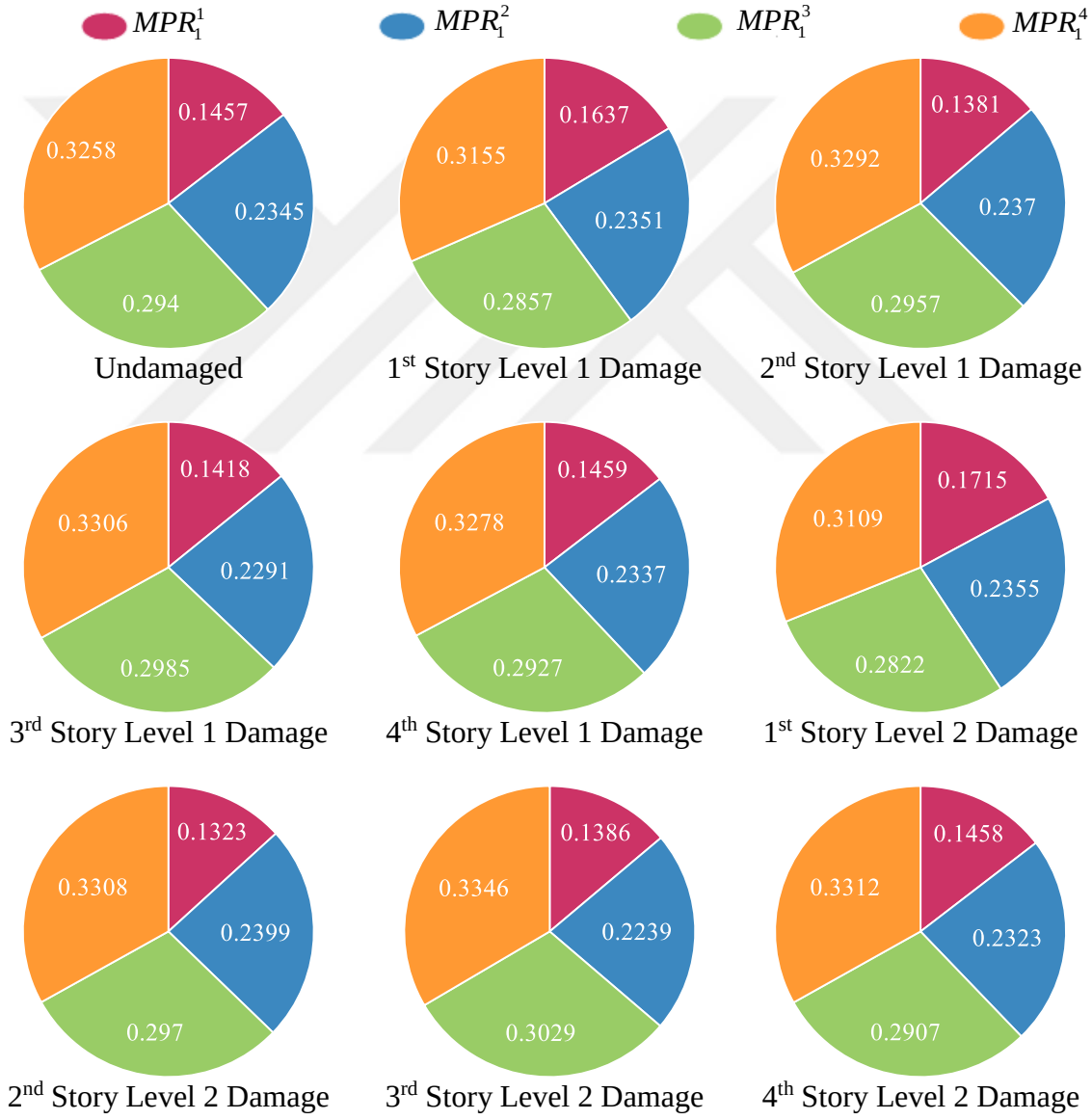


Figure 52. MPR values of undamaged and damaged FE models

MPR value changes ($\Delta MPR$) caused by first level damages are presented below in Figure 53. As mentioned earlier the location of the damage can be found by determining the maximum MPR increase. For instance, in Figures 53(a), 53(b), 53(c) and 53(d) the $\Delta MPR$ value of damaged DOF was the biggest, and therefore the estimated damage location was at the first, second, third and fourth story, respectively. All of the location estimations were correct.

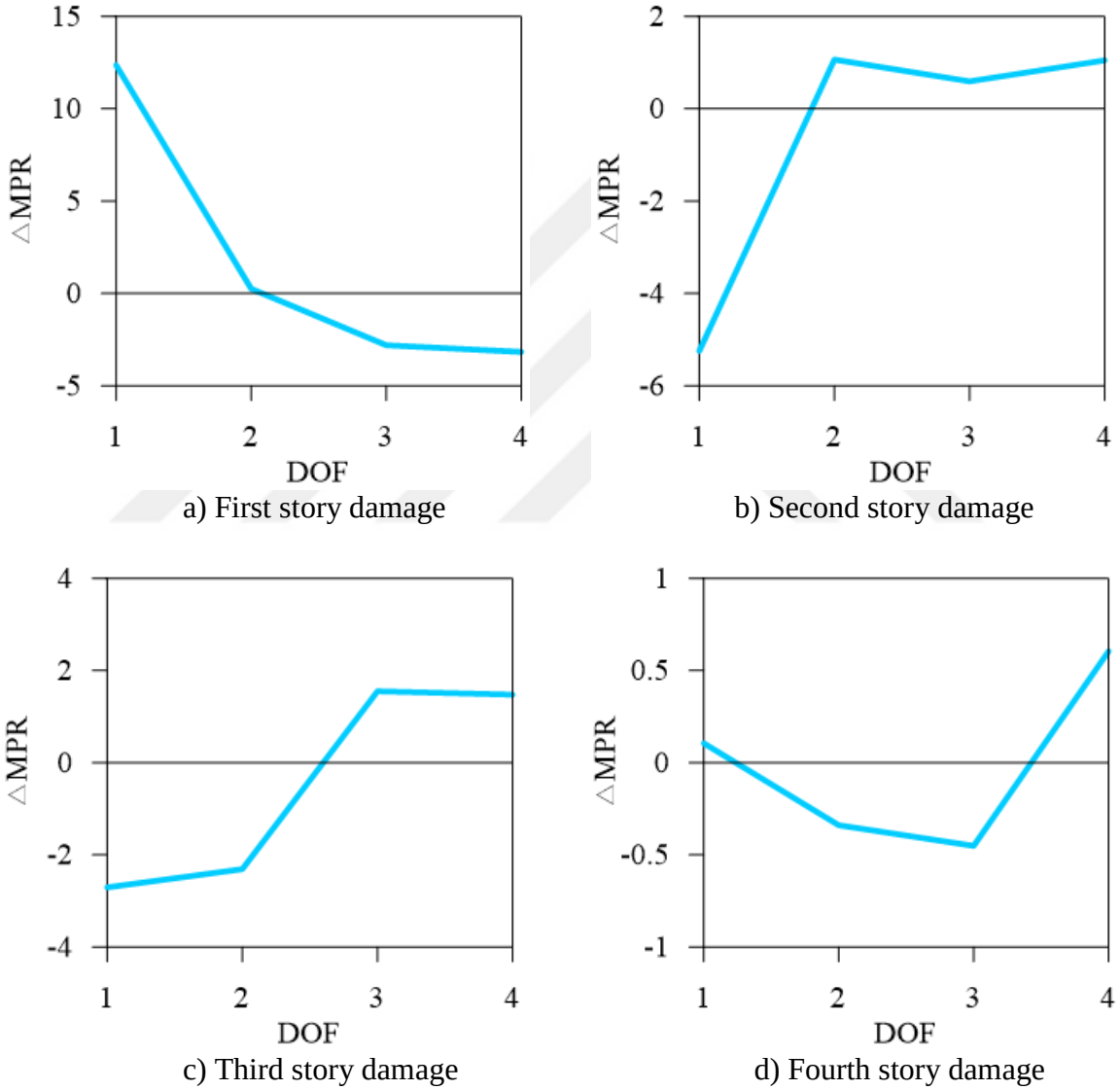


a) First story damage

b) Second story damage

c) Third story damage

d) Fourth story damage

Figure 53. MPR variations of numerical steel frame model

MPR variations for level 2 story damages are shown in Figure 54 along with the level 1 damages. Here, it is aimed to detect the same correlations of damage severity obtained in the numerical RC building model. It has been found that the increasing level of damage

severity results in bigger changes in all MPR values, especially the MPR of damaged DOF. As shown in Figure 54, each $\Delta MPR$ value moved further away from the zero axis with the increasing damage severity level. In other words, the presented parameter is sensitive to damage severity. And therefore, the severity of the damage can be determined using MPR values.

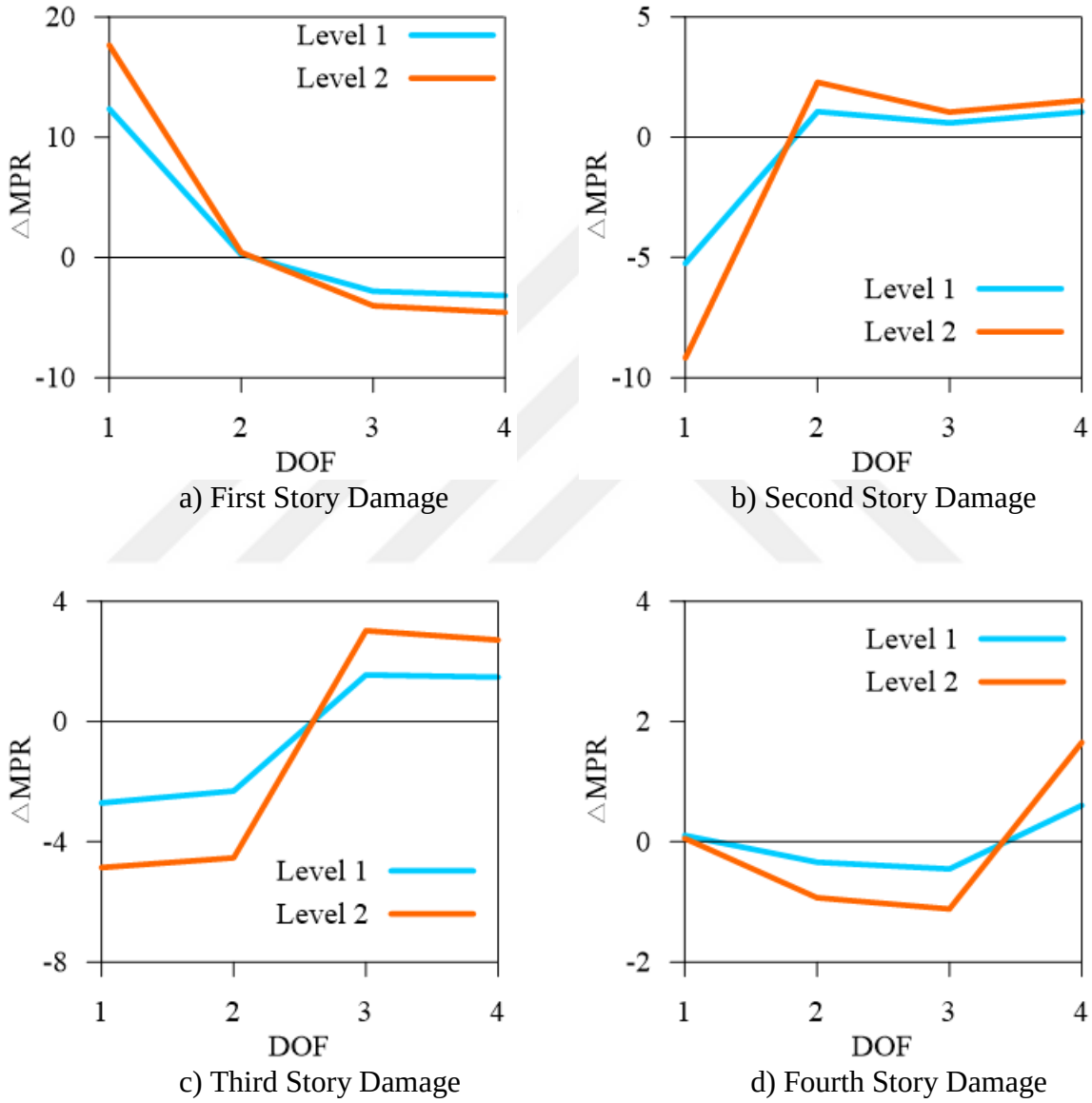


Figure 54. MPR variations of numerical steel frame for both severity levels

### 2.3.5.2. MPR Variations of Experimental Study

In this section, MPR values are obtained through acceleration measurements of the steel frame model. Accelerometers were utilized to collect the dynamic response of the steel frame in ambient conditions. Then, by using these dynamic responses as stated in the methodology section, MPR values were derived. User-defined filtering value is assumed to be 1, but MPR values were not convenient for damage identification. The reason for this behavior in the experimental study is that the acceleration measurement contains more noise data compared to numerical studies. Therefore, a method of filtering through the MAC rejection level is developed for a more reliable derivation of MPR values in experimental studies rather than using user-defined filtering values. Figure 55 shows the interval formed by the 0.9 MAC rejection level. The MAC rejection value varies between 0 and 1. The MAC rejection level searches both sides of the selected peak value for similarities. The search continues until the MAC value reaches the rejection level limits. A lower rejection level means that the final interval is wider (Rainieri et. al., 2007).

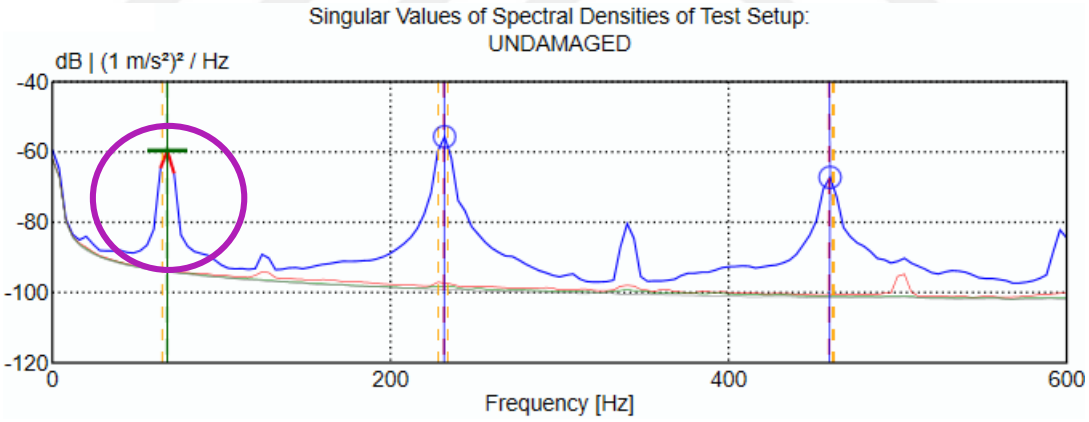


Figure 55. Interval of 0.9 MAC rejection level on singular values of spectral densities

The intervals given by different MAC rejections are shown in Figure 56. However, distances to the right and left from frequency values were uneven. Therefore distance to the closest limit is applied to the other side to obtain symmetrical filtering. Symmetrical filtering showed better results when compared to the $\Delta MPR$ obtained with unsymmetrical filtering.

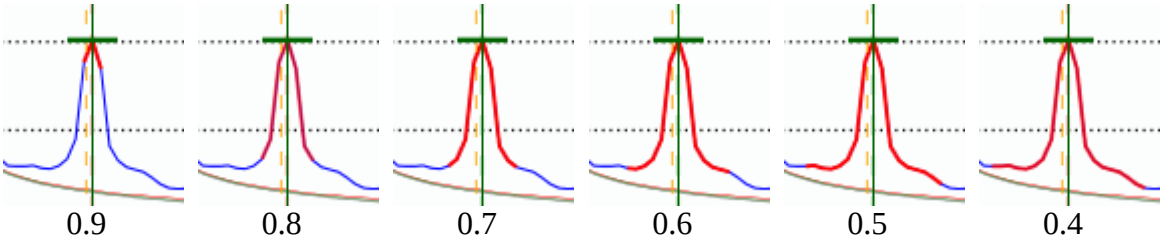


Figure 56. Intervals given by different MAC rejections

Equation 42 shows the calculation of filtering value $x_l$ where $x_{i(\min)}$ and $x_{i(\max)}$ denotes the start and the end values of interval for a specific MAC rejection level. The calculation is repeated as many times as the number of modes considered ( $n_m$ ).

$$x_l = \min\left\{\frac{f_i - x_{i(\min)}}{f_i}, \frac{x_{i(\max)} - f_i}{f_i}\right\} \quad i = 1 \; to \; n_m \tag{42}$$

The frequency domain data of each measurement point is divided into modes using Equation 43, where $f_i$ represents the natural frequency value of the $i$-th mode, and $f_i^r$ is the natural frequency value within the filtering range. From this, frequency domain data of each measurement point for each mode $U_i^j(f)$ is obtained.

$$U_i^j(f) = U^j(f_i^r) \; i = 1 \; to \; n_m \; , \; f_i \times (1 - x_l) \leq f_i^r \leq f_i \times (1 + x_l) \tag{43}$$

$x_{i(\min)}$ , $x_{i(\max)}$ and $x_l$ values for 0.4-0.9 MAC rejection levels of undamaged state are presented in Table 7. The first mode of the undamaged state was found at 67.958 Hz

Table 7. Filtering values for different MAC rejection levels

| Structural State | 1st Mode Frequency (Hz) | MAC Rejection Level | $x_{1(\min)}$ (Hz) | $x_{1(\max)}$ (Hz) | $x_l$ |
|---|---|---|---|---|---|
| Undamaged | 67.958 | 0.4 | 32 | 104 | 0.52912 |
| | | 0.5 | 36 | 100 | 0.47026 |
| | | 0.6 | 44 | 92 | 0.35254 |
| | | 0.7 | 52 | 84 | 0.23482 |
| | | 0.8 | 56 | 80 | 0.17596 |
| | | 0.9 | 64 | 72 | 0.05824 |

Table 7. continued.

| | | | | | |
|---|---|---|---|---|---|
| First Story Level 1 Damage | 61.911 | 0.4 | 28 | 92 | 0.48600 |
| | | 0.5 | 32 | 88 | 0.42140 |
| | | 0.6 | 40 | 80 | 0.29218 |
| | | 0.7 | 44 | 76 | 0.22757 |
| | | 0.8 | 52 | 68 | 0.09835 |
| | | 0.9 | 56 | 64 | 0.03374 |
| Second Story Level 1 Damage | 60.955 | 0.4 | 28 | 92 | 0.50931 |
| | | 0.5 | 32 | 88 | 0.44369 |
| | | 0.6 | 40 | 80 | 0.31244 |
| | | 0.7 | 44 | 76 | 0.24682 |
| | | 0.8 | 52 | 68 | 0.11558 |
| | | 0.9 | 56 | 64 | 0.04995 |
| Third Story Level 1 Damage | 66.676 | 0.4 | 32 | 104 | 0.52007 |
| | | 0.5 | 40 | 96 | 0.40008 |
| | | 0.6 | 44 | 92 | 0.34009 |
| | | 0.7 | 52 | 84 | 0.22011 |
| | | 0.8 | 56 | 80 | 0.16012 |
| | | 0.9 | 64 | 72 | 0.04013 |
| Fourth Story Level 1 Damage | 68.164 | 0.4 | 32 | 104 | 0.52573 |
| | | 0.5 | 40 | 96 | 0.40837 |
| | | 0.6 | 44 | 92 | 0.34969 |
| | | 0.7 | 52 | 84 | 0.23232 |
| | | 0.8 | 56 | 80 | 0.17364 |
| | | 0.9 | 64 | 72 | 0.05628 |
| First Story Level 2 Damage | 58.66 | 0.4 | 32 | 88 | 0.45448 |
| | | 0.5 | 40 | 80 | 0.31810 |
| | | 0.6 | 44 | 76 | 0.24991 |
| | | 0.7 | 48 | 72 | 0.18173 |
| | | 0.8 | 52 | 68 | 0.11354 |
| | | 0.9 | 56 | 64 | 0.04535 |
| Second Story Level 2 Damage | 59.674 | 0.4 | 36 | 84 | 0.39672 |
| | | 0.5 | 40 | 80 | 0.32969 |
| | | 0.6 | 44 | 76 | 0.26266 |
| | | 0.7 | 48 | 72 | 0.19563 |
| | | 0.8 | 52 | 68 | 0.12860 |
| | | 0.9 | 56 | 64 | 0.06157 |
| Third Story Level 2 Damage | 64.868 | 0.4 | 36 | 92 | 0.41826 |
| | | 0.5 | 40 | 88 | 0.35660 |
| | | 0.6 | 48 | 80 | 0.23327 |
| | | 0.7 | 52 | 76 | 0.17161 |
| | | 0.8 | 56 | 72 | 0.10995 |
| | | 0.9 | 60 | 68 | 0.04828 |
| Fourth Story Level 2 Damage | 68.059 | 0.4 | 44 | 92 | 0.35177 |
| | | 0.5 | 48 | 88 | 0.29300 |
| | | 0.6 | 52 | 84 | 0.23422 |
| | | 0.7 | 60 | 76 | 0.11668 |
| | | 0.8 | 60 | 76 | 0.11668 |
| | | 0.9 | 64 | 72 | 0.05791 |

Figure 57(a) shows the frequency domain data graph of the first DOF in the first story level 2 damage. And the first mode of frequency domain data obtained by filtering the

frequency data is shown in Figure 57(b). The filtering is performed using $x_l$ value calculated from the 0.9 MAC rejection level interval.

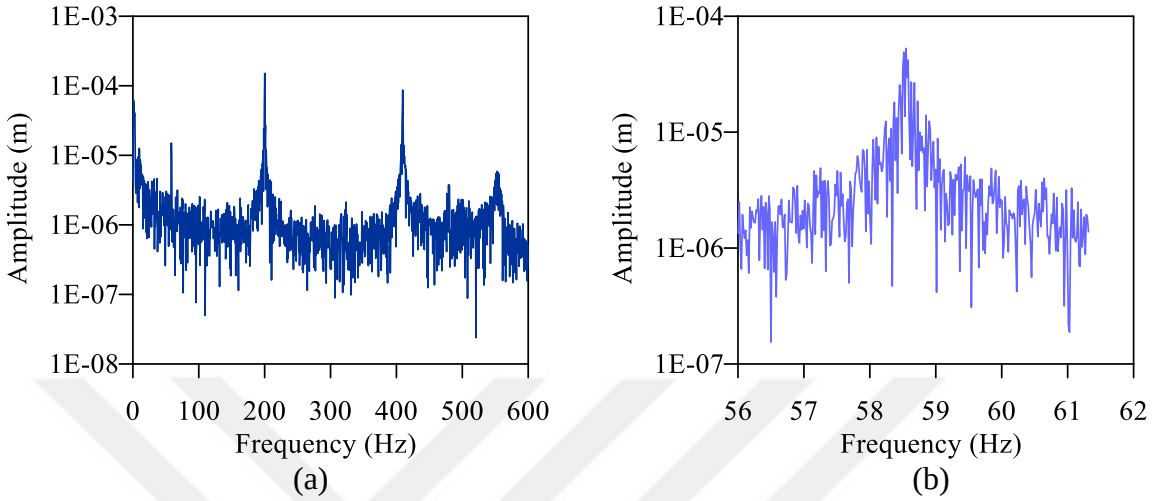


Figure 57. Graph of (a) frequency domain data and (b) the filtered first mode data of the first story second level damage

MPR values of undamaged and damaged models obtained with $x_l$ values derived from the 0.9 MAC rejection level are shown in Figure 58.

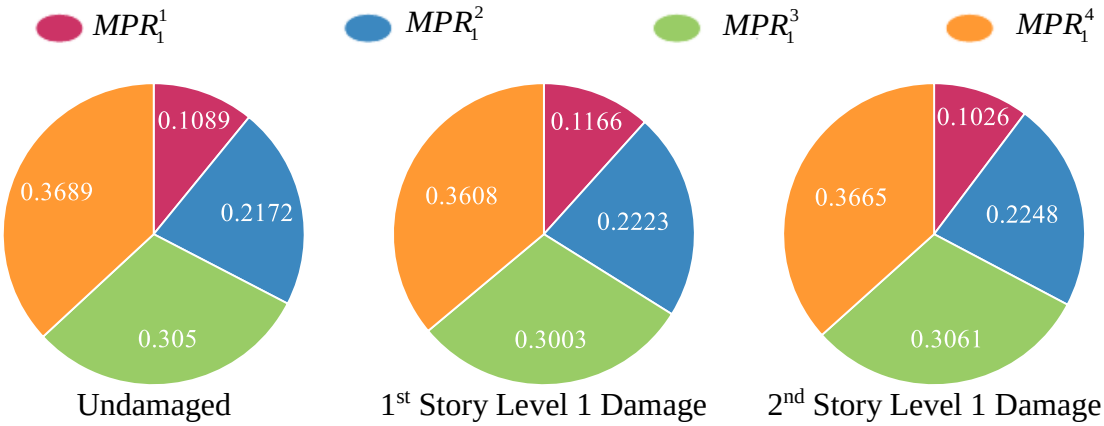


Figure 58. MPR values of frame models

Figure 58 continued.

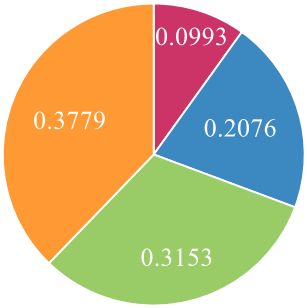


3rd Story Level 1 Damage

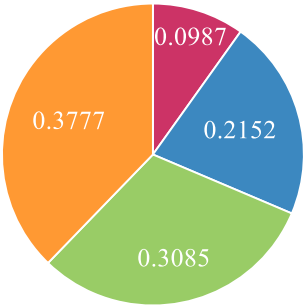


4th Story Level 1 Damage

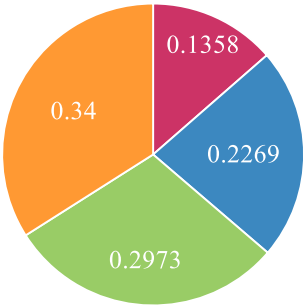


1st Story Level 2 Damage

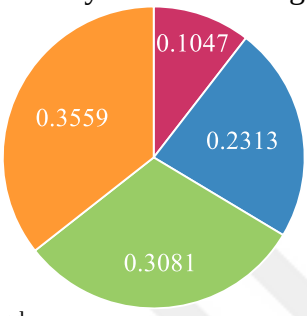


2nd Story Level 2 Damage

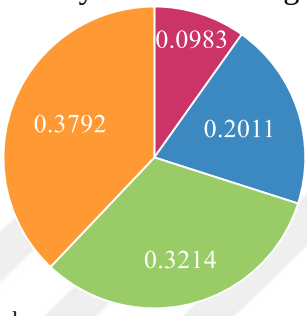


3rd Story Level 2 Damage

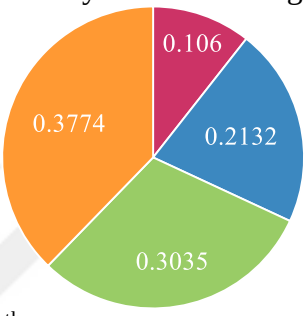


4th Story Level 2 Damage

MPR variations of each damage scenario with different $x_l$ values derived from different MAC rejection levels are shown in Figure 59.

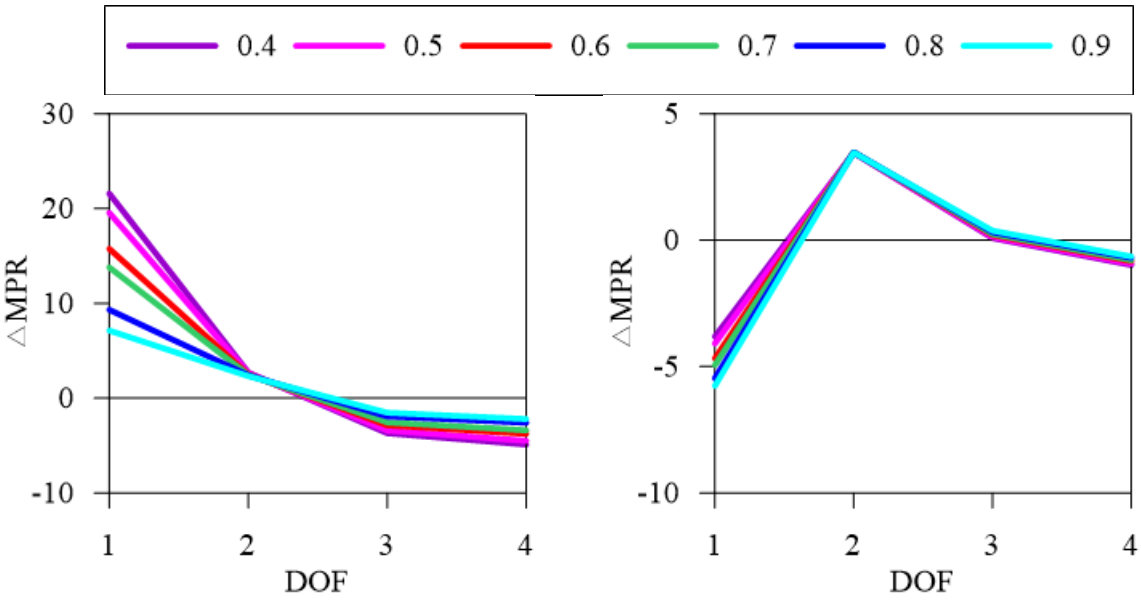


a) The First Story Level 1 Damage b) The Second Story Level 1 Damage

Figure 59. MPR variations of each damage scenario with different $x_l$ values derived from different MAC rejection levels

Figure 59. continued.

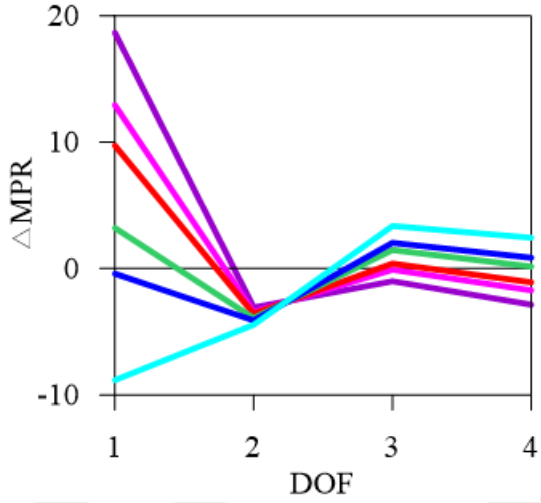


c) The Third Story Level 1 Damage

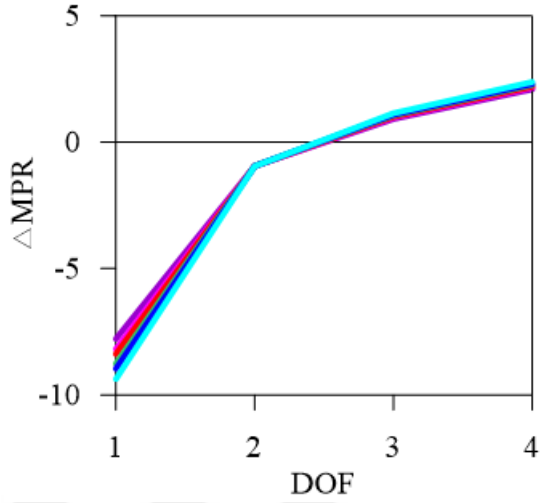


d) The Fourth Story Level 1 Damage

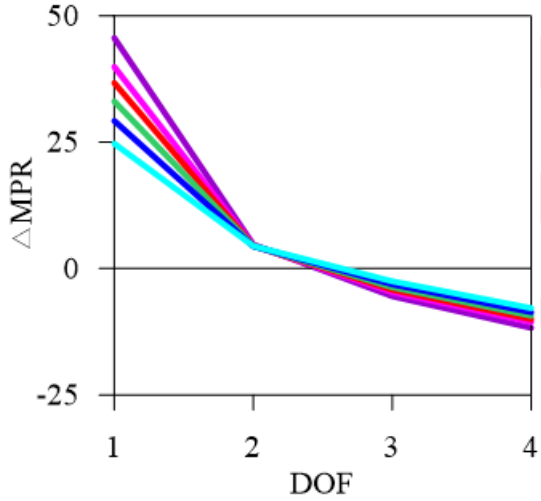


e) The First Story Level 2 Damage

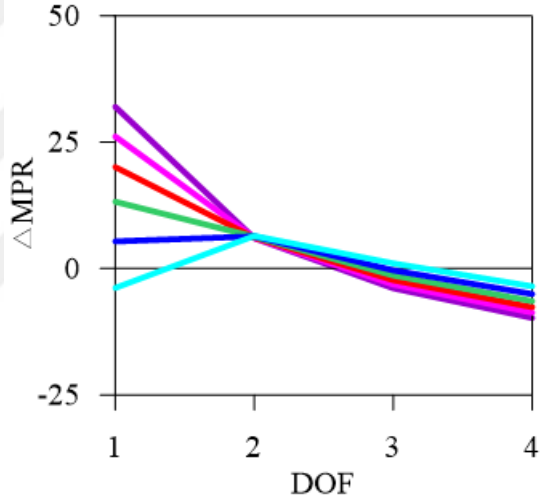


f) The Second Story Level 2 Damage

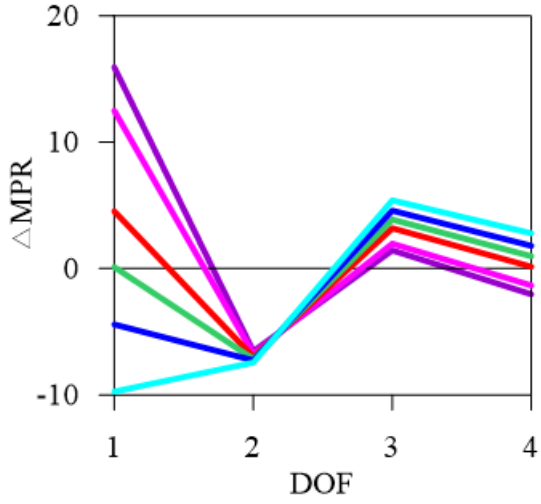


g) The Third Story Level 2 Damage

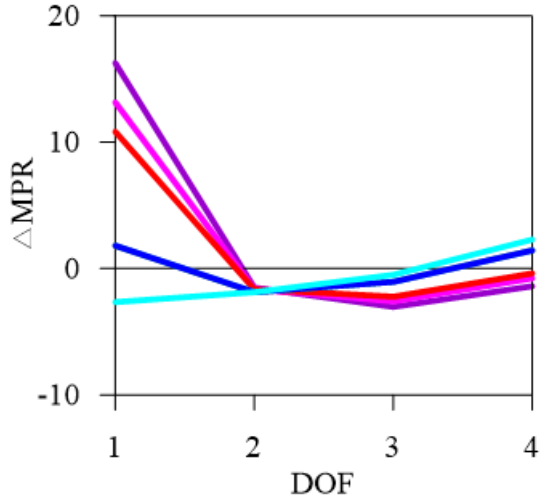


h) The Fourth Story Level 2 Damage

Different filtering values derived from different MAC rejection levels caused minimal changes in level 1 damage $\Delta MPR$ values. However, it was essential to pick smaller $x_l$ values derived from high MAC rejection levels in order to obtain more practical $\Delta MPR$ values. Therefore, $\Delta MPR$ values calculated through the 0.9 MAC rejection level are selected for damage identification. Figure 60 shows the MPR changes caused by the first level damages in different stories. Damage localization can easily be carried out because the highest MPR increase gives the location of the damaged DOF.

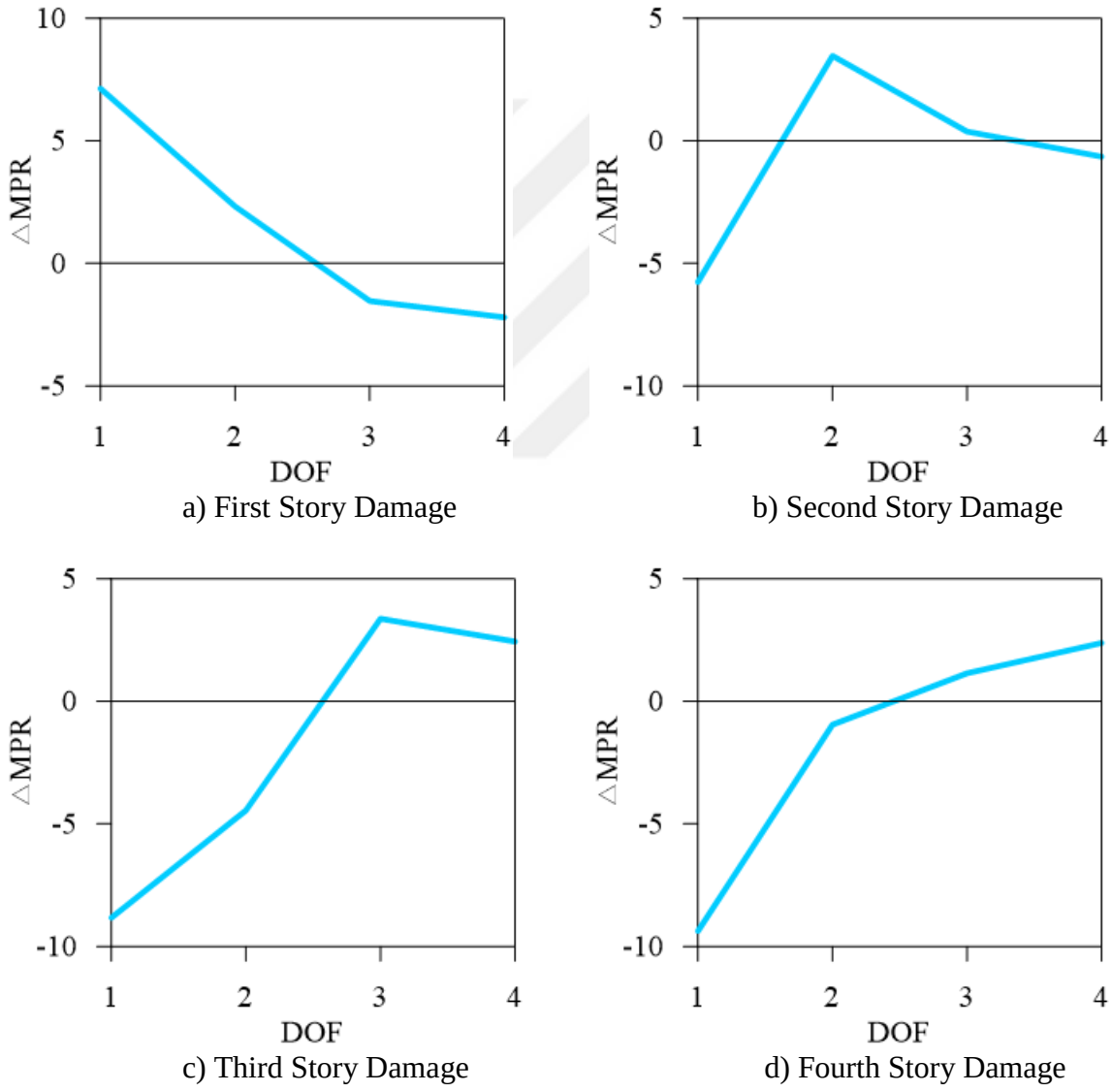


Figure 60. MPR variations obtained from experimental measurements of steel frame model

The MPR changes caused by first and second level damage scenarios are shown in Figure 61. Except for the fourth story damage, an increase in the damage severity was highly

effective on the increase of MPR value of the damaged DOF. Overall, damage localization was possible for each damage scenario, and damage quantification was available for all damage scenarios except for the fourth story damage.

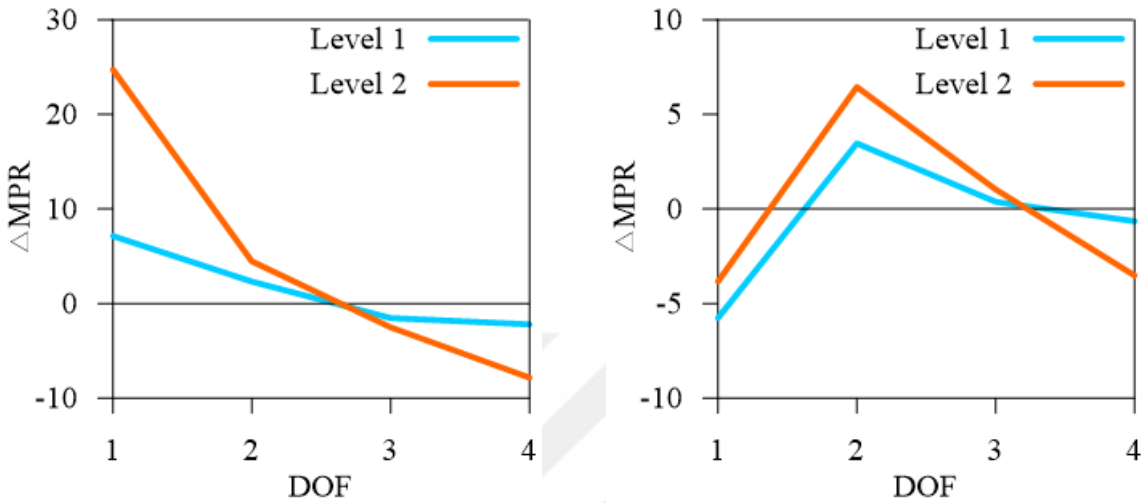


a) The First Story Damage




b) The Second Story Damage

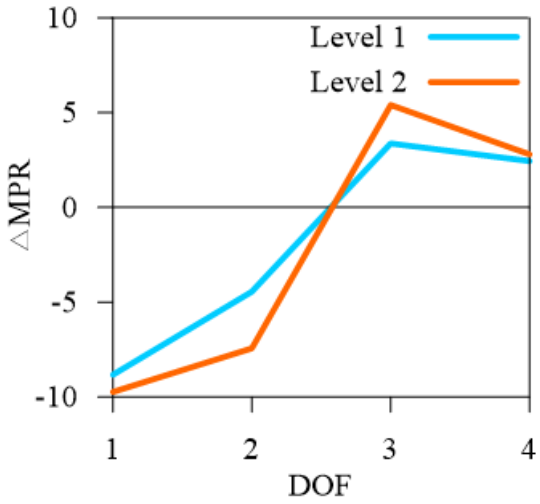


c) The Third Story Damage

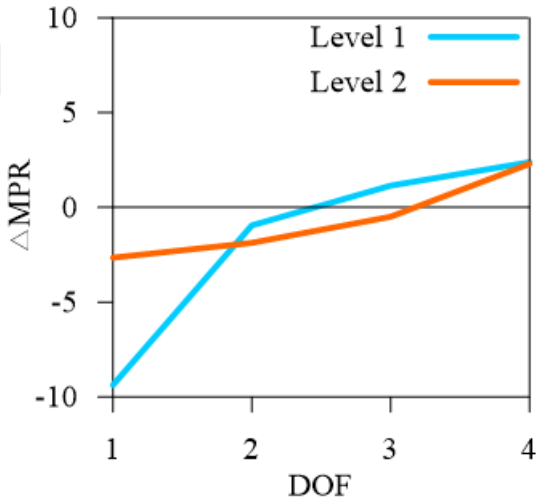


d) The Fourth Story Damage

Figure 61. MPR variations for both severity levels obtained from experimental measurements of steel frame model

### 2.3.6. Results and Discussion

The utilization of the MPR values in damage identification was numerically and experimentally evaluated based on changes caused by single story damage scenarios on the

steel frame model. The structural damage was simulated as a part cut. The results of this study can be summarised as stated below:

- ✓ The expected behavior of the natural frequencies was to decrease with damage occurrence. However, top story damages in both numerical and experimental studies caused natural frequency values to increase. In addition, the mode shapes derived from both studies did not show significant changes in the location and severity variation. Damping ratios were highly reactive to damage occurrence, but a favorable interpretation was not possible for damage identification. For these reasons, the damage presence, severity and location have not been evaluated based on these parameters.
- ✓ The MPR variations of the steel frame were calculated under the effect of part cut. Four MPR values of the first mode (one for each DOF) were evaluated for four different story damage locations and two different damage severity levels.

The Numerical Study of Steel Frame:

- ✓ Modal analysis was carried out for dynamic characterization of the numerical model. And the FE model of the steel frame was excited using white noise acceleration in order to obtain dynamic responses to be used in the MPR calculation. MPR of each structural state (undamaged and damaged) were obtained with a method presented by Park and Oh (2018).
- ✓ $\Delta MPR$ value of damaged DOF was the biggest among other MPR values of the first mode therefore MPR variation is determined to be feasible for the localization of damage. Also, $\Delta MPR$ was positive for DOFs above the damaged story meaning that the participation of that specific DOF also increased with damage. An increase in damage severity level resulted in bigger changes in the MPR values of each DOF. This means that the severity of the damage can easily be determined through this method.

The Experimental Study of Steel Frame:

- ✓ OMA was carried out to measure the acceleration responses of the model. EFDD and SSI methods were employed to determine dynamic characteristics such as natural frequency, mode shape and damping ratio. Measured data were used in the MPR derivation method, but the filtering procedure used in numerical studies was inefficient. User-defined $\gamma$ value requires in-depth knowledge of both structure and environmental conditions. Therefore, a determinate filtering technique was introduced. The technique utilizes intervals provided by different MAC rejection levels to

determine a definite filtering range. It is deduced that in order to obtain more precise MPR values, a smaller filtering range derived from a high MAC rejection level was necessary. Since a smaller filtering range excludes more data it was easier to get rid of noisy data caused by environmental conditions. However, a small filtering range requires precise determination of mode frequency.

- ✓ MPR values and variations obtained with a small filtering range were examined. Similar to numerical study, determination of damage location was possible through detection of the highest $\Delta MPR$ value. The DOF with the highest MPR increase was the damaged DOF. The severity of the damage had a direct proportion to MPR variation. The higher damage severity caused an increase in the $\Delta MPR$ value of the damaged DOF. However, unlike numerical studies, the increasing damage severity level did not cause all $\Delta MPR$ values to move further away from the zero axis.

Finally, based on the results of this case, it is concluded that the MPR variation was effective in both numerical and experimental damage identification. The MPR values provided information on the damage presence, severity and location. It should be noted, that the method requires knowledge of the initial condition of the structure because the method is based on a comparative approach. Moreover, the presented filtering technique can be utilized for structural health monitoring to determine rapid or long-term changes in structural state. For this reason, the numerical model of the monitored structure can also be used to determine the behavior of MPR values for different types of damage scenarios.

## 3. CONCLUSIONS

Within the scope of this thesis, the utilization of MPR values for damage identification was examined. An intensive numerical study on RC building is carried out to determine the capability of MPR variation for damage identification of single story and cumulative damage scenarios with varying damage severity levels. In addition, to test the applicability of the presented damage identification method, MPR values of steel frame models with single story damage scenarios were calculated both numerically and experimentally. The following conclusions can be drawn based on the numerical and experimental results of this study:

✓ MPR changes of the RC building model were calculated under the effect of stiffness reduction that represents the structural damage. The damage location and severity were adjusted to create single story and cumulative damage scenarios. Cumulative damage was studied to examine MPR changes under possible earthquake damage to the buildings, and single story damage scenarios were studied for a detailed examination of 16 MPR values consisting of a combination of 4 modes and 4 DOFs.

✓ Strong correlations between MPR variation and damage location as well as MPR variation and damage severity were created from these different damage types. MPR variation was effective in finding the damage location for both damage types. The severity of the damage was in direct proportion to MPR changes. Therefore, the quantification was practicable.

✓ MPR changes of the experimental steel frame model were calculated under the effect of part removal. OMA was carried out to measure dynamic responses and determine dynamic characteristics meanwhile FE model was utilized for numerical examination of MPR variations to the same effects.

✓ Results of the numerical study showed similarity to the RC building study in which the localization and quantification of the damage were practicable. However, a new technique of filtering was necessary to get rid of noise in experimental measurement data. Upon using this new technique, the filtering process is automated, and results were proved to be more reliable. Eventually, the MPR variations obtained from the experimental study were effective at localization and quantification of the damage.

## 4. RECOMMENDATIONS

In addition to all conclusions given above, the following recommendations may prove beneficial for further studies:

- Numerical study of building type structures with various numbers of stories, varying story heights and cross-sections can be studied. Therefore, the effect of varying story height and cross-section on the MPR variation would be determined.
- Combinations of different story damages can be studied both numerically and experimentally to determine the applicability of the method.
- In the experimental study, the damage given to the steel frame was a part cut. MPR variation for different damage patterns caused by effects such as earthquake, uneven settlement, and corrosion can be studied in order to validate the applicability of the MPR as a damage identification parameter.
- Studying larger-scale models would help determine the effectiveness of the presented method. Thus, MPR can be utilized in the health monitoring of large-scale structures.
- Models with different material types such as concrete and wood can be used to further investigate the MPR variation method.

## 5. REFERENCES


Adams, R.D., Cawley, P., Pye, C.J. and Stone, B.J., 1978. A Vibration Technique for Non-Destructively Assessing the Integrity of Structures, Journal of Mechanical Engineering Science, 20, 2, 93-100.

Adams, R.D., Walton, D., Flitcroft, J.E. ve Short, D., 1975. Vibration Testing as a Non-Destructive Test Tool for Composite Materials, Composite Reliability, ASTM STP 580, 159-175.

Altunışık, A.C., 2010. Karayolu Köprülerinin Yapısal Davranışlarının Analitik ve Deneysel Yöntemlerle Belirlenmesi, PhD Thesis, Karadeniz Technical University, Faculty of Science, Trabzon.

Altunışık, A.C., Okur, F.Y. and Kahya, V., 2017. Modal Parameter Identification and Vibration Based Damage Detection of a Multiple Cracked Cantilever Beam, Engineering Failure Analysis, 79, 154-170.

Bendat, J.S. ve Piersol, A.G., 2004. Random Data: Analysis and Measurement Procedures, 3th Edition, John Wiley and Sons, USA

BK Connect, 2021. Modular Analysis Software, Version 25.1, Hottinger Brüel & Kjaer A/S, Denmark.

Brincker, R., Zhang, L. and Andersen, P., 2001. Modal Identification of Output-Only Systems Using Frequency Domain Decomposition, Smart Materials and Structures, 10, 3, 441.

Brincker, R., Zhang, L. ve Andersen, P., 2000. Modal Identification from Ambient Responses using Frequency Domain Decomposition, 18th International Modal Analysis Conference, San Antonio, USA, 4062, 2, 625-630.

Cawley, P. ve Adams, R.D., 1979. The Location of Defects in Structures from Measurements of Natural Frequencies, Journal of Strain Analysis, 14, 2, 49-57.

Chopra, A.K., 2011. Dynamics of structures: Theory and applications to earthquake engineering, 4th ed. Prentice Hall, New Jersey

Cooley, J.W. and Tukey, J.W., 1965. An Algorithm for the Machine Calculation of Complex Fourier Series, Mathematics of Computation, 19, 90, 297-301.

Curadelli, R.O., Riera, J.D., Ambrosini, D. and Amani, M.G., 2008. Damage Detection by Means of Structural Damping Identification, Engineering Structures, 30, 12, 3497-3504.

Demir, S., Günaydin, M., Atmaca, B., Altunişik, A.C., Hüsem, M., Adanur, S., Angin, Z. and Ateş, Ş., 2021. Performance Evaluation of Reinforced Concrete Buildings

During the Sivrice-Elazığ Earthquake (M w= 6. 8, January 24, 2020) in Accordance with Turkish Earthquake Code. Journal of Earthquake and Tsunami, 15,4, 2150018.

Gade, S., 2006. Frequency Domain Techniques for Operational Modal Analysis, The Shock and Vibration Digest, 38, 6, 537-538.

Gallardo, J.A., Juan, C., Santa María, H. and Chacón, M.F., 2021. Damage and Sensitivity Analysis of a Reinforced Concrete Wall Building During the 2010, Chile Earthquake, Engineering Structures, 240, 112093.

Ghalishooyan, M., Shooshtari, A. and Abdelghani, M., 2019. Output-Only Modal Identification by in-Operation Modal Appropriation for Use with Enhanced Frequency Domain Decomposition Method, Journal of Mechanical Science and Technology, 33, 7, 3055-3067.

Günaydın, M., 2016. Onarılmış ve Lifli Polimer Kompozit Malzemelerle Güçlendirilmiş Betonarme Binaların Dinamik Davranışlarının Deneysel ve Analitik Yöntemlerle İncelenmesi, PhD Thesis, Karadeniz Technical University, Faculty of Science, Trabzon.

Heylen, W., Lammens, S. and Sas, P., 1997. Modal Analysis Theory and Testing, Vol. 200, Katholieke Universiteit Leuven, Leuven, Belgium.

Jacobsen, N.J., Andersen, P. ve Brincker, R., 2006. Using Enhanced Frequency Domain Decomposition as a Robust Technique to Harmonic Excitation in Operational Modal Analysis, Proceedings of ISMA2006, International Conference on Noise and Vibration Engineering, Leuven, Belgium.

Ju, F.D. and Mimovich, M.E., 1988. Experimental Diagnosis of Fracture Damage in Structures by the Modal Frequency Method. ASME J. Vibrat. Acoust. Stress Reliab Design 110, 456-463

Kam, T.Y. and Lee, T.Y., 1992. Detection of Cracks in Structures Using Modal Test Data, Engineering Fracture Mechanics, 42, 2, 381-387.

Khodabandehlou, H., Pekcan, G. and Fadali, M.S., 2019. Vibration-Based Structural Condition Assessment Using Convolution Neural Networks, Structural Control and Health Monitoring, 26,2, e2308.

Lee, Y.S. ve Chung, M.J., 2000. A Study on Crack Detection using Eigen frequency Test Data, Computers and Structures, 77, 327-342.

Liew, K.M. and Wang, Q., 1998. Application of Wavelet Theory for Crack Identification in Structures, Journal of Engineering Mechanics, 124, 2, 152-157.

Matlab, 2018. MATLAB and Statistics Toolbox Release 2018b, The MathWorks, Inc., Natick, Massachusetts, United States.

Mehboob, S., Zaman Khan, Q.U. and Ahmad, S., 2020. Numerical Study for Evaluation of a Vibration Based Damage Index for Effective Damage Detection, Bulletin of the Polish Academy of Sciences. Technical Sciences, 68, 6.

Mehrjoo, M., Khaji, N., Moharrami, H. and Bahreininejad, A., 2008. Damage Detection of Truss Bridge Joints Using Artificial Neural Networks, Expert Systems with Applications, 35, 3, 1122-1131.

Nikolakopoulos, P.G., Katsareas, D.E. and Papadopoulos, C.A., 1997. Crack Identification in Frame Structures, Computers and Structures, 64,1-4, 389-406.

Okur F., 2017. Mühendislik Yapılarında Analitik, Sayısal ve Deneysel Yöntemlere Dayalı Hasar Tespiti, Master of Science Thesis, Karadeniz Technical University, Faculty of Science, Trabzon.

Oppenheim, A.V., Buck, J.R. and Schafer, R.W., 2001. Discrete-Time Signal Processing, Vol. 2, Upper Saddle River, NJ: Prentice Hall.

Ovanesova, A.V. and Suarez, L.E., 2004. Applications of Wavelet Transforms to Damage Detection in Frame Structures, Engineering Structures, 26, 1, 39-49.

Pandey, A.K. ve Biswas, M. 1994. Damage Detection in Structures using Changes in Flexibility, Journal of Sound Vibration, 169, 1, 3-17.

Pandey, A.K., Biswas, M. ve Samman, M.M., 1991. Damage Detection from Changes in Curvature Mode Shapes, Journal of Sound and Vibration, 145, 2, 321-332.

Park, H.S. and Oh, B.K., 2018. Damage Detection of Building Structures Under Ambient Excitation Through the Analysis of the Relationship Between the Modal Participation Ratio and Story Stiffness, Journal of Sound and Vibration, 418, 122-143.

Park, H.S., Kim, J. and Oh, B.K., 2019. Model Updating Method for Damage Detection of Building Structures Under Ambient Excitation Using Modal Participation Ratio, Measurement, 133, 251-261.

Pawar, P.M., Venkatesulu Reddy, K. and Ganguli, R., 2007. Damage Detection in Beams Using Spatial Fourier Analysis and Neural Networks, Journal of Intelligent Material Systems and Structures, 18, 4, 347-359.

Peeters, B. and De Roeck, G., 1999. Reference-Based Stochastic Subspace Identification for Output-Only Modal Analysis, Mechanical Systems and Signal Processing, 13, 6, 855-878.

Prime, M.B. and Shevitz, D.W., 1995. Linear and nonlinear methods for detecting cracks in beams, 14th International Modal Analysis Conference, Michigan, US, 1437-1443.

PULSE, 2021. PULSE Operational Modal Analysis, Version 7.1., Structural Vibration Solution A/S, Denmark.

Radzieński, M., Krawczuk, M. and Palacz, M., 2011. Improvement of Damage Detection Methods Based on Experimental Modal Parameters, Mechanical Systems and Signal Processing, 25, 6, 2169-2190.

Rainieri, C., Fabbrocino, G. and Cosenza, E., 2007. Automated Operational Modal Analysis as Structural Health Monitoring Tool: Theoretical and Applicative Aspects. Key Engineering Materials, 347, 479-484.

Ramos, J.L.F.S., 2007. Damage Idendification on Masonry Structures Based on Vibration Signatures, PhD Thesis, University of Minho, Portugal.

Razak, H.A. and Choi, F.C., 2001. The Effect of Corrosion on the Natural Frequency and Modal Damping of Reinforced Concrete Beams, Engineering Structures, 23, 9, 1126-1133.

Rizos, P.F., Aspragathos, N. and Dimarogonas, A.D., 1990. Identification of Crack Location and Magnitude in a Cantilever Beam from The Vibration Modes, Journal of Sound and Vibration, 138, 3, 381-388.

Salawu, O.S. and Williams, C., 1995. Bridge Assessment Using Forced-Vibration Testing, Journal of Structural Engineering, 121, 2, 161-173.

SAP2000, 2021. Structural Analysis Program, Computers and Structures Inc., Berkeley, California, US.

Sevim, B., 2010. Kemer Barajlarının Dinamik Davranışlarının Sonlu Eleman ve Deneysel Modal Analiz Yöntemleriyle Belirlenmesi, PhD Thesis, Karadeniz Technical University, Faculty of Science, Trabzon.

Srinivasan, M.G. ve Kot, C.A., 1992. Effects of Damage on the Modal Parameters of Cylindrical Shell, 10th International Modal Analysis Conference, San Diego, US, 529- 535.

Stubbs, N., Kim, J.T. and Farrar, C.R., 1995. Field Verification of a Nondestructive Damage Localization and Severity Estimation Algorithm. Proceedings of the SPIE the International Society for Optical Engineering, SPIE International Society for Optical, 210-218.

Trifunac, M.D., 1972. Comparisons Between Ambient and Forced Vibration Experiments, Earthquake Engineering & Structural Dynamics, 1, 2, 133-150.

URL-1, www.bksv.com/en/knowledge/blog/vibration/piezoelectric-accelerometers Piezoelectric Accelerometers. 18 May 2022

URL-2, www.bksv.com/en/transducers/vibration/accelerometers/ccld-iepe/4507-b-005?tab=specifications TYPE 4507-B-005 Accelerometers. 18.05.22

URL-3, www.bksv.com/en/instruments/daq-data-acquisition/lan-xi-daq-system/daq-modules/type-3053 Data Acquisition System. 19.05.2022

URL-4, www.bksv.com/en/transducers/vibration/impact-hammers/8210 Impact Hammer. 19.05.2022

Vandiver, J.K., 1975. Structural evaluation of fixed offshore platforms, Doctoral dissertation, Massachusetts Institute of Technology, Massachusetts.

Verderame, G.M., Ricci, P., De Luca, F., Del Gaudio, C. and De Risi, M.T., 2014. Damage Scenarios for RC Buildings During the 2012 Emilia (Italy) Earthquake. Soil Dynamics and Earthquake Engineering, 66, 385-400.

Wolff, T. and Richardson, M., 1989. Fault detection in structures from changes in their modal parameters. Proceedings of the 7th international modal analysis conference, Las Vegas, Nevada, Vol. 1, 87-94.

Yu, D.J. and Ren, W.X., 2005. EMD-Based Stochastic Subspace Identification of Structures From Operational Vibration Measurements, Engineering Structures, 27, 12, 1741-1751.

Yu, Y., Wang, C., Gu, X. and Li, J., 2019. A Novel Deep Learning-Based Method for Damage Identification of Smart Building Structures, Structural Health Monitoring, 18, 1, 143-163.

Yuen, M.M.F., 1985. A Numerical Study of the Eigenparameters of a Damaged Cantilever, Journal of Sound and Vibration, 103, 3, 301-310.

## RESUME

He completed his primary, middle and high schools in 2007, 2010 and 2014, respectively. In 2014, he started his bachelor's study in the Civil Engineering Department of Abdullah Gül University. During his bachelor's study, he was awarded first prize in the "Design Sustainable Future" Competition organized by Ronesans Inc and third prize in the "3rd National Spaghetti Bridge Competition" organized by Kalyoncu Institute of Technology. He completed his bachelor's degree in 2019 as a high honor student and was the second-best in his class. He currently works as a research assistant at the Civil Engineering Department, Karadeniz Technical University. He has an English proficiency score of 7.5 in IELTS.

His completed academic publications are listed below:

- ✓ Yılmaz Z., Uzal N., Saki S., "Effect of L-Dopa additive in coagulation bath on the performance of PSF membrane incorporated with Al2O3 nanoparticles" ICOCEE 2017-International Conference on Civil and Environmental Engineering, Cappadocia, TURKEY, 8-10 May 2017

- ✓ Yılmaz. Z., Okur F. Y., Günaydın M., Altunışık A. C., "Structural Modeling in Object-Oriented Based Software by Utilizing Data Tables", Journal of Construction Engineering, Management & Innovation, 4 (2021) 267-273, https://doi.org/10.31462/jcemi.2021.04267273

- ✓ Okur E., Altunışık A. C., Genç A. F, Günaydın M., Okur F. Y., Karahasan O. Ş., Yılmaz Z., "Dynamic Response of a Traditional Hımış Mansion using Updated FE Model with Operational Model Testing", Journal of Building Engineering, 43 (2021): 103060 https://doi.org/10.1016/j.jobe.2021.103060